

Optically Transparent, Thermally Insulating and Soundproofing (OTTIS) Aerogel for High-Efficiency Window Applications

by
Elise Strobach

S.M. Mechanical Engineering (2017)
Massachusetts Institute of Technology

B.S. Mechanical Engineering (2014)
Milwaukee School of Engineering

Submitted to the Department of Mechanical Engineering in
Partial Fulfillment of the Requirements for the
Degree of Doctor of Philosophy in Mechanical Engineering
at the
Massachusetts Institute of Technology
February 2020

©2020 Massachusetts Institute of Technology
All rights reserved

Signature redacted

Signature of Author:

Department of Mechanical Engineering
January 15th, 2020

Signature redacted

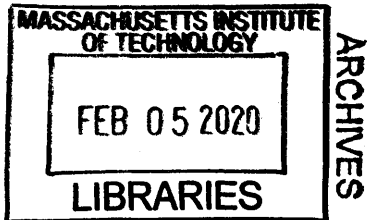
Certified by:

Evelyn N. Wang
Department Head of Mechanical Engineering
Thesis Supervisor

Signature redacted

Accepted by:

Nicolas Hadjiconstantinou
Professor of Mechanical Engineering
Chairman, Committee on Graduate Students



Optically Transparent, Thermally Insulating and Soundproofing (OTTIS) Aerogel for High-Efficiency Window Applications

by

Elise Strobach

Submitted to the Department of Mechanical Engineering on January 15th, 2020,
in Partial Fulfillment of the Requirements for the Degree of Doctor of Philosophy

Abstract

Building heating, ventilation and air conditioning (HVAC) accounts for about 13.6 quadrillion BTU (“quads”) per year or 14% of the total energy consumption in the United States.¹ Accounting for 39% of annual US carbon dioxide emissions, this consumption is directly related to the energy efficiency of the building envelopes.² Windows form an essential but lossy part of building envelopes, particularly during cold weather. Thermal losses in the U.S. from controlled indoor environments to outdoors climates account for \$20 billion dollars in energy each year, signifying a need for more energy efficient windows.³ However, insulating windows represent a thermal challenge due to the needs for optical clarity and thermal performance. Successful application of window design requires an in-depth understanding of both fundamental heat transfer and the occupant needs of our buildings.

One promising solution to these energy losses is the use of silica aerogel, a porous material with super-insulating properties. Previous studies have explored the use of aerogels for energy efficient window glazing due to its low thermal conductivity and promise of transparency. However, its adoption in the general window market has been limited by its low optical clarity characterized by a blue haze. In this work, we present the development of a high-clarity silica aerogel that is able to achieve visible transmittance $> 98\%$ and thermal conductivity $< 13\text{ mW/mK}$ that has been optimized for use in building windows. This performance was achieved by careful tailoring of the interconnected particle network driven by optical modeling to reduce effective scattering size within the material below 10 nm diameter. Next, clarity and thermal conductivity of the material was improved by optimization of the solution-gelation

synthesis across over 300 unique samples and 80 recipes. This provided a framework for achieving a variety of low-haze aerogels with varied thermal, sound-proofing, and mechanical properties.

After achieving high-clarity through optimization of the solution-gelation chemical recipe, several 5 inch diameter double-pane prototypes were to measure the optical, thermal, and acoustic performance. Results indicate that sealing high-clarity aerogel into the gaps of existing double-pane window designs, we can achieve a center-of-glazing U-factor of 0.20 BTU/h/ft²/F, which is 35-50% more insulating than current building codes across North America. These early thermal results and a production-scale techno-economic analysis indicate the aerogel has the ability to achieve cost-effective thermal performance that is competitive with traditional double- and triple-pane windows. Additionally, the aerogel is able to withstand exposure to extreme conditions, such as temperature > 200 °C, relative humidity > 60%, and ultraviolet exposure for more than 6 months without degradation of the nanostructure or optical quality. These results show a promising proof-of-concept design for an aerogel double-pane window that is capable of state-of-the-art performance without a prohibitive cost to consumers. Successful development and commercialization of this high-clarity aerogel has the potential to save billions of dollars in annual building energy losses while satisfying the diverse and complex needs of our buildings.

Thesis Committee:

Thesis Supervisor: Professor Evelyn N. Wang, Department of Mechanical Engineering

Professor Gang Chen, Department of Mechanical Engineering

Professor Nicholas X. Fang, Department of Mechanical Engineering

Acknowledgements

The journey is often as important as the end result – the years of work that made this thesis possible were shaped by many incredible individuals during my educational journey at MIT, and I would like to thank them for their contributions. The dedication and passion provided by those in my professional and personal life were essential to this thesis and to my training as a professional researcher.

I would like to acknowledge the members of the Device Research Laboratory (including past and present). I have had the privilege of working with some of the most inspirational individuals I have met in life. My advisor, Professor Evelyn Wang, has been a role model of excellence in her support of both the research and the researchers. It has only been through her management and guidance that this work was possible, and I thank her for the amazing opportunity she has given me. I would also like to acknowledge Professor Sungwoo Yang, Professor Bikram Bhatia, and Dr. Lin Zhao for their dedication and contributions to this work. Finally, I would like to thank Dr. Kyle Wilke for his support and motivation to complete this work.

In addition to the Device Research Laboratory, I would like to thank my thesis committee advisors, Professor Gang Chan and Professor Nicholas Fang. Their insight and guidance throughout this process not only helped me to tackle the technical challenges, it also taught me how to approach and think about research. Additionally, they both facilitated collaborations within their labs (Nanoengineering Group and the Nanophotonics and 3D Nanomanufacturing Laboratory).

I would also like to thank the funding sources and facilities that have allowed me to accomplish this work at MIT. I have had the great honor of being an MIT Energy Initiative Fellow as well as an NSF Graduate Research Fellow. The foundational work of this thesis was supported by funding from the ARPA-E program of the Department of Energy as part of the FOCUS project call.

The material development and early market research was supported by the NSF I-Corps Program and the Deshpande Center for Technology Innovation. Prototype fabrication and testing was supported by the Massachusetts Clean Energy Center Catalyst grant. The MRSEC Shared Experimental Facilities at MIT (and particularly Dr. Charlie Settens, who supported this work immensely through his knowledge of and enthusiasm for materials characterization) were also fundamental to this thesis.

This research was also made possible through the support of my friends and family. They have supported me throughout my graduate studies both as a professional and as an individual. My parents, Dale and Bernadette Strobach, and my brothers have always demonstrated the dedication and passion that inspires me to tackle new challenges each day. I also want to express my deep appreciation and gratitude to the friends that I have made and grown closer to during my time at MIT.

Finally, I would like to acknowledge the influence of the MIT community for its contribution to this work. The support of the faculty, students, alumni, and affiliates has provided an amazing set of resources and opportunities that have uniquely shaped this work and myself. To all that have offered support, suggestions, connections, questions, words of encouragement, patience, etc., a most humble and sincere thank you.

Table of Contents

1. INTRODUCTION	15
1.1 AEROGEL FOR ENERGY-EFFICIENT WINDOWS	15
1.2 THESIS OBJECTIVES AND OUTLINE	18
2. STATE-OF-THE-ART ENERGY EFFICIENT WINDOWS.....	20
2.1 FIGURES OF MERIT	21
2.2 MEASURING & APPLYING FIGURES OF MERIT	25
2.3 HEAT TRANSFER THROUGH WINDOWS.....	28
2.4 WINDOW TECHNOLOGIES & DESIGNS	34
2.5 SUMMARY	40
3. ACHIEVING TRANSPARENT AEROGELS	41
3.1 FUNDAMENTAL PRINCIPLES OF TRANSPARENT AEROGELS.....	41
3.2 STRUCTURAL CHARACTERIZATION OF TRANSPARENT AND INSULATING AEROGELS.....	48
3.3 STRUCTURAL DEPENDENCE ON AEROGEL SYNTHESIS	52
3.4 SUMMARY	56
4. OPTIMIZING TRANSPARENT AEROGELS FOR WINDOWS	58
4.1 THERMAL PERFORMANCE	62
4.2 ACOUSTIC PERFORMANCE	63
4.3 MECHANICAL PERFORMANCE.....	66
4.4 COMBINED PROPERTY OPTIMIZATION FOR APPLICATION.....	69
4.5 SUMMARY	70
5. TRANSPARENT & STABLE AEROGELS FOR WINDOWS	72
5.1 GRADIENT-INDUCED STRESSES	73
5.2 NON-UNIFORMITY IN CRITICAL POINT DRYING.....	75
5.3 INTERDEPENDENT DEFECTS.....	76
5.4 POST-SYNTHESIS ANNEALING	78
5.5 SUMMARY	80
6. INTEGRATING TRANSPARENT AEROGELS INTO WINDOWS	82
6.1 INITIAL AEROGEL DOUBLE-PANE PROTOTYPES.....	82
6.2 FULL-SCALE AEROGEL PROTOTYPE.....	88
6.3 DOUBLE-PANE DURABILITY	93
6.4 SUMMARY	100
7. TECHNO-ECONOMIC VIABILITY OF AEROGEL WINDOWS	101

7.1	AEROGEL COST	102
7.2	COST-EFFECTIVENESS OF AEROGEL WINDOWS	107
7.3	SUSTAINABILITY & IMPACT OF AEROGEL WINDOWS	109
7.4	SUMMARY	110
8.	SUMMARY, PERSPECTIVE, AND FUTURE WORK	111
8.1	FUTURE WORK	111
8.2	PERSPECTIVE ON THE FUTURE OF DAYLIGHTING	114
	BIBLIOGRAPHY	115

List of Figures

FIGURE 1: (A) HIGH OPTICAL CLARITY OF OUR AEROGEL COMPARED TO COMMERCIALY AVAILABLE MATERIALS. (B) ULTRA HIGH INSULATING PROPERTIES OF AEROGEL MATERIAL COMPARED TO TRADITIONAL WINDOW MATERIALS.17

FIGURE 2: TYPICAL STRUCTURE OF AN OPTICALLY TRANSPARENT SILICA AEROGEL. SMALL PRIMARY SILICA PARTICLES (<1 NM DIAMETER) AGGREGATE TOGETHER TO FORM LARGER SECONDARY SILICA PARTICLES (~2 NM DIAMETER). THESE SECONDARY PARTICLES BOND TOGETHER TO FORM AN INTERCONNECTED NECKLACE STRUCTURE THAT SUPPORTS A HIGHLY MESOPOROUS NETWORK. PORE SIZES VARY GREATLY IN THE MATERIAL, BUT MEAN PORE SIZE IS ~ 10 NM.¹²18

FIGURE 3. SIMPLE DIAGRAM OF A RESIDENTIAL, DOUBLE-PANE WINDOW ILLUSTRATING SOME OF THE KEY ELEMENTS. DIFFERENT STYLES OF WINDOWS WILL USE COMBINATIONS OF THESE AND OTHER ELEMENTS TO ACHIEVE DESIRED OPTIMUM PERFORMANCE IN VARIED APPLICATIONS.....20

FIGURE 4. SUMMARY OF THE KEY FIGURES OF MERIT DEFINED FOR WINDOWS: A) U-FACTOR IS THE MEASURE OF HEAT FLOW PER UNIT AREA FOR A GIVEN TEMPERATURE DIFFERENCE THROUGH THE AREA OF A WINDOW. B) CONDENSATION RESISTANCE (CR) IS THE MEASURE OF LOCAL AREA-AVERAGED CONDENSATION (SCALED FROM 0 TO 100) ON THE INNER SURFACE OF A WINDOW. C) SOLAR HEAT GAIN COEFFICIENT (SHGC) IS THE FRACTION OF SOLAR ENERGY THAT IS TRANSMITTED TO THE INNER ENVIRONMENT ON A SCALE OF 0 TO 1. D) VISIBLE TRANSMITTANCE (VT) IS THE AMOUNT OF VISIBLE LIGHT THAT IS TRANSMITTED THROUGH THE WINDOW NORMALIZED ON A SCALE OF 0 TO 1.....25

FIGURE 5. ENERGY STAR PERFORMANCE CRITERIA FOR RESIDENTIAL WINDOWS BASED ON CLIMATE ZONE IN THE UNITED STATES.²⁸ NOTE THAT FOR HEATING-DOMINATED CLIMATES (NORTHERN) SHGC LIMITS ARE FORCED TO BE GREATER THAN 0.32, BUT FOR COOLING-DOMINATED CLIMATES (SOUTHERN) THE SHGC MUST BE KEPT BELOW 0.25. THIS ILLUSTRATES THE DIVERSE USE OF FIGURES OF MERIT TO OPTIMIZE PERFORMANCE FOR VARIOUS APPLICATION NEEDS.....27

FIGURE 6. (A) DIAGRAM SHOWING DIFFERENT THERMAL TRANSPORT CONTRIBUTIONS FOR A TYPICAL DOUBLE-PANE WINDOW. (B) SIMPLIFIED THERMAL RESISTANCE NETWORK SHOWING THE INTERACTION OF DIFFERENT HEAT TRANSFER PATHWAYS.³⁰29

FIGURE 7. IDEAL SPECTRAL TRANSMITTANCE FOR GLAZINGS IN WARM AND COLD CLIMATES.^{34,35} SPECTRAL DISTRIBUTION OF HUMAN EYE RESPONSE, SOLAR SPECTRUM AND BLACKBODY RADIATION AT 25 °C ALSO SHOWN FOR REFERENCE.....30

FIGURE 8. PLOT SHOWING THE EFFECT OF CHANGING CENTER-OF-GLAZING EMISSIVITY AND SOLAR TRANSMITTANCE ON THE U-VALUE AND SOLAR HEAT GAIN COEFFICIENT (SHGC) OF SINGLE-, DOUBLE- AND TRIPLE-PANE WINDOWS. THE BLUE SYMBOLS REPRESENT THE EFFECT OF LOW-E COATINGS – WHEN THE EMISSIVITY OF THE INNER SURFACES OF GLAZINGS (SURFACE #2 FOR SINGLE-PANE, SURFACE #3 FOR DOUBLE-PANE AND SURFACES #3 AND #5 FOR TRIPLE-PANE) CHANGE TO 0.85, 0.65, 0.45, 0.25 AND 0.05 (TOP TO BOTTOM). THE RED SYMBOLS REPRESENT THE EFFECT OF GLAZING SOLAR TRANSMITTANCE (T_{sol} , ASSUMED EQUAL TO T_{vis} FOR THIS ANALYSIS) CHANGING TO 0.65, 0.45, 0.25 AND 0.05 (RIGHT TO LEFT). WINDOW 7³⁶ WAS USED TO MODEL THE PERFORMANCE, ASSUMING STANDARD NFRC 100-2010 ENVIRONMENTAL CONDITIONS, GENERIC CLEAR GLASS PANES AND AIR-FILLED GAPS; ALL PARAMETERS OTHER THAN THOSE MENTIONED ABOVE WERE UNCHANGED. .31

FIGURE 9. PLOT SHOWING HOW DOUBLE-PANE CENTER-OF-GLAZING U-VALUE VARIES WITH CHANGING THERMAL CONDUCTIVITY OF THE FILL LAYER (THICKNESS = 12 MM), WITH AND WITHOUT LOW-E COATING ($e = 0.05$) ON INTERNAL SURFACE OF THE INNER PANE (SURFACE #3). THE U-VALUES FOR SINGLE-PANE WINDOW, AS WELL AS THERMAL CONDUCTIVITY OF AIR, ARGON AND KRYPTON ARE ALSO SHOWN FOR REFERENCE. WINDOW 7³⁶ WAS USED FOR THIS ANALYSIS, ASSUMING STANDARD NFRC 100-2010 ENVIRONMENTAL CONDITIONS AND GENERIC CLEAR GLASS PANES.33

FIGURE 10. (A) CROSS-SECTIONAL HIGH RESOLUTION TEM OF A $TiO_2/Cu/TiO_2$ LOW-E COATING.⁴⁶ (B) TRANSMITTANCE AND REFLECTANCE SPECTRUM OF AN $AlN/Ag/AlN$ LOW-E COATING WITH HIGH VISIBLE TRANSMITTANCE (82%) AND LOW INFRARED EMITTANCE (8%).⁴⁸36

FIGURE 11. (A) AN EVACUATED MONOLITHIC AEROGEL GLAZING IN A WELL-INSULATED FRAME. THE VIEW THROUGH SHOWS NO DISTORTION OF THE IMAGE BUT A SLIGHTLY HAZINESS CAN BE OBSERVED. (B) TILED MONOLITHIC AEROGEL GLAZING SANDWICHED BETWEEN TWO GLASS PANES. (C) DOUBLE PANE WINDOW UNITS FILLED WITH GRANULAR AEROGEL: (LEFT) EMPTY REFERENCE, (MIDDLE) 3-5 MM GRANULAR PARTICLE, (RIGHT) 0.5 MM GRANULAR PARTICLE. (D) HIGH-TRANSPARENCY AEROGEL SAMPLE IN COMPARISON WITH A SINGLE PANE GLASS.

(E) HAZE AND TOTAL VISIBLE TRANSMITTANCE OF TRANSPARENT MONOLITHIC AEROGEL SAMPLES PREVIOUSLY REPORTED. SOLID LINES ARE THE MODEL PREDICTIONS FOR DIFFERENT SCATTERING ASYMMETRIC FACTOR G (0, ISOTROPIC; >0 , FORWARD) AND SINGLE SCATTERING ALBEDO Ω (1, PURE SCATTERING; <1 , INCLUDING ABSORPTION). PERFORMANCE OF A SINGLE-PANE GLASS IS INDICATED BY THE GREEN SHADED AREA. GRANULAR SAMPLES HAVE MUCH LOWER TRANSMITTANCE AND HAZE, HENCE ARE OUT OF THE PLOTTED RANGE. FIGURES REPRODUCED WITH PERMISSION: (A) FROM [59], (B) FROM [60], (C) FROM [63], AND (D, E) FROM [73].	39
FIGURE 12: A) IMAGE AND STRUCTURAL REPRESENTATION OF AN OPTICALLY TRANSPARENT SILICA AEROGEL FABRICATED WITH SOLAR TRANSPARENCY $>97\%$. SMALL PRIMARY SILICA PARTICLES (<1 NM DIAMETER) AGGREGATE TOGETHER TO FORM LARGER SECONDARY SILICA PARTICLES (~ 2 NM DIAMETER). THESE SECONDARY PARTICLES BOND TOGETHER TO FORM AN INTERCONNECTED NECKLACE STRUCTURE THAT SUPPORTS A HIGHLY MESOPOROUS NETWORK. B) SEM IMAGE SHOWING THE INTERCONNECTED STRUCTURE. PORE SIZES VARY GREATLY IN THE MATERIAL, BUT MEAN PORE SIZE IS ~ 10 NM. C) TRANSMISSION SPECTRA OF A 4 MM TRANSPARENT AEROGEL SAMPLE COMPARED TO THE AM1.5 SOLAR SPECTRUM.	42
FIGURE 13. SCANNING ELECTRON (A) AND TUNNELING ELECTRON (B) MICROSCOPIC IMAGING OF SILICA AEROGEL. RESOLUTION IS LIMITED BY THE INSULATING NATURE OF SILICA BUT SHOWS THE BASIC STRUCTURAL FEATURES THAT FORM DURING SOLUTION-GELATION.	44
FIGURE 14. AEROGEL PRODUCTION, CONSISTING OF MEASURING AND MIXING CHEMICALS, WHICH ARE THEN POURED INTO SHEETS FOR GELATION. THESE SHEETS FORM A WET GEL. FINALLY, THIS WET GEL IS DRIED VIA CRITICAL POINT DRYING.	46
FIGURE 15. (A) HIGHLY TRANSPARENT MONOLITHIC SILICA AEROGEL SAMPLE FABRICATED IN THE DEVICE RESEARCH LABORATORY. (B) IMAGE OF COMMERCIALY AVAILABLE SILICA AEROGEL. ⁹¹	47
FIGURE 16: TYPICAL SILICA AEROGEL SCATTERING PATTERN. BY ASSUMING SPHERICAL, DISPERSE SCATTERS WE CAN MAKE APPROXIMATIONS ABOUT PORE AND PARTICLE SIZES, AS WELL AS THE INTERCONNECTIVITY OF THE STRUCTURAL NETWORK.	49
FIGURE 17: EFFECTIVE SCATTERING SIZE (REPRESENTING SCATTERING FROM BOTH PORE AND PARTICLES) AND SEM IMAGES OF SILICA AEROGEL. (A) HIGHLY TRANSPARENT ($>96\%$) TMOS AEROGEL WITH A DENSITY OF 220 KG/M^3 . (B) MS-51 AEROGEL WITH A DENSITY OF 75 KG/M^3 .	50
FIGURE 18. VISIBLE TRANSMITTANCE AND HAZE AS A FUNCTION OF EFFECTIVE SCATTERING SIZE AS CHARACTERIZED BY SMALL ANGLE X-RAY SCATTERING (SAXS). SCATTERING IS THE PRIMARY LOSS MECHANISM FOR VISIBLE TRANSMITTANCE AND RESULTS IN HIGHER HAZE. THE MODELING LINES SHOWN ARE TAKEN FROM THE MODEL DESCRIBED IN ZHAO ET AL ^{18,19} .	52
FIGURE 19. IMAGES OF SAMPLES OF VARIED AMMONIA RATIO MADE WITH TMOS PRECURSOR. HAZINESS CAN BE SEEN BY THE BLUE COLOR OF DIFFUSELY SCATTERED LIGHT OF SHORT WAVELENGTHS. FROM THESE IMAGES, IT IS CLEAR TO SEE THE LOWEST HAZE SAMPLE IS SECOND FROM THE RIGHT.	53
FIGURE 20. INFLUENCE OF VARYING THE CHEMICAL RATIOS NORMALIZED BY PRECURSOR ON THE VISIBLE HAZE OF SILICA AEROGEL. (A) VARIATION OF AMMONIA HYDROXIDE WHICH FUNCTIONS AS THE CATALYST. BOTH THE TMOS AND MS-51 PRECURSORS SHOW AN OPTIMUM RATIO TO MINIMIZE HAZE. (B) VARIATION OF WATER, THE REACTANT WITH TMOS AND MS-51 RESPECTIVELY. HIGHER RATIOS SHOW LOWEST HAZE. (C) VARIATION OF METHANOL WHICH SERVES TO CONTROL CONCENTRATION OF REACTANTS AND CATALYST, AND ALSO INFLUENCES THE DENSITY OF THE AEROGELS.	54
FIGURE 21. RELATIONSHIP BETWEEN THE PRODUCT OF DENSITY AND SCATTERING DIAMETER AND VISIBLE HAZE. DENSITY AND SCATTERING DIAMETER INFLUENCE THE SCATTERING COEFFICIENT AND ARE THEREFORE RELATED TO DIFFUSE REFLECTION AND THEREFORE HAZE. THE MODELING LINE WAS CALCULATED USING THE MODEL DESCRIBED IN ZHAO ET AL ¹⁸ .	55
FIGURE 22. EFFECTIVE SCATTERING SIZE ACHIEVED THROUGH VARIOUS RECIPE RATIOS. EACH AXIS IS NORMALIZED BY THE MINIMUM AND MAXIMUM VALUES SELECTED FOR FABRICATION. THIS WAS A RATIO OF 2-75 FOR METHANOL, 1-47 FOR WATER, AND 0.002-0.30 FOR AMMONIA. FROM THE PLOT, WE SEE THAT HIGHER AMMONIA AND WATER CONTENT RESULTS IN CONSISTENTLY LOWER SCATTERING SIZE, AND THEREFORE HIGHER CLARITY.	56
FIGURE 23. TRANSMISSION SPECTRA OF A 4 MM TRANSPARENT AEROGEL COMPARED TO A 3 MM THICK SAMPLE OF TRADITIONAL CLEAR FLOAT GLASS. HAZE SPECTRA FOR THE SAME AEROGEL IS SHOWN BY THE DASHED LINE. DUE TO THE LOW REFLECTANCE AND HIGH CLARITY OF THE TRANSPARENT AEROGEL, TOTAL TRANSMISSION IN THE VISIBLE SPECTRUM (375-800NM) IS HIGHER THAN THAT OF GLASS. HOWEVER, GLASS HAZE IS VERY CONSISTENT IN THE VISIBLE WAVELENGTHS ($\sim 0.5\%$, NOT SHOWN) COMPARED TO THE WAVELENGTH DEPENDENT BEHAVIOR FOR THE AEROGEL SAMPLE SHOWN HERE (AVERAGE HAZE 1.6% IN VISIBLE WAVELENGTH RANGE). BOTH TRANSMISSION AND HAZE OF THE AEROGEL ARE HIGHLY DEPENDENT ON THE NANOFEATURE SIZES,	

DENSITY, AND THICKNESS, PROVIDING AN OPPORTUNITY TO TAILOR THE MATERIAL TO ACHIEVE HIGHER PERFORMANCE IN APPLICATION.59

FIGURE 24. TRANSPARENT AEROGEL HAZE NORMALIZED TO A 4 MM THICKNESS (AS DESCRIBED IN ZHAO ET AL¹⁹) AS A FUNCTION OF A) AVERAGE VISIBLE TRANSMISSION, B) AVERAGE SCATTERING SIZE, AND C) BULK DENSITY. A) HAZE AND TRANSMISSION ARE FUNDAMENTALLY RELATED BY THE ISOTROPIC SCATTERING THAT DOMINATES OPTICAL LOSS IN THE VISIBLE AND UV WAVELENGTHS AS SHOWN BY THE DATA TREND.¹⁹ SINCE THE THRESHOLD OF DESIRED HAZE IS MORE LIMITING THAN VISIBLE TRANSMISSION, BY STUDYING THE PROPERTY RELATIONSHIPS OF HAZE WE CAN ALSO MEET ACCEPTABLE VISIBLE TRANSMISSION. B) SCATTERING SIZE, AS MEASURED BY SAXS, SHOWS THAT HAZE IS VERY SENSITIVE TO THE AVERAGE NANOFEATURE SIZE WITHIN THE MATERIAL. THE MODELED LINE SHOWS GOOD AGREEMENT WITH EXPERIMENTAL RESULTS WHEN Banded BY THE RANGE OF DENSITIES WITHIN THE EXPERIMENTAL DATASET (89 TO 249 KG/M³). C) THE RELATIONSHIP BETWEEN DENSITY AND HAZE IS NOISIER EXPERIMENTALLY THAN PREDICTED BY THE MODEL DUE TO THE HIGH UNCERTAINTY WHEN ESTIMATING DENSITY. THE BANDS ON THE MODEL CAPTURE THE RANGE OF SCATTERING SIZES WITHIN THE EXPERIMENTAL DATASET (2.72 TO 4.08 NM).....61

FIGURE 25. EFFECTIVE THERMAL CONDUCTIVITY AS A FUNCTION OF APPARENT DENSITY. THERMAL CONDUCTIVITY WAS MEASURED IN A NETZSCH 436 HFM ON 12-15 CM DIAMETER SAMPLES WITH THICKNESS OF 4 – 7 MM. THE LINE REPRESENTS PREDICTED THERMAL CONDUCTIVITY AT STANDARD TEMPERATURE AND PRESSURE FROM THE RELATIONSHIPS DESCRIBED IN HRUBESH & PEKALA¹⁰⁰ WITH THE BANDS REPRESENTING THE RANGE OF AVERAGE PORE DIAMETER WITHIN THE EXPERIMENTAL DATASET (11 – 20 NM), AS MEASURED BY NITROGEN SORPTION. BOTH THE DATA AND EXPERIMENTAL CHARACTERIZATION AGREE WELL AND PREDICT AN OPTIMUM POINT AT ABOUT 140 KG/M³.63

FIGURE 26. SOUND TRANSMISSION LOSS COMPARISON OF A 4 MM THICK AEROGEL AND A 4 MM GLASS SHEET IN AMBIENT CONDITIONS AS MEASURED BY AN IMPEDANCE TUBE. REFLECTION IS THE DOMINANT SOUND TRANSMISSION LOSS MODE IN BOTH THE AEROGEL AND GLASS SHEET, SHOWING SIMILAR BEHAVIOR.64

FIGURE 27: ABSORPTION AND REFLECTION COEFFICIENTS FOR A 3 MM THICK TMOS AEROGEL. THE REFLECTION COEFFICIENT IS MEASURED BY THE RATIO OF THE REFLECTED AMPLITUDE RELATIVE TO THE INCIDENT AMPLITUDE AND IS THE DOMINANT SOUND TRANSMISSION LOSS MODE, INDICATING THAT INCREASING SOUND REFLECTION IN THE PORE AND PARTICLE STRUCTURE WILL INCREASE OVERALL SOUND LOSS.65

FIGURE 28. SOUND TRANSMISSION LOSS OF THE AEROGEL MATERIAL AVERAGED FROM 80-1600 HZ AS A FUNCTION OF AEROGEL THICKNESS. EACH MEASUREMENT WAS REPEATED AT LEAST 3 TIMES AND AVERAGED TO OBTAIN EACH DATA POINT. THE DEPENDENCE OF SOUND TRANSMISSION LOSS ON THICKNESS INDICATES THAT SOUND IS MOST IMPEDED BY AN INCREASE IN OVERALL AEROGEL MASS, AS PREDICTED BY PRIOR WORKS ON GLASS PANES.¹⁰⁴ ..66

FIGURE 29: COMPRESSIVE STRENGTH OF TMOS AND MS-51 AEROGELS FABRICATED IN THE DEVICE RESEARCH LABORATORY COMPARED TO TYPICAL LITERATURE VALUES¹⁰⁷. WHILE IT IS GENERALLY TRUE THAT A DENSER AEROGEL HAS A HIGHER COMPRESSIVE STRESS⁷⁷ WE SEE THAT THE LESS DENSE MS-51 AEROGEL STILL HAS A VERY HIGH COMPRESSIVE STRENGTH, INDICATING IT IS A GOOD CANDIDATE RECIPE FOR STRONG, LOWER DENSITY AEROGELS AS NEEDED IN WINDOW APPLICATIONS.67

FIGURE 30. YOUNG’S MODULUS AS A FUNCTION OF APPARENT AEROGEL DENSITY. THE VALUES OF E WERE DETERMINED BY A SLOPE FIT OF EXPERIMENTAL DATA FROM A STANDARD INDENTATION TEST USING THE HERTZ INDENTATION THEORY. PREVIOUS LITERATURE INDICATES THE EXPONENTIAL TERM OF A POWER FIT SHOULD FALL IN THE RANGE OF 2.59 TO 3.53. THE DATA COLLECTED HAS A POWER FIT OF 2.87, AGREEING WELL WITH PRIOR WORKS. THIS RELATIONSHIPS ALSO SHOWS THAT WHILE THE STRENGTH CAN BE IMPROVED BY OPTIMIZING THE MATERIAL DENSITY, THE AEROGEL STILL HAS A YOUNG’S MODULUS THAT IS 3 ORDERS OF MAGNITUDE LOWER THAN TRADITIONAL FLOAT GLASS.68

FIGURE 31. DIAGRAM ILLUSTRATING THE SIMPLIFIED FLOW OF HEAT FROM AN INTERIOR CHAMBER TO AN EXTERIOR CHAMBER. TEMPERATURES AND CONVECTIVE COEFFICIENTS ARE PRESCRIBED BY THE U-FACTOR STANDARDS. HERE, R_{WINDOW} CAN BE CALCULATED FROM MODELED OR EXPERIMENTALLY MEASURED EFFECTIVE THERMAL CONDUCTIVITY FROM THE AEROGEL. AS A NOTE, THE ADDITION OF GLASS TO THIS MODEL HAS NO APPRECIABLE EFFECT ON U-FACTOR DUE TO THE HIGHLY INSULATING NATURE OF THE AEROGEL (R_{WINDOW}) THAT IS MUCH LARGE THAN ANY THERMAL RESISTANCE FROM THE GLASS PANES.69

FIGURE 32. A) HAZE AND U-FACTOR AS A FUNCTION OF APPARENT DENSITY FOR THE AEROGEL NORMALIZED TO 4 MM THICKNESS. MODEL BANDS ENCOMPASS THE AVERAGE SCATTERING SIZE (2.72 – 4.08 NM) FOR HAZE AND AVERAGE PORE DIAMETER (11 – 20 NM) FOR U-FACTOR THAT ARE REPRESENTED BY THE INCLUDED DATASETS. B) HAZE AND U-FACTOR AS A FUNCTION OF AEROGEL THICKNESS. MODEL BANDS ENCOMPASS THE DENSITIES (112 – 249 KG/M³) FOR BOTH HAZE AND U-FACTOR THAT ARE REPRESENTED BY THE INCLUDED DATASETS..... 70

FIGURE 33: (A) VISIBLE TRANSMITTANCE OF THE ULTRA-CLEAR SILICA AEROGEL (BLUE) COMPARED TO BOROSILICATE GLASS AND COMMERCIAL SILICA AEROGEL (FROM AEROGEL TECHNOLOGIES). THE ULTRA-CLEAR AEROGEL IS MORE TRANSPARENT THAN BULK GLASS DUE TO THE REDUCTION IN REFLECTANCE FROM THE HIGHLY POROUS AEROGEL. (B) SCATTERING SIZE DISTRIBUTION (CHARACTERIZED BY SMALL ANGLE X-RAY SCATTERING) COMPARING FEATURE SIZES OF COMMERCIAL AEROGEL TO THE ULTRA-CLEAR STRUCTURE. SCATTERING SIZE QUANTIFIES BOTH PORE AND PARTICLE FEATURES. (C) SCANNING ELECTRON MICROSCOPE IMAGE OF THE ULTRA-CLEAR AEROGEL NANOPOROUS STRUCTURE, SHOWING THE COMPLEX PARTICLE AND PORE NANOFEATURES.72

FIGURE 34: A) SURFACE DEFECTS ON A MONOLITHIC AEROGEL SHEET. SPECIAL LIGHTING WAS USED TO ACCENTUATE THE DEFECTS, WHICH FORM CELLS WITH A CHARACTERISTIC PERIOD OF ~ 0.2 IN, CONSISTENT WITH TYPICAL BENARD-MARANGONI CONVECTION CELL SIZES OBSERVED IN LITERATURE.¹¹¹ TO AID THE EYE TWO CELLS HAVE BEEN TRACED IN YELLOW. B) SIDE VIEW OF A MONOLITHIC AEROGEL SHEET SITTING ON TOP OF A BEAKER AFTER SUPERCRITICAL DRYING. NON-UNIFORM STRESSES IN THE SHEET CAUSE WARPING, PREVENTING THE FORMATION OF A FLAT SHEET. THE THICKNESS OF THE SHEET IS MARKED IN BLACK. C) DRIED COLLOIDAL SUSPENSION WITH CRACKING AND STRESSES DUE TO BENARD-MARANGONI CONVECTION.¹⁰⁹73

FIGURE 35. THE EXOTHERMIC REACTION DURING GELATION, EVAPORATION AT SURFACES, AND HEAT TRANSFER THROUGH THE MOLD (CONTAINER), LEAD TO TEMPERATURE GRADIENTS WITHIN THE MIXTURE. THESE TEMPERATURE GRADIENTS CAN DRIVE BOTH MARANGONI CONVECTION AND RAYLEIGH CONVECTION.....74

FIGURE 36: BIREFRINGENCE VARIATIONS WITHIN DRIED AEROGEL SAMPLES OF 5 IN NOMINAL DIAMETER SHOWING RELATIVE CHANGES TO STRESS WITHIN THE SAMPLE. (A) SAMPLE THAT CRACKED DURING AN ERROR CRITICAL POINT DRYING. STRESS BUILD-UP AROUND THE EDGES OF THE CRACKS SHOW WHERE NON-UNIFORM SHRINKAGE LEAD TO COMPLETE SEPARATION OF THE DIFFERENT SECTIONS WITHIN THE SAMPLE. (B) SAMPLE THAT WAS MADE WITH A SIMILAR PROCESS TO (A) BUT WAS DRIED USING A WELL-CONTROLLED PROCESS. WHILE WE STILL SEE SOME STRESS VARIATIONS WITHIN THE SAMPLE, OVERALL THE BIREFRINGENCE IS MUCH MORE UNIFORM. (C) SAMPLE THAT HAD SIGNIFICANT SHRINKAGE DURING CRITICAL POINT DRYING BUT WAS ABLE TO REMAIN CRACK-FREE. CAREFUL STUDY OF THE PHOTO SHOWS STRESS LINES THAT EXTEND RADIALLY OUTWARD, BUT THE CHANGES IN STRESS ACROSS THESE LINES SHOW LESS CONTRAST THAN (A), THE SYMMETRY OF STRESSES CREATED AND THEIR LOW RELATIVE DIFFERENCE BETWEEN THE BULK SAMPLE RESULTED IN THIS SAMPLE SHRINKING WITHOUT CRACKING OR WARPING.76

FIGURE 37: TRANSPARENT SILICA AEROGEL BEFORE AND AFTER ANNEALING AT 400 °C FOR 2 WEEKS. TRANSMITTANCE IS 97.6% IN THE ANNEALED SAMPLE COMPARED TO 94.8% BEFORE ANNEALING. HOWEVER THE SAMPLE ALSO DENSIFIED 4.5%, INCREASING EFFECTIVE THERMAL CONDUCTIVITY AND INDICATING A NEED FOR OPTIMIZATION.....79

FIGURE 38: STRUCTURAL CHANGE AS MEASURED BY SAXS OF A TRANSPARENT SILICA AEROGEL ANNEALED FOR 1 HOUR AT PROGRESSIVELY INCREASING TEMPERATURES. AVERAGE PORE SIZE, PARTICLE SIZE, AND OVERALL DENSITY SHOW APPRECIABLE CHANGE AT HIGHER TEMPERATURES, EVEN WITH SHORT EXPOSURE.79

FIGURE 39. SMALL ANGLE X-RAY SCATTERING (SAXS) DATA FOR TMOS SAMPLES ANNEALED AT 400 °C SHOWING THE STRUCTURAL CHARACTERIZATION OF THE PARTICLE AND PORE NETWORK. (A) SCATTERING DATA OF A SAMPLE BEFORE AND AFTER ANNEALING FOR 336 H. ASSUMING THAT STRUCTURAL FEATURES ARE SPHERICAL, THE PARTICLE ($Q\sim 0.03$), PORE ($Q\sim 0.1$), AND MEAN SCATTERING SIZE (FULL DATA RANGE) CAN BE FOUND FROM THE DATA¹². BECAUSE THE DATA IS SPREAD OVER A LARGE RANGE OF SIZES, A SUBTLE CHANGE TO THE RAW SCATTERING CURVE RESULTED IN AN APPRECIABLE CHANGE IN SIZE. (C) THE STRUCTURAL FEATURE CHANGES OF A TMOS SAMPLE ANNEALED UP TO 336 H AT 400 °C ARE SHOWN. THE DATA POINTS FOR EACH ANNEALING TIME REPRESENT THE SCATTERING RADIUS BEFORE THE INDICATED ANNEALING TIME (BEFORE ANNEALING), AND IMMEDIATELY AFTER ANNEALING (ANNEALED). PARTICLE SIZE WAS NOT AFFECTED SIGNIFICANTLY BY ANNEALING, BUT THE PORE SIZE DECREASED MORE WITH ANNEALING TIME, CAUSING THE MEAN SCATTERING VALUE TO DECREASE WITH ADDITIONAL ANNEALING.80

FIGURE 40. PROPOSED DOUBLE-PANE WINDOW DESIGN USING DRL AEROGEL. THE AEROGEL WILL REPLACE THE GAS-FILLED GAP AND THE EDGE-SPACERS OF A TYPICAL DOUBLE-PANE (LEFT) TO ACHIEVE SUPERIOR PERFORMANCE (RIGHT).82

FIGURE 41. A) ULTRA-CLEAR AEROGEL SHEET (6" DIAMETER) WITH A POROSITY OF 94%. AVERAGE PORE AND PARTICLE FEATURE SIZES ARE <10 NM DIAMETER, ALLOWING TRANSMITTANCE $>98\%$, HAZE $<2.0\%$, AND THERMAL CONDUCTIVITY <13 MW/MK THROUGH 3 MM THICKNESS. B) PROPOSED AEROGEL DOUBLE-PANE WINDOW WITH INSET SHOWING THE ULTRA-CLEAR AEROGEL COMPARED TO FLOAT GLASS. THE AEROGEL REPLACES THE AIR GAP IN A DOUBLE-PANE WINDOW.83

FIGURE 42. DOUBLE-PANE WINDOW PROTOTYPE USING DRL AEROGEL. THE AEROGEL WILL REPLACES THE GAP TRADITIONAL FILLED WITH GAS AND THE EDGE-SPACERS SUPPORT THE DOUBLE-PANE STRUCTURE.....83

FIGURE 43. (A) EXPERIMENTAL VISIBLE TRANSMISSION PLOTTED AGAINST PREDICTED VISIBLE TRANSMISSION. A LINE OF $Y=X$ WAS ADDED TO THE GRAPH TO SHOW THAT EXPERIMENTAL VALUES ALIGN VERY WELL WITH PREDICTED VALUES. (B) EXPERIMENTAL HAZE PLOTTED AGAINST PREDICTED HAZE. A LINE OF $Y=X$ WAS ADDED TO THE GRAPH, WHICH SHOWS THAT EXPERIMENTAL HAZE VALUES DIFFER MORE AS THE PREDICTED HAZE VALUE INCREASES.84

FIGURE 44. VISIBLE LIGHT TRANSMISSION OF AEROGEL SAMPLE0246 COMPARED TO PILKINGTON’S ENERGY ADVANTAGE LOW-E COATING AND OPTIFLOAT GLASS, AS WELL AS TRANSMISSION OF INSULATED GLASS UNIT STACKS THAT INCLUDE SAMPLE0246 WITH THE GLASS. DUE TO THE AEROGEL’S HIGH TRANSPARENCY, IT DOES NOT SIGNIFICANTLY AFFECT OTHER STRATEGIES TO CONTROL SHGC.85

FIGURE 45: SOUND TRANSMISSION LOSS COMPARISON OF A 4 MM THICK AEROGEL AND A 4 MM GLASS SHEET IN AMBIENT. REFLECTION IS THE DOMINANT SOUND TRANSMISSION LOSS MODE IN BOTH THE AEROGEL AND GLASS SHEET. THE DATA SHOWS THAT SOUND TRANSMISSION CAN BE INCREASED BY ADDING THE AEROGEL LAYER TO THE GLASS LAYER, WITH LARGE ENHANCEMENT EXPECTED WHEN THE AEROGEL PORE PRESSURE IS DECREASED.86

FIGURE 46: SOUND TRANSMISSION LOSS COMPARISON OF A 4 MM THICK AEROGEL SEALED IN A DOUBLE-PANE, A 4 MM AIR GAP AT ~ 1 KPA, AND A 4 MM GLASS SHEET IN AMBIENT. REFLECTION IS THE DOMINANT SOUND TRANSMISSION LOSS MODE IN BOTH THE AEROGEL AND GLASS SHEET. THE DATA SHOWS THAT SOUND TRANSMISSION CAN BE INCREASED BY ADDING THE PARTIALLY EVACUATED AEROGEL LAYER TO THE GLASS STACK.87

FIGURE 47: U-VALUES AT CENTER-OF-PANE FOR DIFFERENT WINDOW DESIGNS AS MODELED FROM THERMAL CONDUCTIVITY (NO CONSIDERATION FOR CONVECTION) PER THE NFRC STANDARD CONDITIONS. TO BE COMPETITIVE IN THE WINDOW MARKET, IT IS NECESSARY TO BE AT OR BELOW $2.5 \text{ W/M}^2\text{K}$. AEROGEL AT BOTH AMBIENT AND MODESTLY REDUCED PRESSURE SHOW SIGNIFICANTLY BETTER PERFORMANCE AT REASONABLE THICKNESSES.88

FIGURE 48. AEROGEL DOUBLE-PANE PROTOTYPE MADE OF ~ 4 INCH TILED HEXAGONS. THE FULL PROTOTYPE IS 12” X 12” FEATURING A 2 MM THICK LAYER OF NOMINALLY IDENTICAL AEROGELS.89

FIGURE 49. ROTATABLE GUARDED HOT BOX USED TO MEASURE HEAT FLOW ACROSS A WALL AREA. (A) DIAGRAM SHOWING GENERAL DESIGN OF METERED CHAMBER SYSTEM.¹¹⁸ (B) SYSTEM USED FOR U-FACTOR CHARACTERIZATION AT OAK RIDGE NATIONAL LABORATORIES. FOR WINDOW PROTOTYPE TESTING, THE INSULATED GLASS UNIT IS MOUNTED INTO THE CENTER WALL SECTION AND SEALED IN BETWEEN THE “COLD” AND “HOT” CHAMBERS. HEAT FLOW ACROSS THE PROTOTYPE IS MEASURED BY MONITORING THE HEAT NEEDED TO MAINTAIN THE SETPOINT TEMPERATURES.90

FIGURE 50. EXPERIMENTAL AND MODELED U-FACTOR OF 1 X 1 SQFT AEROGEL DOUBLE-PANE PROTOTYPE. EXPERIMENTAL MEASUREMENTS WERE PERFORMED IN A ROTATABLE GUARDED HOTBOX AT CONDITIONS DESCRIBED IN TABLE 4. THE PROTOTYPE WINDOW WAS MADE USING TILED 2 MM AEROGEL SAMPLES.90

FIGURE 51. EXPERIMENTAL AND MODELED U-FACTOR OF 1 X 1 SQFT AEROGEL DOUBLE-PANE PROTOTYPE UTILIZING VARIOUS ADDITIONAL DESIGN STRATEGIES TO IMPROVE INSULATING PERFORMANCE. DESCRIPTION OF MODEL-SUGGESTED DESIGN IMPROVEMENTS ARE SHOWN IN TABLE 5. BOTH THE EXPERIMENTAL AND MODEL PREDICTIONS OF THE PROTOTYPE CAN BE IMPROVED SIGNIFICANTLY BY UTILIZING OPTIMIZED AEROGELS IN COMBINATION WITH ARGON GAS-FILLS.92

FIGURE 52. EXPERIMENTAL SETUP FOR EXTREME ENVIRONMENTAL TESTING. THE HOT PLATE EXPOSES THE AEROGEL TO $>400 \text{ }^\circ\text{C}$ ON THE BOTTOM SURFACE WHILE THE HUMIDIFIER CONTINUES TO BRING IN ROOM TEMPERATURE AIR AT $>80\%$ HUMIDITY. THE SAMPLE IS EXPOSED TO THESE CONDITIONS FOR 8 TO 24 HOUR INCREMENTS AND THEN CHARACTERIZED FOR OPTICAL PERFORMANCE.94

FIGURE 53. TOTAL TRANSMITTANCE COMPARISON OF TMOS SAMPLE BEFORE, AFTER 8, 16, 32 AND 100 HOURS OF ANNEALING AT 400°C IN 80% HUMIDITY. TRANSMITTANCE IS SHOWN TO INCREASE WITH EXPOSURE TO HIGH-TEMPERATURE ANNEALING, WITH NO ADVERSE EFFECTS CAUSED BY THE EXPOSURE TO THE HIGH HUMIDITY ENVIRONMENT.95

FIGURE 54. HYDROPHILIC (LEFT) AND HYDROPHOBIC (RIGHT) AEROGEL SAMPLES MOUNTED ON A COPPER BLOCK. THE COPPER BLOCK IS COOLED VIA A COOLING LOOP TO $-8 \text{ }^\circ\text{C}$ AND THEN PLACED INTO A HUMIDITY CHAMBER.97

FIGURE 55. COMPARABLE INSULATED GLASS UNITS ILLUSTRATING THE DEGRADATION OF PERFORMANCE AS THE ARGON FILL IS REPLACED BY AIR. THE AEROGEL INSULATED GLASS UNIT CAN UNDERGO AN ADDITIONAL 25% FILL LOSS BEFORE REACHING THE SAME U-FACTOR AT FAILURE AS THE GAS-FILLED WINDOW.99

FIGURE 56. TYPICAL MANUFACTURING PROCESS FOR WINDOWS INCLUDING THE AEROGEL MATERIAL. INSULATED GLASS UNIT (IGU) MANUFACTURES SIMPLY BUY AND SEAL THE AEROGEL INTO A GLAZING UNIT, REPLACING GAS FILLS IN THE CURRENT PROCESS. FOR PRODUCTION LAUNCH, AEROGEL MANUFACTURING WILL BE CO-

LOCATED AND INCLUDE PILOTS TARGETED TO REDUCE ANY IMPACT THE AEROGEL MATERIAL HAS ON TRADITIONAL MANUFACTURING. SELLING DIRECTLY TO IGU MANUFACTURERS ALLOWS US TO TAKE ADVANTAGE OF THE EXISTING EQUIPMENT AND DISTRIBUTION CHANNELS.....103

FIGURE 57. UNIT COST OF AEROGEL PRODUCTION DRIVEN BY CHEMICALS NEEDED FOR PRODUCTION. THIS COST CAN BE REACHED AT A 4.5 MILLION SQFT PRODUCTION VOLUME.104

FIGURE 58. KEY RISKS, PROBABILITY OF OCCURRENCE, POTENTIAL IMPACT, AND MITIGATION STRATEGIES FOR COMMERCIAL PRODUCTION AND INTEGRATION OF THE AEROGEL INTO THE EXISTING MANUFACTURING CHAIN.107

FIGURE 59. COMPARISON OF COST ADDED TO A SIMPLE DOUBLE-PANE WINDOW FOR VARIOUS SOLUTIONS TO INCREASE THERMAL PERFORMANCE. THE AEROGEL MATERIAL CAN BE ADDED TO A DOUBLE-PANE WINDOW AT A PRICE POINT SIGNIFICANTLY LOWER THAN TRIPLE-PANE, WITH UP TO 50% BETTER PERFORMANCE THAN EXOTIC GASES.108

Chapter 1

1. Introduction

Since the first dawn, humans have counted on the sun to provide light, heat, demarcation of time, religious inspiration, etc. People have grown to depend on sunlight so much that if we are deprived of it, our physical and mental health can be affected. What makes this abundant energy source so special? The spectrum of radiant energy coming from the sun provides a range of ultra-violet, visible, and near-infrared light which humans have adapted to use in a variety of ways (such as vitamin D conversion, vision and color, and heat, respectively). This light shines on the Earth's surface as a collimated source, allowing it to be concentrated and directed.

But, when modern life requires us to spend more than 80% of our time indoors, the benefits of natural lighting can soon be lost. We try to emulate the benefits of the solar spectrum through various strategies, but studies have shown that natural lighting increases happiness, color perception, productivity, and performance in a way that is difficult to match.⁴ An obvious solution to this problem is to use the light that is already falling into our laps; daylighting uses the sun's natural light to provide illumination, particularly in building interiors. In architecture, daylighting has the potential to not only increase happiness and productivity, but it can also be an energy efficient and aesthetic solution.

Fenestration-based daylighting is the oldest and simplest form of natural lighting seen in buildings. However, the basic single-pane windows that dominated the last millennia can no longer meet the energy and comfort needs that modern buildings demand. Windows today focus on maximizing comfort and performance, and designs must consider many factors including visual performance, thermal comfort and energy loss, and shading and light control. Glazing systems are being designed to meet these needs with specificity for building location, climate, and occupancy needs with a precision that surpasses what has been developed in the past.

1.1 AEROGEL FOR ENERGY-EFFICIENT WINDOWS

The diverse needs of buildings require windows to be varied in their thermal and optical properties. Considerations for climate, orientation, occupancy, etc. all vary the performance needs of the windows used. However, a growing unmet need across all climates is the limitations of affordable, thermally insulating glazing elements. Existing products rely on three primary

strategies to improve performance: 1) add more layers of glass, 2) fill the space between the glass layers with insulating gases, 3) add solar and thermal coatings to one or more of the glass panes.⁵ By adding more layers and insulating gases, thermal performance can be significantly increased (by as much as 10 times) but it also raises the cost significantly – sometimes quadrupling the cost. While adding coatings to glass panes is a cheap, effective solution to reduce radiative losses, it cannot prevent convection or conduction through the window and has, therefore, reached its limit for effectiveness.

These strategies can be used in combination to meet the diverse needs of buildings, but often this results in products that are either highly cost prohibitive or sacrifice energy performance, forcing consumers to choose between efficiency and affordability. Installed triple pane windows in the United States account for less than 5% of all windows, but with no affordable high-performance options, this is not a surprising number.⁶ The thermal limitations and high cost of traditional windows result in large sacrifices of energy and/or comfort in more than 80% of new buildings installed each year.⁷ The lack of affordable, energy efficient windows results in Americans wasting over \$20 billion in energy annually.⁸

The next generation of windows needs to meet the rigorous standards we have for optical and thermal performance, while remaining relatively inexpensive and durable. One path of materials that enables this performance is silica aerogel, a nanoporous material made up of aggregated glass nanoparticles. Transparent, insulating aerogels provide a unique blend of intrinsic properties (heat loss suppression, visible transmission, lightweight, etc., see Figure 1) that have the potential to increase window performance with minimal impact to existing design and cost.⁹⁻¹¹

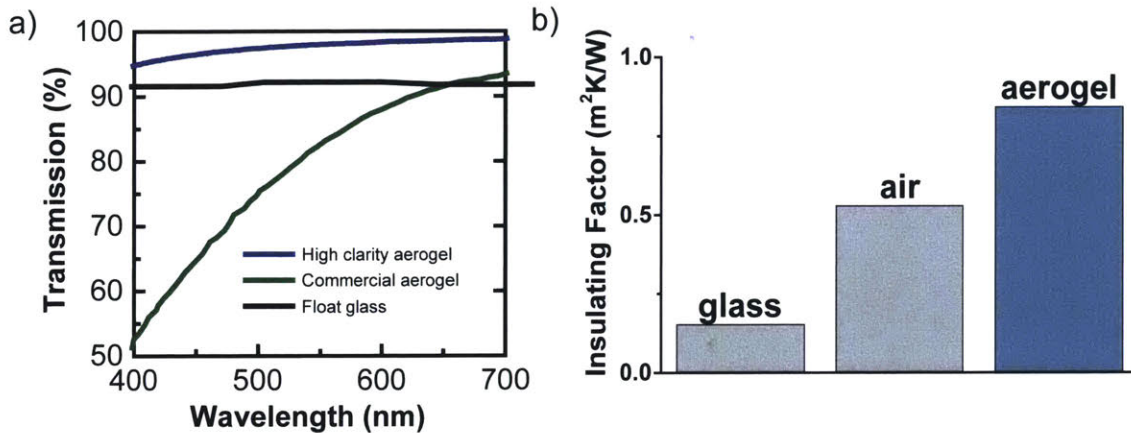


Figure 1: (a) High optical clarity of our aerogel compared to commercially available materials. (b) Ultra high insulating properties of aerogel material compared to traditional window materials.

The aerogel structure consists of a cross-linked silica particle backbone supporting a highly mesoporous (2-50 nm) network comprised of aggregated particles, as seen in Figure 2.^{12,13} With such a low solid volume fraction and pore sizes smaller than the mean free path of air, the solid and gaseous thermal conductivity of aerogels is very low (less than the thermal conductivity of air at room temperature).¹⁴ The radiative thermal conductivity is also very low due to the high absorptivity of the silica particles in infrared (IR) wavelengths; the particles absorb incident radiation and re-radiate in all directions, greatly reducing transmitted IR radiation.¹⁵ These small feature sizes of the particles and pores also allow the transmission of solar wavelengths (300-2000 nm); the only barrier to transmission through the structure is the refractive index difference between the aerogel backbone (silica particles) and air. But, by fabricating aerogels with very small pore and particle sizes (less than 10 nm diameter average), almost all of the visible spectrum can be transmitted (Figure 1a).¹⁶⁻¹⁹ This high transparency and incredibly low thermal conductivity means that very little material and added cost is required to achieve state-of-the-art window performance, opening a new avenue for energy efficient windows.

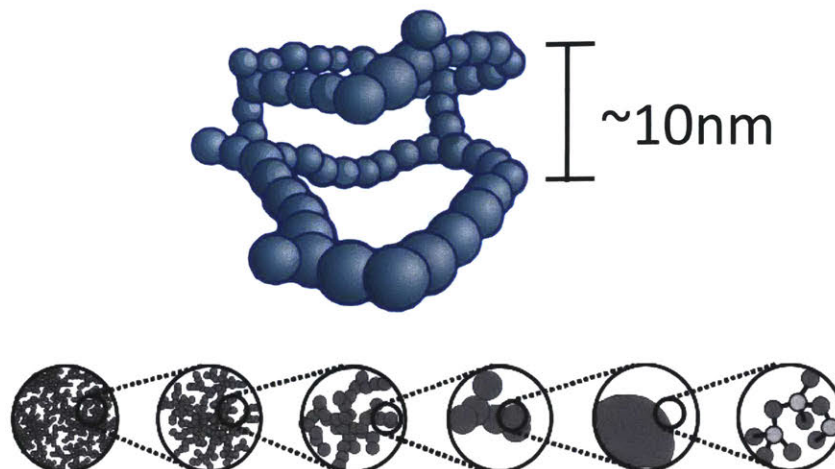


Figure 2: Typical structure of an optically transparent silica aerogel. Small primary silica particles (<1 nm diameter) aggregate together to form larger secondary silica particles (~2 nm diameter). These secondary particles bond together to form an interconnected necklace structure that supports a highly mesoporous network. Pore sizes vary greatly in the material, but mean pore size is ~ 10 nm.¹²

1.2 THESIS OBJECTIVES AND OUTLINE

The objective of this thesis is to outline the methodology for creating optically clear, thermally insulating, and sound-proofing silica aerogels for energy efficient windows. To do this, we present the development of a high-clarity silica aerogel that is able to achieve visible transmittance > 98 % and thermal conductivity < 13 mW/mK. This performance was achieved through iteration and characterization of over 300 unique samples guided by robust optical modeling, providing an understanding of the interconnected nanostructure and its influence on the optical, thermal, and acoustic properties. After achieving high-clarity through optimization of the solution-gelation chemical recipe, several 6 inch diameter double-pane prototypes were assembled and tested to industry standards for optical and thermal performance. Early thermal results and techno-economic analysis indicate the aerogel has the ability to achieve cost-effective thermal performance that is competitive with traditional double- and triple-pane windows. Overall, these elements provide a framework for achieving high-clarity aerogels that can be optimized for the various needs of windows in buildings. The structure of this thesis is outlined below:

In Chapter 1, the motivation and background information for silica aerogel in windows is discussed.

In Chapter 2, we present an overview of thermally insulating windows and the fundamental principles that drive state-of-the-art development.

In Chapter 3, we introduce transparent silica aerogels and the synthesis process. We then explore the relationship between the unique nanostructure and the optical properties, and use these relationships to optimize the aerogel chemical recipe to yield low-haze aerogels.

In Chapter 4, the aerogel structural properties and optical, thermal, acoustic, and mechanical properties are characterized to create a framework for optimization.

In Chapter 5, we explore the various sources of defects unique to the high-clarity aerogel samples and how these defects can be minimized. This includes analysis of the solution-gelation synthesis, critical point drying, and the use of annealing.

In Chapter 6, the integration of optimized aerogels into a double-pane insulated glass unit is described. This includes development and testing of small-scale prototypes for optical, thermal, and acoustic performance to industry standards. Additionally, in this chapter we discuss potential modes of failure and preliminary testing of these modes.

In Chapter 7, the feasibility and practicality of aerogel windows is discussed. This includes a techno-economic analysis of the aerogel synthesis projected to commercial production. It also includes an analysis of the economic and energy savings potential of aerogel double-pane windows based on measured aerogel properties.

In Chapter 8, we summarize the work presented and discuss future directions.

Chapter 2

2. State-of-the-Art Energy Efficient Windows

Building heating, ventilation and air conditioning (HVAC) accounts for about 13.6 quadrillion BTU (“quads”) per year or 14% of the total energy consumption in the United States.¹ This consumption is directly related to the energy efficiency of the building envelopes, where windows form an essential but thermally lossy part of the exterior. Thermal losses in the U.S. from controlled indoor environments to outdoors climates account for \$20 billion dollars in energy each year, signifying a need for more energy efficient windows.³ But with more than 80% of the average person’s time spent indoors, these solutions also need to consider the various aspects of daylighting, comfort, and reliability. Modern windows need to use many designs and strategies to meet the needs of both the building and the occupants.

Traditional, transparent fenestration can be broken into two parts: the optically clear center-of-glazing, and the frame used as the structural element for incorporation into the wall. Many variations of these elements exist to satisfy the diverse needs of our buildings, but the glazing and the frame are universal features. Figure 3 shows an example of a typical double-pane window system designed for residential buildings.

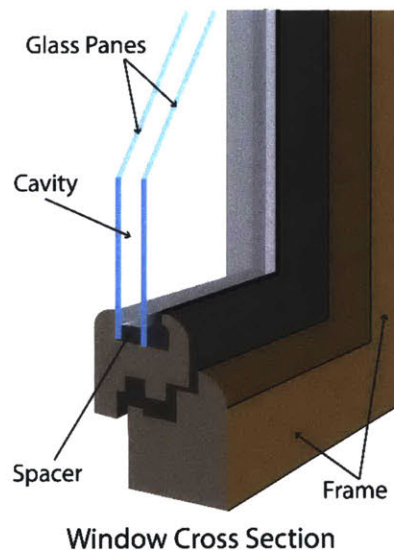


Figure 3. Simple diagram of a residential, double-pane window illustrating some of the key elements. Different styles of windows will use combinations of these and other elements to achieve desired optimum performance in varied applications.

While windows can have a variety of elements based on their performance needs in application, the common components include:

- Glass pane(s)
- Spacer
- Cavity fill(s) (such as gasses)
- Glass coating (on one or more glazing surfaces)
- Structural frame materials (sash, frame, etc.)
- Sealants, claddings, etc.

Generally, building occupants think about the most important window properties – transparency and thermal insulation – as center-of-glazing properties. However, the full window assembly (including the frame, sealing elements, spacers, etc.) can all have a significant influence on performance. Different applications use varied combinations of these elements, which can make it challenging to compare performance, especially in state-of-the-art products where strategies can focus on improving one aspect of the window assembly independently. Therefore, standard figures of merit have been adopted as a way to describe and compare both center-of-glazing and full window performance.

2.1 FIGURES OF MERIT

The diverse needs of buildings require windows to be varied in their thermal and optical properties. Considerations for climate, orientation, occupancy, etc. all vary the performance needs of the windows used. However, there are several standards by which the performance of windows can be quantified and compared.⁵ Here we discuss the most universally applicable figures of merit.

2.1.1 U-factor

The U-factor or U-value is an area averaged heat transfer coefficient used to quantify the thermal transmittance of a material or stack of materials. It was established as a standard measure of window insulating performance by the National Fenestration Rating Council (NFRC). For a fixed inside and outside temperature (as described in NFRC-100),²⁰ the U-factor quantifies the rate of heat transfer per unit area per unit indoor-outdoor temperature difference. As discussed later in this chapter, the thermal energy flow through the window is a summation of the conduction, convection, and radiation heat transfer through elements of the window such as the center-of-glazing, or through the entire window assembly. Including the frame and support elements generally increases the total window's heat transfer rate over just the center-of-glazing, but is a

more representative metric of performance in application, and necessary to quantify for modeling and selecting windows for building performance. Total U-factor for a window, U_t , is defined as

$$U_t = \frac{Q_t}{A_{pf}(T_{out} - T_{in})}$$

under typical indoor and outdoor conditions described as

$$T_{in} = 21.0^{\circ}C$$

$$T_{out} = -18.0^{\circ}C$$

$$V_{wind} = 5.5 \text{ m/s}$$

$$I_{solar} = 0 \text{ W/m}^2$$

where Q_t is the total heat transfer from the indoors to outdoors, A_{pf} is the projected area of the fenestration. The fixed conditions defined as T_{in} and T_{out} are the internal and external environmental temperatures, V_{wind} is the external wind speed, and I_{solar} is the normal incident solar irradiance.

Individual elements can be quantified using a similar approach, and total U-factor of the window can be estimated using an area-average summation of U-factors of individual elements using the equation:

$$U_t = \frac{[\sum(UA)_{frame} + \sum(UA)_{divider} + \sum(UA)_{edge-of-glazing} + \sum(UA)_{edge-of-divider} + \sum(UA)_{center-of-glazing}]}{A_{pf}}$$

Related to the U-factor is the insulating factor, or R-value or R-factor, which is defined as the reciprocal of the U-factor. While a low U-factor indicates good performance by describing a low thermal transmittance, a high R-factor indicates good performance by describing its high thermal resistance.

2.1.2 Condensation Resistance (CR)

Condensation Resistance (CR) is a numerical metric varying between 1 and 100 that quantifies resistance to water condensing on the interior surface of the window due to humidity. This condensation happens when the local temperature of the interior surface drops below the dew point of the water (dependent on the internal environmental relative humidity). A higher number indicates that condensation is less likely to occur on the window. The NFRC has established the standard method for determining CR per standard NFRC 500.²¹ The overall CR assumes indoor

and outdoor temperatures and wind speeds same as those used to define the U-factor (see Section 2.1.1), while indoor relative humidity is varied across relative humidities of 30%, 50%, and 70%.²²

At these conditions, the CR is calculated as the relative area which experiences condensation at the various humidity levels normalized by the total window areas. The CR also includes terms that account for the degree to which surface temperatures are below the dew point at different humidity levels. The CR can be used to describe any portion of the window (center-of-glazing, edge-of-glazing, frame) or the window assembly as a full product.

It is important to note that the CR and U-factor both describe aspects of the thermal transport through the window, but are not necessarily related. The U-factor describes total area-averaged energy transfer, whereas CR will capture local occurrences of low inner surface temperature. CR describes the magnitude of thermal short circuits within the window that the U-factor metric cannot. However, it is generally true that if a window has good thermal performance CR will be high and U-factor will be low.

The CR should not be used as a way to predict condensation in application (which creates visual issues, degrades window elements, and can affect U-factor), but instead indicate the relative effectiveness of the window design to insulate throughout the surface area of the product.

2.1.3 Solar Heat Gain Coefficient (SHGC)

The Solar Heat Gain Coefficient (SHGC) is a measure of the amount of solar energy that can pass from the exterior of the building into the interior through the fenestration in question. Unlike solar transmittance, the SHGC is a measure of both the direct and indirect solar radiation that can be absorbed and re-emitted into the interior of a building. The heat gain is quantified from 0 to 1, with 0 representing 0% of solar energy transmission and 1 meaning 100% of solar energy is transmitted through the fenestration as defined per standard NFRC 200.²³ As with U-factor, performance can also vary between the center-of-glazing and the full window assembly SHGC. Conditions for testing the SHGC are defined as

$$T_{in} = 24.0^{\circ}C$$

$$T_{out} = 32.0^{\circ}C$$

$$V_{wind} = 2.75 \text{ m/s}$$

$$I_{solar} = 783 \text{ W/m}^2$$

This metric is particularly important in heating or cooling dominated climates, where precise control of the amount of solar energy allowed to enter the building can have a dramatic effect on indoor environmental control and building energy consumption. Practically, to simplify development and comparison of technologies it is common to use a closely related quantity, solar transmittance, T_{sol} , to estimate center-of-glazing properties. The difference between SHGC and T_{sol} is due to the absorbed and re-emitted solar radiation by the glazing, which is typically very small (up to 15%) in common windows. For performance comparisons and simple energy modeling either metric can be used.

2.1.4 Visible Transmittance (VT)

Visible Transmittance (VT) is a measure of the visible light that is transmitted through a full window assembly or individual components, such as center-of-glazing. As with SHGC, the metric is scaled from 0 to 1 (equivalent to 0% and 100% of visible light transmitted). The VT is measured as the total hemispherical transmitted light within the spectrum defined from 390 to 750 nm, normalized to an uncovered baseline (100% transmission) as described in standards NFRC 200²³ and 202²⁴. It is typically desirable to maximize VT in order to utilize as much daylight in a building as possible, but increasing VT will also increase the SHGC, as they are both related to the transmission of the solar spectrum. While VT can be applied to all elements of a window, full window values will always have a VT lower than 1 due to the inclusion of the framing elements that cannot transmit 100% of incoming light.

It is also important to note that VT does not quantify the clarity of transmitted light, which is directly related to the angle at which the visible spectrum is transmitted. There is a related metric for haze that is used to quantify the amount of light scattered at more than 2.5° as it travels through the medium,²⁵ but even this standard does not account for the effects on visual aesthetics when incoming light is at a high angle. It is necessary to use VT and haze metrics to meet minimum performance requirements and compare to prior works, but the full visual experience must be considered for a successful application of a window technology.

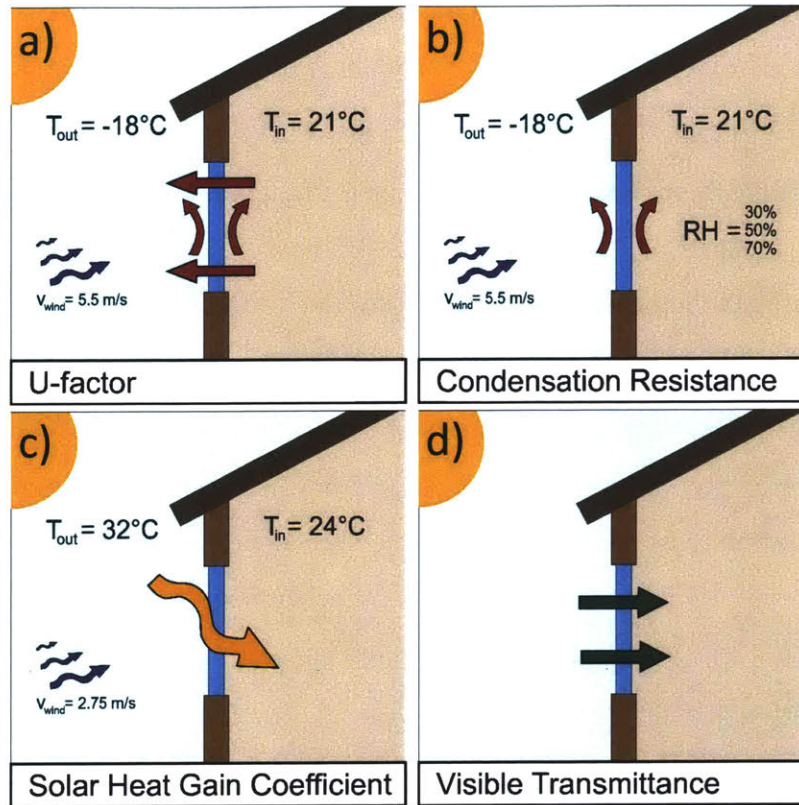


Figure 4. Summary of the key figures of merit defined for windows: a) U-factor is the measure of heat flow per unit area for a given temperature difference through the area of a window. b) Condensation Resistance (CR) is the measure of local area-averaged condensation (scaled from 0 to 100) on the inner surface of a window. c) Solar Heat Gain Coefficient (SHGC) is the fraction of solar energy that is transmitted to the inner environment on a scale of 0 to 1. d) Visible Transmittance (VT) is the amount of visible light that is transmitted through the window normalized on a scale of 0 to 1.

2.2 MEASURING & APPLYING FIGURES OF MERIT

The various figures of merit for windows are measured per the defined NFRC standards as discussed above. Generally, figure of merit values that are reported for a full-window require test chambers to replicate the prescribed standard conditions. For U-factors, two carefully controlled chambers are placed in thermal communication via an insulating wall as described in ASTM standard C1363.²⁶ This wall can then be replaced in part by a material or material stack (such as a double pane window with full frame element) and affixed with thermocouples on both sides and a metering box on the “internal room temperature” side. This setup can measure surface temperatures and heat flux across the tested material. These test setups require careful construction and calibration to provide accurate, reliable results. To meet NFRC standards, setups where the standard figures of merit are measured and reported must be certified to ensure accuracy. It is common practice for new window designs and technologies to work with simulations and center-

of-glazing tests at unofficial measuring sites before measuring the full U-factor performance. Other standards, such as ASTM C177²⁷ describing a guarded hot plate apparatus, can provide a smaller-scale platform to test the performance for new materials to approximate full-scale.

Several figures of merit, such as visible or solar transmittance, can be measured at the center-of-glazing easily and inexpensively on small to large samples or prototypes. These values are often measured directly throughout the development process.

It is important to note that figures of merit only provide a quantifiable standard for comparison, and do not represent the complete list of performance requirements for energy efficient windows. Varied applications may require other properties such as visual aesthetics (coloring, reflectivity, clarity), cost (both upfront cost and time to payback over other products), and durability (life of the window, total energy or cost savings for expected performance lifetime). In this chapter, we focus on the figures of merit to compare state-of-the-art and traditional design strategies that exist at various stages of product development.

Well-established figures of merit provide us with a standard basis for comparing performance of our windows. This becomes especially useful when considering the variety of climate, occupancy, and usage characteristics of the buildings around the world. Whether we are comparing the needs of a home to those of an office building across the street, or an arctic survey station to a tropical hotel, the metrics that are used to select windows must be adaptable.

Figure 5 shows the distribution of residential ENERGY STAR qualified windows based on regional climate in the United States. Differences in the U-factor and SHGC limits (particularly the switching inequalities for heating versus cooling dominated regions) illustrate the importance of prescribing a window's optical and thermal performance to meet energy standards. By quantifying the limits of heat transfer (U-factor) and solar energy transmission (SHGC) independently, homes in both hot and cold climates can use these figures of merit to ensure they meet minimum energy efficiency standards unique to their location.

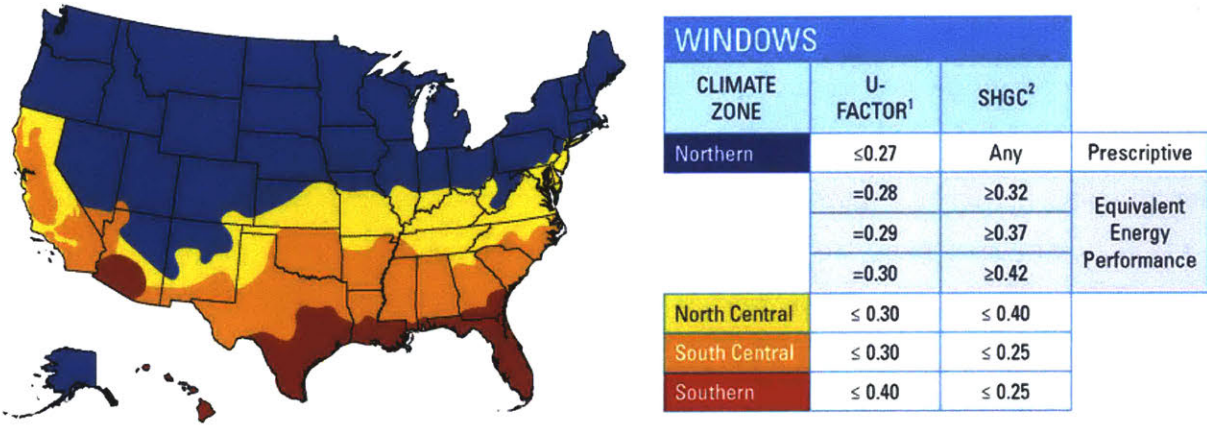


Figure 5. ENERGY STAR performance criteria for residential windows based on climate zone in the United States.²⁸ Note that for heating-dominated climates (Northern) SHGC limits are forced to be greater than 0.32, but for cooling-dominated climates (Southern) the SHGC must be kept below 0.25. This illustrates the diverse use of figures of merit to optimize performance for various application needs.

In order to use the previously defined figures of merit to effectively guide window design, it is important to understand fundamentals of heat and light transfer through the window in order to control overall performance. Even in the most common installed window products (double-pane windows in which two panes of glass are separated by a spacer and insulated with a gas) it is non-obvious what combination of VT, SHGC, and U-factor is optimal. Table 1 shows typical values for common double-pane windows installed in various climates and occupancy types. The differences in light and heat transfer through the window illustrate the variations based on climate.

Table 1. Examples of typical performance values for double-pane, casement windows for residential buildings in various climate zones within the United States.²⁹

Window Description	Climate Region	Glass Thickness	U-factor	CR	SHGC	VT
	Style: double-pane casement Frame: aluminum & wood Gas fill: 90% argon, 10% air	Southern	3 mm	0.35	48	0.24
3 mm			0.32	52	0.25	0.43
Northern		6 mm	0.28	42	0.27	0.41
		6 mm	0.28	41	0.37	0.46
North-Central		6 mm	0.29	41	0.17	0.36
		3 mm	0.29	41	0.35	0.46
South-Central		6 mm	0.28	42	0.17	0.36
		3 mm	0.28	41	0.42	0.24

2.3 HEAT TRANSFER THROUGH WINDOWS

Windows fulfill their various functions – including thermal comfort, daylighting, UV protection, and visual experience – by controlling various transport pathways. The assembly and characteristics of different window components are designed to minimize electricity consumed by HVAC and artificial lighting, diminish UV exposure, and provide a clear view of the outdoors. These objectives are accomplished by controlling the transmission in the solar spectrum – including in the UV, visible and near-infrared, thermal radiation in the mid-infrared, as well as minimizing heat transfer through conduction and convection. As shown in Figure 6a, a typical double glazed window unit comprising two panes of glass, separated by a gap and supported by a frame, acts as an optical and thermal barrier between the outdoor ambient environment and indoor room-temperature surroundings.

Energy transport between the indoor and outdoor happens through all three modes of heat transfer – radiation, conduction and convection – all of which can be significant. Figure 6b shows different heat transfer pathways using a simplified thermal resistance network. These include the radiative transfer of solar energy and blackbody radiation emitted by the surroundings, conduction through the glass panes, filler material and frame, and convection in the fluid medium outside and within the spacer layer. Energy efficient windows are designed to maximize the thermal resistance of the window envelope to minimize heat losses and thermally decouple the indoor from outdoor. When all modes of heat transfer are well-controlled, thermal comfort is maximized and energy costs for building HVAC are minimized. This section looks at each of the above mentioned transport mechanisms and how they can be tuned to achieve the desired window performance.

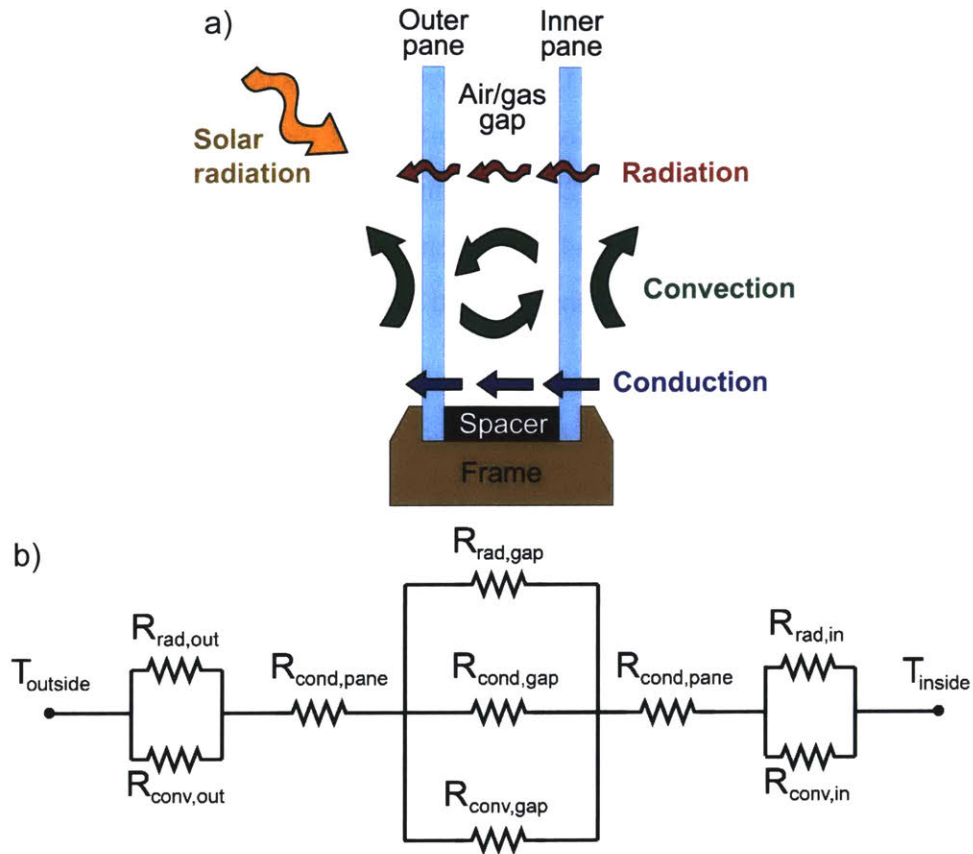


Figure 6. (a) Diagram showing different thermal transport contributions for a typical double-pane window. (b) Simplified thermal resistance network showing the interaction of different heat transfer pathways.³⁰

2.3.1 Radiation

Radiative transfer is the primary mode of optical and thermal transport, and is central to the purpose of a window. Depending on the window configuration and climate, radiation is potentially the dominant heat transfer mechanism, and is consequently the focus of most strategies used to control heat transfer.

Radiative transport through a window is regulated by altering the spectral transmittance of the center-of-glazing. Figure 7 presents the different wavelength-dependent factors that need to be considered to achieve optimal radiative control. First and foremost, a glazing unit needs to be transparent in the visible wavelengths (400-700 nm) that provides daylighting and clear visual access. This not only necessitates a relatively high visible transmittance (typically 0.5-0.9)⁵ to reduce electric lighting costs, but also requires a relatively uniform transmittance in the visible spectral band – where the human eye is sensitive – to minimize coloration of transmitted light and haziness.^{31,32} In addition to controlling radiation at visible wavelengths, windows also need to

control solar radiation in other wavelength bands as well, including UV and near-infrared (near-IR). The ozone layer blocks 97-99% of the UV radiation, which is comprised of UVA, UVB and UVC radiation. This includes practically all of the harmful UVC radiation (100-280 nm) and most of the skin-burn-causing UVB radiation (280-315 nm) radiation (which is blocked by glass). However, 50% of the UVA radiation (315-400 nm) can still be transmitted through windows (if not blocked using coatings or chemical absorbers) and can cause material degradation as well as skin ailments upon long exposure.³³

While UV is confined to a narrow spectral region, the near-IR (0.7-3 μm) comprises the largest spectral range of incoming solar radiation and is an important regime for thermal management and energy efficiency of windows. In order to reduce the cooling load in a warm climate, it is desirable to reject all near-IR solar radiation. Similarly, in order to reduce the heating load in a cold climate, it is desirable to allow near-IR solar radiation transmission. Finally, in order to thermally insulate the indoor environment and minimize radiation transfer between room-temperature objects and ambient-temperature outdoors, most-energy efficient windows are made reflecting in the mid-IR wavelength range (3-40 μm).

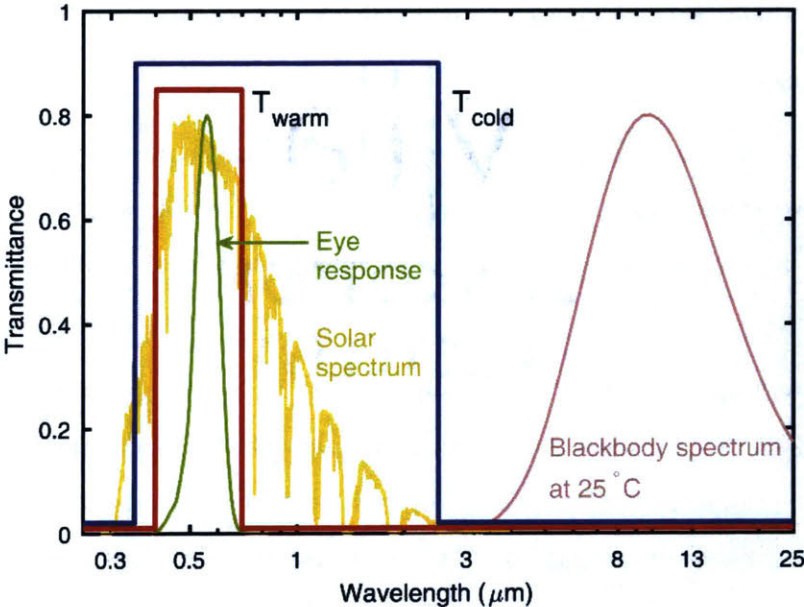


Figure 7. Ideal spectral transmittance for glazings in warm and cold climates.^{34,35} Spectral distribution of human eye response, solar spectrum and blackbody radiation at 25 °C also shown for reference.

The desired radiative properties of glazing systems, described above, are typically achieved using spectrally-selective coatings applied on one or multiple clear glass panes (that are transparent in the visible and near-IR and emissive in mid-IR). Figure 8 plots the variation in SHGC and U-values when glazing surface emissivity and solar transmittance is varied – typically achieved using low-e coatings and tints (discussed in detail in Section 2.4.2).⁵ While the infrared emissivity dictates the heat transfer between indoor and outdoor – a lower ϵ resulting in a lower U-value, the solar transmittance determines the SHGC – a lower T_{sol} resulting in a lower SHGC. Even though we vary the surface emissivity and glass transmittance independently in this analysis, in reality glazing treatments (including varying number of layers, type of glass, tints, and low-e coatings) will vary both these properties simultaneously and affect the U-value as well as SHGC. The results shown in Figure 8 provide a range of expected performance variation for different configurations. The ultimate choice of glazing depends upon the climate and a wide range of practical considerations including durability, weight, and cost.

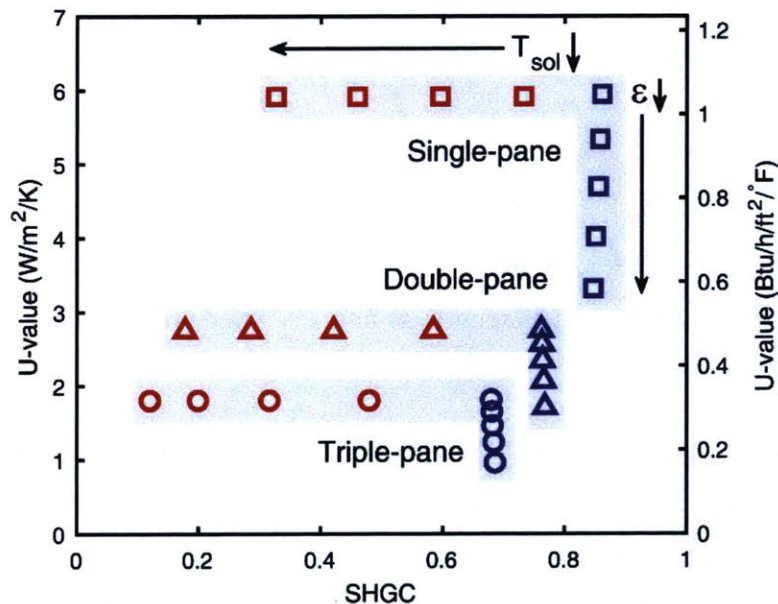


Figure 8. Plot showing the effect of changing center-of-glazing emissivity and solar transmittance on the U-value and Solar Heat Gain Coefficient (SHGC) of single-, double- and triple-pane windows. The blue symbols represent the effect of low-e coatings – when the emissivity of the inner surfaces of glazings (surface #2 for single-pane, surface #3 for double-pane and surfaces #3 and #5 for triple-pane) change to 0.85, 0.65, 0.45, 0.25 and 0.05 (top to bottom). The red symbols represent the effect of glazing solar transmittance (T_{sol} , assumed equal to T_{vis} for this analysis) changing to 0.65, 0.45, 0.25 and 0.05 (right to left). WINDOW 7³⁶ was used to model the performance, assuming standard NFRC 100-2010 environmental conditions, generic clear glass panes and air-filled gaps; all parameters other than those mentioned above were unchanged.

2.3.2 Conduction

Once the radiative transport is regulated using the strategies described above, conduction becomes the dominant heat loss mechanism in a window. Heat conduction pathways include heat transfer through the center-of-glazing, spacers, and frame. The thermal resistance of these elements is often in parallel with each other, making it crucial to minimize the conductance of all elements proportionally to prevent thermal shorts through the window.

The primary method of minimizing heat transfer through the center-of-glazing relies on the use of low-thermal conductivity gas fills. This is primarily because glass panes offer low conduction resistance in comparison to an air gap – the thermal conductivity of glass is about 40× that of stagnant air – so there is little benefit of increasing glass thickness which adds weight and cost without thermal benefit. Figure 9 shows the effect of thermal conductivity of the gap layer on the center-of-glazing U-value for a window for different mid-IR emissivity. We note that the effect of thermal conductance of the fill layer is more pronounced when low-e coatings are used, which increases the relative contribution of conduction in comparison to radiation. Furthermore, the reduction in U-value is the greatest at sufficiently-low gap thermal conductance which can be achieved by evacuating the cavity or using super-insulating fillers such as aerogel (see Section 2.4.4). While the plot shows U-value at a fixed thickness for simplicity, the optimal gap spacing varies for different gases with different thermal conductivity and viscosity to minimize convective currents (discussed in Section 2.4.1). In the extreme case, the gas fill and corresponding conductive transport is almost entirely eliminated by using vacuum-insulated units that maintain a gap spacing as small as practically possible.

Window spacers and frames are essential elements of a glazing unit that maintain a fixed gap spacing between glass panes and hold the insulated glass unit (IGU) assembly in place, and also impact the thermal performance. While spacers between two panes may serve several purposes including accommodating temperature- and pressure-induced stresses and serving as a gas and moisture barrier, from a heat transfer perspective it serves as a thermal bridge which ideally reduces the overall U-value of the IGU to below its center-of-glazing value. The two primary strategies to minimize this heat loss include: (1) using spacer materials that are thermally less conductive (e.g. silicone instead of aluminum) and (2) spacer designs that reduce the effective heat transfer area by using innovative designs. These two strategies are also useful in minimizing heat

transfer through the frame through the choice of low thermal conductivity materials (such as wood and vinyl) instead of high-thermal conductivity metal frames, and using frame designs that have thermal breaks that minimize heat conduction between the IGU and its surroundings.

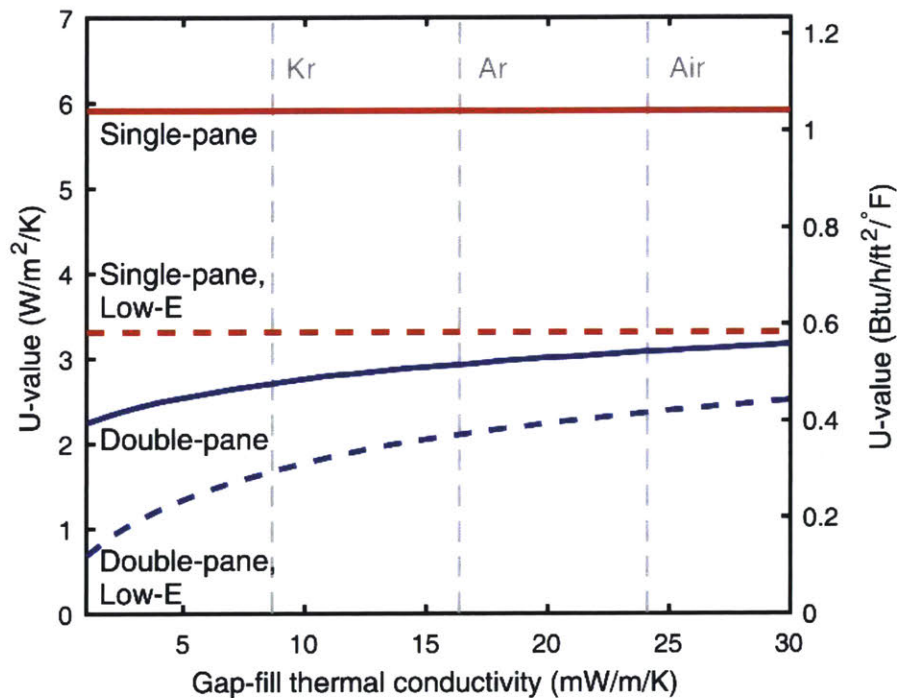


Figure 9. Plot showing how double-pane center-of-glazing U-value varies with changing thermal conductivity of the fill layer (thickness = 12 mm), with and without low-e coating ($\epsilon = 0.05$) on internal surface of the inner pane (surface #3). The U-values for single-pane window, as well as thermal conductivity of air, argon and krypton are also shown for reference. WINDOW 7³⁶ was used for this analysis, assuming standard NFRC 100-2010 environmental conditions and generic clear glass panes.

2.3.3 Convection

Convective transport is not only responsible for heat transfer from the outside ambient indoor and indoor room environment, but also for heat transfer within enclosed IGUs. While the outdoor and indoor convective heat transfer coefficients depend on surrounding temperature and wind velocity, the natural convection within the window cavity is dependent on the window geometry, fill properties, and temperature difference. While an optimal gas-filled IGU is designed to operate in the conduction regime where there are no convection currents and heat loss is minimum, that is sometimes not the case when the Rayleigh number, a dimensionless number associated with buoyancy-driven flow, is above a critical value.³⁷⁻³⁹ Specifically, for a given fill gas, when the gap thickness is large and/or the temperature gradient between two panes becomes large, secondary

flow patterns emerge that transition the heat transfer from a conduction-dominant regime to multicellular flow regime corresponding to a higher average Nusselt number. It has been shown that the velocity profile due to natural convection within a window not only depends on the aspect ratio of the window and boundary temperature, but also the fill gas properties and the number of panes in the window.⁴⁰

2.4 WINDOW TECHNOLOGIES & DESIGNS

Design strategies and technologies used in transparent energy efficient window products must address a wide range of challenges associated with the complex thermal transport while still remaining visually clear. This has led to much interest in the research and development fields on advancing all aspects of window performance as much as possible. Here we provide an overview of prior works and ongoing works to improve various elements of windows for transparent, energy efficient products.

The primary focus of energy-efficient window development has targeted the center-of-glazing. By area, the center-of-glazing represents the most dominant part of the window and, therefore, also has the most influence on total window performance. Many strategies for controlling these properties are required to meet the diverse needs of windows. The assembly and characteristics of different window components are designed to minimize electricity consumed by HVAC and artificial lighting, diminish UV exposure, and provide a clear view of the outdoors. These objectives are accomplished by controlling the transmission in the solar spectrum – including in the UV, visible and near-infrared, thermal radiation in the mid-infrared, as well as minimizing heat transfer through conduction and convection. When all modes of heat transfer are well-controlled, thermal comfort is maximized and energy costs for building HVAC are minimized.

Design strategies and technologies used in transparent energy efficient window products must address a wide range of challenges associated with the complex thermal transport while still remaining visually clear. The primary focus of window development has targeted the center-of-glazing, which is the dominant window element for performance. Traditional center-of-glazing elements are transparent, affordable, and ubiquitous, requiring research efforts to at least match their performance to be competitive.

However, the necessity of being visibly clear means that the array of materials available for good energy performance is limited. In particular, the traditional elements require high energy

intensity for manufacturing, highly-processed materials and structures, as well as high volumes. Even high-performance windows often times come with greenhouse gas (GHG) and lifecycle challenges that make them the less-sustainable choice.⁴¹ This is why windows represent the second highest embodied energy of a residential building, despite the fact that windows often represent less than 15% of total wall area.⁴² Here we present and evaluate the technical approach and sustainability challenges associated with energy efficient glazings.

2.4.1 Gas-Fills

The first insulated glass units relied on an air gap to provide insulation between panes due to its ubiquity and relatively low thermal conductivity (approximately 0.026 W/mK at room temperature and pressure).⁴³ However, with the advent of low-e coatings for radiation control and overall better performing window systems, conduction and natural convection within the gaps of multi-pane windows has become a dominant mode of heat transfer. This has led to the use of more exotic gases within IGU layers.

The most common gas used is argon, but krypton and xenon are also used in high performance windows for their low thermal conductivities.⁵ Mixtures of air and various noble gases are also used to optimize the cost and performance. To balance the trade-off between convection and conduction, each gas will have a different optimum gap thickness in order to achieve the lowest total U-factor. This leads to a variety of window thicknesses and sealing strategies depending on the amount and type of gas or gas mixture used in the gap.

Table 2. Comparison of common gas-fills and their associated design properties for increased center-of-glazing thermal performance for use with plain glass (no coatings).^{43,44}

Gas	Thermal Conductivity	Gap Thickness	GHG emissions
Air	26 mW/m ² K	20 mm	-
Argon	18 mW/m ² K	16 mm	95 kg
Krypton	9.5 mW/m ² K	12 mm	210 kg
Xenon	5.5 mW/m ² K	8 mm	1100 kg

While gas-fills offer an easily-adapted insulating strategy, the limitations on thickness and the high cost of embodied energy quickly reduce the GHG savings. For example, krypton is twice as insulating as argon, yet the ideal gap thickness combined with a much larger embodied energy

means that in application krypton windows result in more GHG emissions than argon windows. If we also consider the ubiquity of argon is 1000 times higher, it becomes clear that the limitations of gas-fills are very real. Other gases have trouble with degradation of the glazing, sealing issues, or cost. Industry has chosen to stay with dry air and argon, and this has yielded the most affordable and sustainable products to-date.

2.4.2 Low Emissivity Coatings

Emissivity controlling films and coatings are the most ubiquitous materials used in windows besides glass panes. These low emissivity (low-e) coating suppress the radiative heat transfer between a window pane and its surroundings by reflecting the incident infrared radiation. Typically, the low-e coating is applied on the inside surface of the outer pane in a double pane window. The low-e material is typically applied to a window pane as a multi-layer coating by chemical vapor deposition (CVD), magnetron sputtering, or a self-applicable adhesive film. The common composition of the low-e coating includes transparent conducting oxides (TCOs), such as indium tin oxide (ITO) and fluorine-doped tin oxide (FTO), and ultrathin metal (silver, copper, and gold) sandwiched between dielectric layers.⁴⁵⁻⁴⁷ The TCO coating is usually incorporated in the glass making process and referred to as a hard coating. Ultrathin metal coating is applied after the glass is hardened and hence referred to as a soft coating. While soft coatings usually have higher performance, hard coatings are more robust in terms of mechanical strength. However, both of these coating types have already achieved very low emissivity values (~ 0.01) and further reducing the emissivity only has a small marginal benefit.

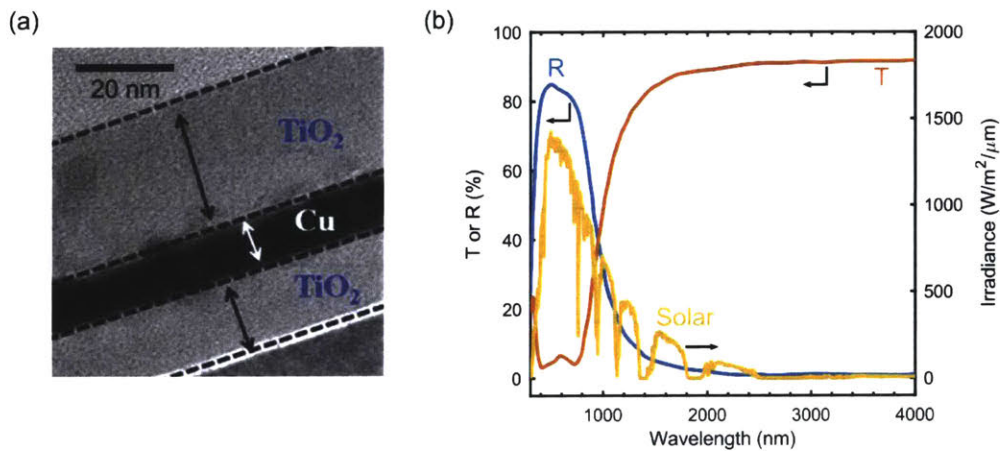


Figure 10. (a) Cross-sectional high resolution TEM of a TiO₂/Cu/TiO₂ low-e coating.⁴⁶ (b) Transmittance and reflectance spectrum of an AlN/Ag/AlN low-e coating with high visible transmittance (82%) and low infrared emittance (8%).⁴⁸

When considering the sustainability of such coatings, it is important to consider the impact of processing and lifetime performance. Hard coatings often require more upfront processing energy, such as Pilkington's pyrolytic coatings that cure in excess of 400°C, but have higher stability and longer lifetimes.⁴⁹ Comparatively, the thinner and more delicate soft coatings can degrade with exposure to environmental conditions. These soft coatings often have to be sealed in a full window within 6 months of initial fabrication, or efficacy will be greatly reduced. This often leads to hard coatings employed for commercial buildings, where size and lifetime limitations outweigh upfront costs compared to soft coatings. In residential buildings where window areas are smaller and performance is dominated by framing elements, soft coatings are more economically favorable. With either coating, it has been found that for the majority of applications only a single coated surface leads to the greatest gain of sustainability.⁵⁰ Additional coatings provide thermal comfort but the added cost, energy to produce, and diminished returns leave the GHG higher than the single-coated counterparts.

2.4.3 Vacuum Insulated Glazings

Vacuum Insulated Glazings (VIGs) use a reduced-pressure air gap (typically 0.1MPa or lower) to drastically reduce conduction and convection in the center-of-glazing element. When combined with radiation control, these windows can have U-factors that are an order of magnitude lower than traditional double and triple pane windows.⁵¹

However, there are many challenges to achieving this performance in a full, durable window design. The biggest challenges are the support array needed to keep the glazings separated, and the edge seal that must maintain internal pressures over the window lifetime.⁵² Current research focuses on making the spacer arrays less visible than traditional metal elements while still maintaining robust mechanical performance.⁵³ Other groups have looked at using individually sealed glass tubes to mitigate seal failure.⁵⁴ However, most of the advancements in this area are being done in the commercial sector, particularly focused on developing better edge seals and advancing spacer arrays to support large area windows.

The largest sustainability challenge with VIGs rests on their very short lifetimes, and limited areas. The complexity of sealing glass at a low pressure requires a nearly perfect, high cost process. More than 25 years of development on VIGs have yet to result in a guarantee that even at small scale these seals will last more than 5 years. The resultant windows suffer from a cost 10 times

higher than comparable triple-panes, and with a greatly reduced lifetime. Cost-prohibitive adoption aside, these windows cannot recoup the energy and materials costs embodied in the end-product.

2.4.4 Transparent Aerogels

Aerogels are a unique class of highly nanoporous materials that can have a variety interesting properties based on the composition and structure of their solid backbones.⁵⁵ In particular, silica aerogel has been of interest as a super-insulating material for windows due to its high solar and visible transmittance as well as its low thermal conductivity (Figure 11a and b).⁵⁶⁻⁶¹ Additionally, the use of ultra-low conductivity solids to replace traditional air gaps also enables these windows to utilize reduced pressure to increase performance even further.⁵⁹ In fact, several commercial products exist that utilize granular aerogel infused windows for diffuse lighting (Figure 11c).^{62,63}

However, prior works fail to achieve high enough transparency to be integrated into a window design that can optically compare to traditional window products.⁶⁴⁻⁶⁷ Several variations of translucent silica aerogel windows have been proposed.^{60,68-70 71} For example, Duer and Svendsen proposed a sealed double pane aerogel window featuring a monolith, which featured very low thermal conductivity but could only achieve up to 74% visible transparency.⁶⁸ Similarly, Wittwer reports optical transparency of 77% and indicates that it is more practical to focus on granular windows for such translucent aerogels.⁶⁹ While some later works have achieved higher transparency, such as Venkateswara Rao et al⁷² (85%), the limitations of optical performance have been a barrier to truly transparent windows ($T > 90\%$).

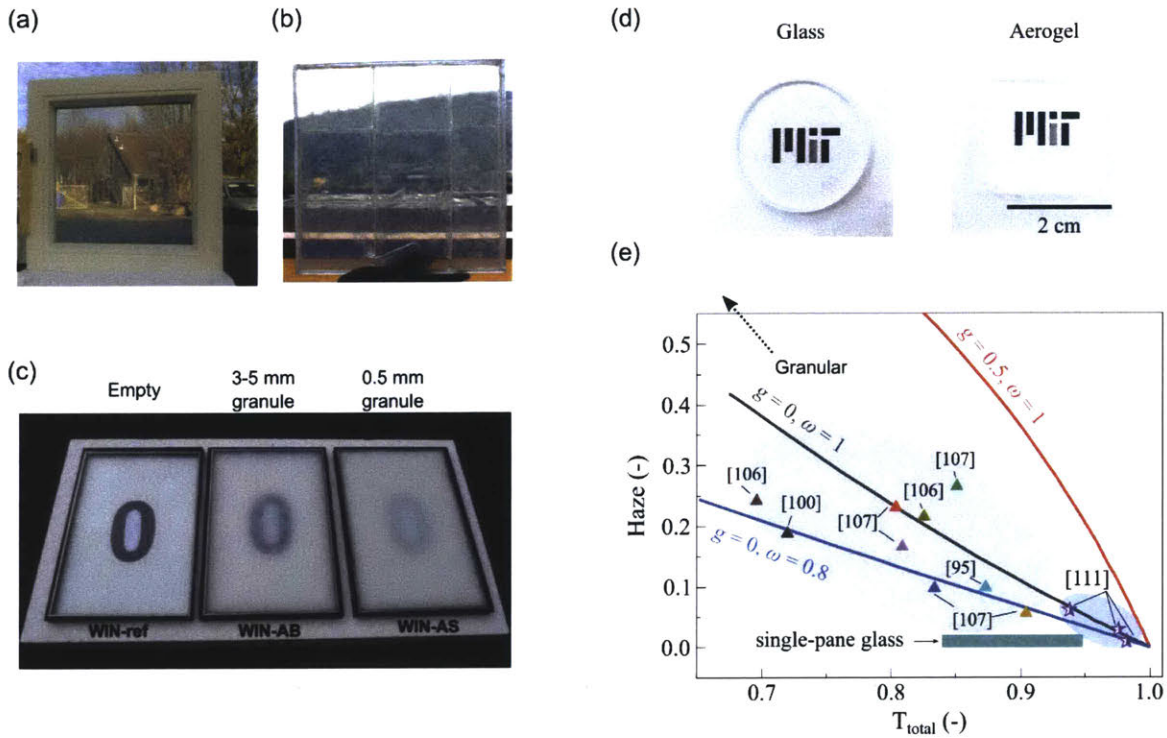


Figure 11. (a) An evacuated monolithic aerogel glazing in a well-insulated frame. The view through shows no distortion of the image but a slightly haziness can be observed. **(b)** Tiled monolithic aerogel glazing sandwiched between two glass panes. **(c)** Double pane window units filled with granular aerogel: (left) empty reference, (middle) 3-5 mm granular particle, (right) 0.5 mm granular particle. **(d)** High-transparency aerogel sample in comparison with a single pane glass. **(e)** Haze and total visible transmittance of transparent monolithic aerogel samples previously reported. Solid lines are the model predictions for different scattering asymmetric factor g (0, isotropic; >0 , forward) and single scattering albedo ω (1, pure scattering; <1 , including absorption). Performance of a single-pane glass is indicated by the green shaded area. Granular samples have much lower transmittance and haze, hence are out of the plotted range. Figures reproduced with permission: (a) from [59], (b) from [60], (c) from [63], and (d, e) from [73].

Other nanoporous materials are also being studied and developed for incorporation into high-performance glazing, such as hybrid structures and polymer aerogel-like materials.^{74,75} However, these materials often face challenges in achieving low thermal conductivity due to high solid backbone heat conduction, and/or undesirable optical effects (often scattering that creates a hazy appearance) caused by mesoporous feature sizes. These materials have not yet demonstrated acceptable performance at lab-scale, and therefore their feasibility for mass production is still unknown.

2.5 SUMMARY

Windows are the primary source of energy loss in building envelopes. In this chapter, we compared the thermal performance of existing and state-of-the-art window technologies by using industry-established figures of merit for quantifying window performance in a variety of climates and applications:

- U-factor: measure of thermal transfer through material(s) normalized by envelope area and temperature difference.
- Condensation Resistance (CR): measure of the area-averaged resistance to condensation forming on a window or window system used to quantify localized temperature peaks.
- Solar Heat Gain Coefficient (SHGC): measure of the fraction of solar energy that enters a building through a window or window system through direct transmission or absorption and re-emission.
- Visible Transmittance (VT): measure of the fraction of total solar light within the visible spectrum that is transmitted through a window or window system.

We provide an overview of the heat transport mechanisms that include radiation in different wavelength ranges, conduction through the center-of-glass, and convection outside and inside the window panes. We discuss designs and technologies that address radiative, convective, and/or conductive heat transfer using a variety of approaches, such as glass coatings, active transmittance control, noble gas fills, and the current role of silica aerogels.

The center-of-glazing of windows is the key element for optimal optical and thermal properties, but many strategies are required to meet the diverse needs of windows. Therefore, coating technologies are being developed to tailor the radiative properties of windows. However, the selection of windows will always require a combination of strategies in order to meet the optimal price and performance balance. Successful application of window designs requires an in-depth understanding of both fundamental heat transfer and the needs of our buildings. The state-of-the-art windows reviewed here all focus on bringing the next level of thermal performance to our buildings to solve our needs, but it is the cost-effective and scalable solutions that will truly have the largest impact on our building energy consumption and occupant comfort.

3. Achieving Transparent Aerogels

Silica aerogel has a history dating back to its discovery in 1931 by Dr. Samuel Stephens Kistler. Since then, this class of nanoporous glass has been studied extensively and applied in many uses, ranging from the collection of comet dust in space, to radiators for detector systems in fundamental physics experiments, to pipe insulation in harsh environments.⁷⁶ It is the highly porous, interconnected particle structure that allows silica aerogel to have a unique blend of properties such as ultra-low thermal conductivity (15 mW/mK), high solar transmittance (>90%), low density (~50-250 kg/m³), and thermal stability (up to 800 °C). This has led to extensive prior works to study the synthesis, structure, and properties, particularly the optical and thermal transport through the material.⁷⁷

Despite this development and study by many, application as a truly transparent insulator has eluded aerogel because of the limitations on visual performance. Silica aerogels are super-insulating, lightweight, thermally stable, highly-functional materials, but without transparency their cost-effectiveness has limited application to niche areas. It is the promised combination of super-insulating and high-clarity that has made silica aerogels an area of interest in the built environment for decades. Therefore, to open up the huge potential energy impact silica aerogels could have in buildings, it is necessary to first achieve high-clarity aerogels.

3.1 FUNDAMENTAL PRINCIPLES OF TRANSPARENT AEROGELS

The process to achieve high-clarity aerogels must begin with an intimate understanding of the aerogel structure and the propagation of light, particularly visible light, through the bulk material. Figure 12 shows the full optical spectrum of a silica aerogel sample (4 mm thick) compared to the AM1.5 solar spectrum. From prior works of the structural and optical properties, the propagation of electromagnetic radiation through can be divided into two distinct loss regimes.^{19,78,79} For wavelengths larger than 1000 nm, absorption is the dominant transmission loss mechanism. Absorption occurs when an incident photon is absorbed and its energy is converted to another form, often to heat.⁸⁰ in the wavelength range of 250-1000 nm, the dominate loss mechanism is caused by isotropic scattering. Light scattering is the mechanism by which a path of light is affected by a change in refractive index.⁸¹ In an aerogel, this is caused by the difference in the

index of refraction between the silica particles and the pores. At smaller wavelengths, as the average distance between interfaces (particle backbone and void interfaces) becomes closer in size to the propagating wavelength, the intensity of scattering increases. In traditional aerogels, this scattering leads to a bluish coloration (similar to atmospheric scattering that causes a blue sky) with an intensity that is approximately proportional to pore size.

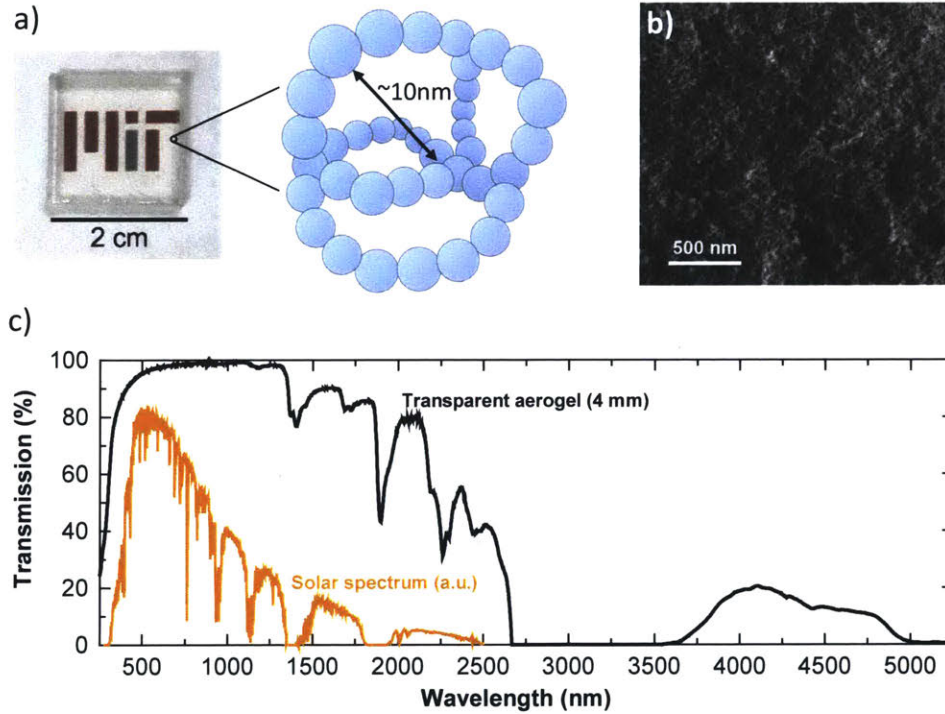


Figure 12: a) Image and structural representation of an optically transparent silica aerogel fabricated with solar transparency >97%. Small primary silica particles (<1 nm diameter) aggregate together to form larger secondary silica particles (~2 nm diameter). These secondary particles bond together to form an interconnected necklace structure that supports a highly mesoporous network. b) SEM image showing the interconnected structure. Pore sizes vary greatly in the material, but mean pore size is ~10 nm. c) Transmission spectra of a 4 mm transparent aerogel sample compared to the AM1.5 solar spectrum.

This transport of light through the aerogel as a participating medium can be described via the 1-D Radiative Transfer Equation. In this model, the aerogel is treated as a homogeneous absorbing and scattering medium, allowing us to use the 1-D azimuthal symmetric Radiative Transfer Equation to describe the radiation intensity as a function of polar angle and spatial position⁸²

$$\mu \frac{\partial I_{\lambda}(\xi_{\lambda}, \mu)}{\partial \xi_{\lambda}} = -I_{\lambda}(\xi_{\lambda}, \mu) + \frac{\omega_{\lambda}}{2} \int_{-1}^1 I_{\lambda}(\xi_{\lambda}, \mu') d\mu' \quad (1)$$

where $\mu = \cos(\theta)$ is the cosine of the polar angle with respect to the incident direction. $\xi = \beta x$ is the optical depth where β_λ is the extinction coefficient and x is the spatial coordinate along the incident direction ($0 < x < t$, t is the sample thickness). ω is the scattering albedo ($0 < \omega < 1$). Wavelength dependent quantities are indicated by subscript λ in Eq. (1).

This modeling approach provides a quantitative measure of the likelihood that an incident photon is scattered, described by the intrinsic property known as the scattering coefficient, σ_s .¹⁹ Similarly, during the same calculation the absorption coefficient, σ_a , can be found. The following relationships can be used to calculate these optical coefficients as

$$\begin{aligned}\sigma_a &= (1 - \omega)\beta \\ \sigma_s &= \omega\beta\end{aligned}$$

By characterizing the scattering and absorption coefficients, density, and thickness of the aerogel, the effective optical scattering radius can be calculated and used to describe the optical scattering of the material.¹⁹ Using the Rayleigh scattering model, a monodisperse effective scattering diameter can be defined which represents a structure with equivalent transparency behavior of the aerogel, defined as

$$d = \sqrt[3]{\frac{10^{b-9}}{4\pi^4 \frac{\rho_{ap}}{\rho_{SiO_2}} \left(\frac{n^2-1}{n^2+2}\right)^2}} \quad (2)$$

where b is a data fitting parameter from the scattering coefficient over 250-1000 nm, ρ_{ap} and ρ_{SiO_2} are the apparent density of the aerogel and the density of the silica, respectively, and n is the refractive index of silica.¹⁹ From this equation, we find that the scattering coefficient has a cubic dependence on the average chord length between the silica backbone and void interfaces. This means that high transparency aerogel that require low scattering losses must have sufficiently small features (relative to the wavelength of interest). In prior works, pores are significantly larger than particle or particle aggregation sizes, meaning the pore size has the largest chord length and therefore the most significant contribution to transmission losses. Therefore, synthesizing aerogels with smaller pore sizes will have the largest impact on increasing aerogel clarity.

3.1.1 Silica Aerogel Synthesis

Silica aerogels are traditionally made via solution-gelation chemistry, in which a chemical reaction of a solution causes formation of a solid gel consisting of a 3-dimensional interconnected network. This solution self-assembles into a gel with a uniform porous structure supported by a sparse particle network. There are many methods of forming silica gel using a variety of chemicals and steps, but generally a silane precursor is reacted to form silica nanoparticles in a disperse network (see Figure 13).⁸³ Regardless of the gelled structure or how it was obtained, the next step is to dry the material by removing the liquid from within the voids. However, traditional drying techniques like evaporation create surface tension forces within the pore structure. The aerogel structure is weak due to the small amount of solid material, and the force of surface tension in pores at the nanometer scale (reaching MPa) can easily deform and/or destroy the structure. Because the material properties are highly dependent on pore size, even small amounts of damage to the structure can greatly affect performance. The typical structure of a dried aerogel is shown in Figure 13 via scanning electron microscope and tunneling electron microscope image.

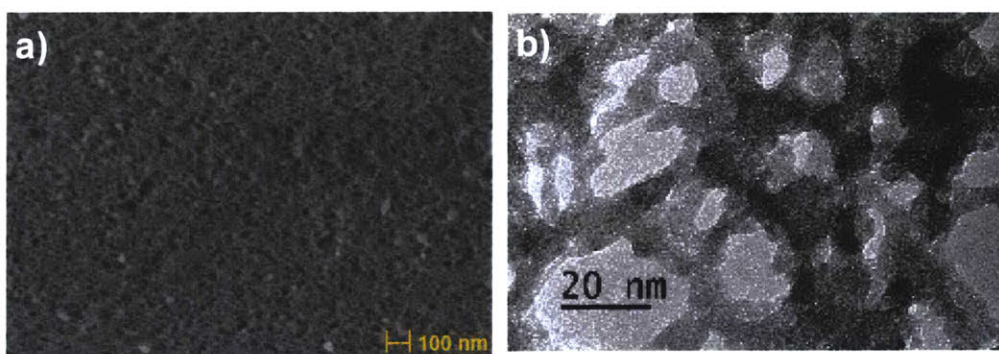


Figure 13. Scanning electron (a) and tunneling electron (b) microscopic imaging of silica aerogel. Resolution is limited by the insulating nature of silica but shows the basic structural features that form during solution-gelation.

The primary approach to dry the gel while avoiding damage to the structure is to remove the liquid inside of the pores without creating a liquid-gas interface. One method often used is freeze-drying, in which the liquid is rapidly cooled to the point of solidification and then sublimated out of the structure.⁷⁷ These are often referred to as cryogels. However, the small feature size and high thermal resistance often makes the solidification step challenging and results in a granular aerogel.

Recent works have achieved some monoliths, but only in small form-factors and with transparency < 50%.⁸⁴

The most common method used is critical point drying, in which the liquid inside the aerogel is brought above the critical point, a liquid-specific temperature and pressure above which the liquid and gas phases become indistinguishable and there is no surface tension force. Transitioning from the liquid to this critical point phase, and then from the critical point to gas phase, avoids the formation of stresses that destroy the structure. With this method, the resultant material can be virtually unchanged by the drying step. Carbon dioxide has a very favorable critical point temperature (31 °C) and has few hazards associated with its use. Methanol, ethanol, and various other liquids have also been used for critical point drying, but their cost and flammability can be prohibitive at larger scale production of samples compared to carbon dioxide.

After the solvent is extracted from the wet gels, they are fully-formed aerogels (alternatively called cryogels if freeze-dried, or ambigels/xerogels if drying is performed at or near ambient pressures). Post-synthesis treatments such as annealing or surface modifications can be used to alter the aerogels, but generally the process is complete after drying.

3.1.2 Transparent Aerogel Synthesis

Each of the steps needed to create a silica aerogel (solution-gelation, critical point drying) have a large, direct impact on the final aerogel product and its optical properties. There are many variations, combinations, and extensive prior works on how the chemicals and process used can impact the resultant aerogel properties, particularly density and spectral transmittance. Several studies have examined the effect of the sol-gel synthesis process on the final structure of aerogel¹², including investigation of different chemical precursors^{85,86}, different aging conditions⁸⁷, and varied drying conditions^{88,89} to control the pore and particle networks. Others have investigated how the variations in the structure (pore size, particle size, density) relate to variations in the properties of interest, such as optical and thermal transmission.^{16,90,17,91} Yet all of these prior works have failed to produce aerogels of high enough optical quality to meet the needs for application to transparent windows.

The achievement of high-clarity aerogel in this work was enabled by the numerous prior works and understandings developed over the best 50 years and guided by the optical model presented by *Zhao et al*^{18,19}. We began by selecting a simple one-step solution-gelation

chemistry. This had been shown by prior works in *Tabata et al*⁸⁹ and *Adachi et al*¹⁷ to have a very low index of refraction and high visible transmittance. It also offered a more direct step to achieving wet gel materials that could be dried in the same manner to reduce the amount of variables changing between batches of samples. As described above, other methods offered a greater degree of control, but subsequent steps created more opportunities for variation between batches, and the optical modeling predicted that a small change in nanostructure (0.5 nm difference in average size) would have a significant impact on the optical clarity.

We therefore chose to work with a silane precursor reaction with water, catalyzed by ammonia and diluted using methanol. After gelation the wet gels could either be dried directly using carbon dioxide critical point drying or first be put through a variety of treatments, aging, surface modifications, etc. in order to make finite, controlled changes to the nanostructure. The drying process itself could also be modified to accommodate different conditions or wet gel form factors (e.g. the difference in pressure and flow rate for a thin sheet compared to a square-like sample can be significant). The core steps of synthesis are outlined in Figure 14.

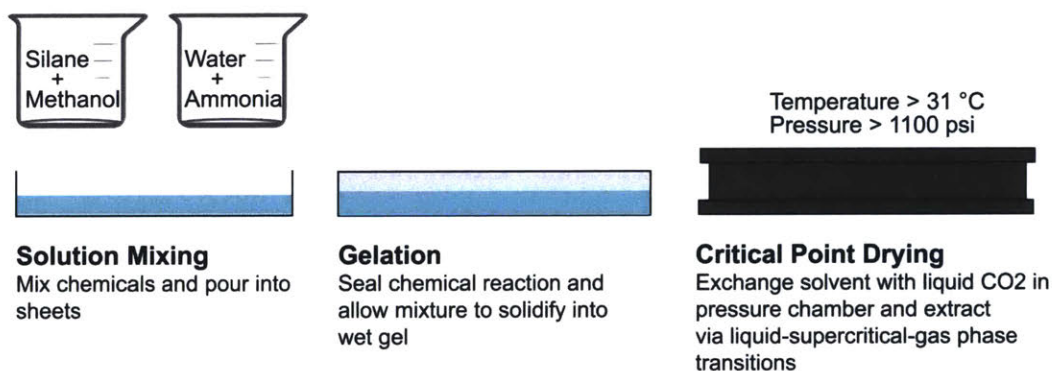


Figure 14. Aerogel production, consisting of measuring and mixing chemicals, which are then poured into sheets for gelation. These sheets form a wet gel. Finally, this wet gel is dried via critical point drying.

The method selected for synthesizing transparent aerogels within this work was done by sol-gel polymerization of a silicate precursor such as tetramethyl orthosilicate (TMOS, 131903, Sigma Aldrich) or Methyl Silicate 51 (MS-51, CAS#12002-26-5, Austin Chemical Company). An ammonia solution (NH₃, 2.0M in methanol, 341428, Sigma Aldrich) was used as a catalyst to promote both hydrolysis and condensation reactions. Reactants were diluted by methanol (MeOH, 322415, Sigma Aldrich) followed by addition of NH₃ and water. The mixing molar ratio of chemicals varied among recipes, as is discussed later in Section 3.2.2 After gelation and varied aging times (ranging from 1-14 days), the sol-gels were removed from molding containers and the

mother solvent was replaced with ethanol (EtOH, 89234-848, VWR) to be prepared for critical point drying (CPD, model 931, Tousimis) as EtOH is miscible with liquid CO₂.

Generally, this process yielded high transparency monoliths (visible transmittance > 94%) that exceeds prior works (see Figure 15). However, the fragile nature of silica aerogel monoliths makes them easy to damage, break, or scuff, which often results in inaccuracies when measuring visible transmittance. This proved a significant challenge to refining the optical clarity if we relied only on measurements from a spectrophotometer. Additionally, misalignment during measurements and changes to lab conditions (such as humidity) also caused changes to the optical properties that were not a result of changes to the recipe or synthesis process. Efficient optimization of the transparent aerogel recipe therefore requires a more fundamental understanding of the structural features.

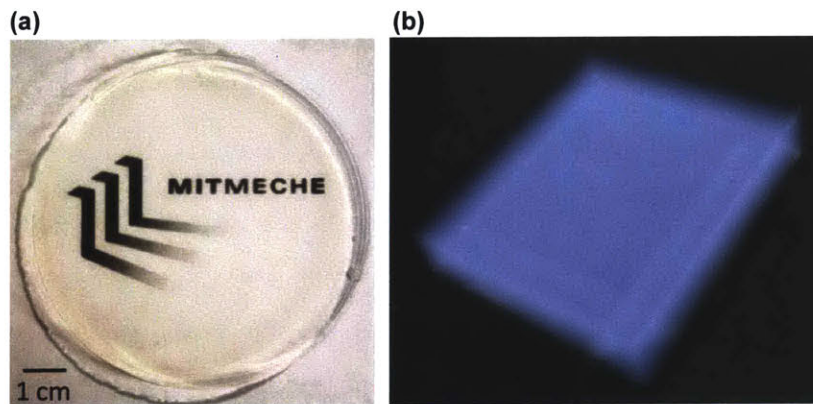


Figure 15. (a) Highly transparent monolithic silica aerogel sample fabricated in the Device Research Laboratory. (b) Image of commercially available silica aerogel.⁹²

We knew from the requirements of the window application space that we needed to achieve higher transparency (~98%), and we also knew from the model presented in *Zhao et al*^{18,19} that this required smaller feature sizes within the nanostructure. But without a clear understanding of how the nanostructure was changing between samples it was challenging to identify which factors within the aerogel synthesis were improving the optical clarity, let alone to what degree. We therefore needed to develop an understanding of the relationship between synthesis, resultant structure, and visible performance before we could methodically optimize the aerogel for application.

3.2 STRUCTURAL CHARACTERIZATION OF TRANSPARENT AND INSULATING AEROGELS

The ultra-nanoporous structure of silica aerogel enables both low thermal conductivity and high transparency, but achieving transparency comparable to glass while maintaining super-insulating properties is not trivial. The aerogel structure consists of a cross-linked silica particle backbone supporting a highly mesoporous (2-50 nm) network comprised of aggregated particles.^{12,13} These small feature sizes of the particles and pores allow the transmission of visible; the only barrier to transmission through the structure is the refractive index difference between the aerogel backbone (silica particles) and air. However by fabricating aerogels with very small pore and particle sizes (less than 10 nm diameter average), almost all of the visible spectrum can be transmitted.¹⁶⁻¹⁹ Prior works have already established a strong correlation between the average structural scattering size (often approximated as an effective pore diameter) and both visible transmittance and haze.^{18,78}

3.2.1 Small Angle X-ray Scattering of Aerogels

To accurately and repeatedly probe the structure of the transparent aerogels, we chose to use a well-understood and non-destructive method called small angle x-ray scattering (SAXS). Small angle scattering is the use of either neutrons or electrons to probe small feature sizes within a material via deflection of a collimated source. While each source type (neutrons or electrons) can operate over range of conditions, the principles of scattering and data processing are similar.⁹³ For study of our transparent silica aerogel, small angle x-ray scattering (SAXS) was used to investigate the nanometer-scale porous structure. A Cu-k-alpha x-ray source was used to direct highly collimated electrons at a thin (2-10 mm) sample of aerogel. The electrons were scattered by the sample and a photon detector collected a 2D pattern of the forward-scattered electrons over an optimized duration of time. The x-y position of each scattered photon that is collected on the detector is related to the scattering angle by the sample-to-detector distance via the scattering vector, which is defined as

$$Q = \frac{4\pi}{\lambda} \sin(\theta) \quad (3)$$

The number of photons collected at a particular detector position is related to the relative frequency of occurrence of a particular material feature length.⁹⁴ Because aerogel is isotropic, we

see that the scattering vector does not vary circumferentially and we can integrate the data at each radius to further reduce data noise. We can plot this integrated photon intensity vs the scattering vector as shown in Figure 16 to obtain the key SAXS plot that allows for analysis of the structure.⁹⁵

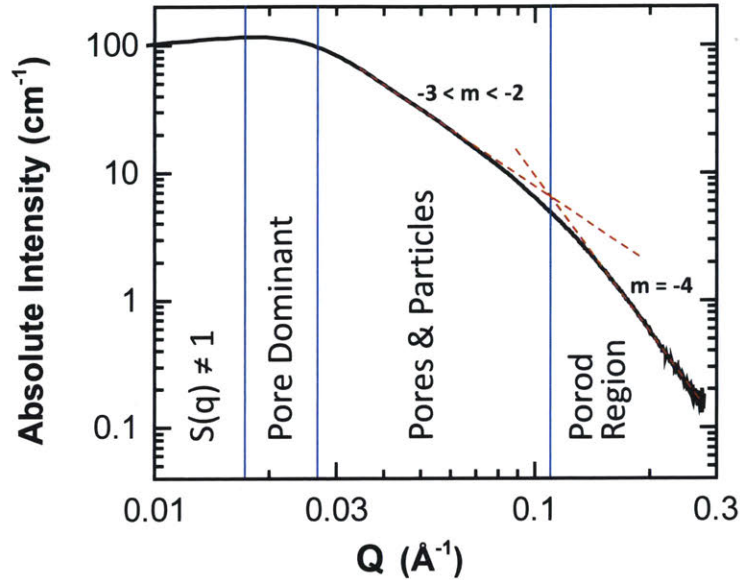


Figure 16: Typical silica aerogel scattering pattern. By assuming spherical, disperse scatters we can make approximations about pore and particle sizes, as well as the interconnectivity of the structural network.

As seen graphically in Figure 16 we can separate the intensity, I , into its components in the form of

$$I(Q) = (\rho_p - \rho_s)^2 \phi_p V_p P(Q) S(Q) \quad (4)$$

where $\rho_p - \rho_s$ is the difference in density of the scatterers and the medium, ϕ_p is the concentration of scatters, V_p is the shape of the scatterer/scattering center, P is the form factor, and S is the structure factor. The difference in densities, or scattering length density, represents the refractive index difference of the pores and particles related to how the x-rays are scattered. Because this quantity is a difference, the scattering intensity will be the same whether the scatterers are solids in a void, or voids in a solid. This equivalent scattering behavior is known as Babinet's principle and is important for understanding the combined effects of particle and pore scattering in silica aerogel.⁹⁴ The form factor is the distribution of scattering length sizes as a function of Q . This part of I is key to understanding pore and particle size distributions and interactions. Finally, the structure factor is a complex underlying contribution based on the interactions of the scatterers at each value of Q . However, S is often simplified to 1 to represent dilute, non-interacting particles.

By using this assumption for a restricted Q range, we can use a spherical scattering model to relate the form function, $P(Q)$, to effective scattering radii in order to simplify many complex or unknown factors.

There are several regions of interest in Figure 16 to consider when understanding all the complexities of the aerogel structure. However, the most influential factor on optical performance is the effective scattering size within the nanostructure, which can also be described as the average scattering length and variance of the particle and pore networks. This scattering distribution can be found using many methods, but the most common assumption is to use a spherical scatterer model to relate $I(Q)$ to $P(Q)$ via a numerical method such as curve fitting (SasView⁹⁶ software) or Monte Carlo iteration (MCSAS software⁹⁷). Figure 17 shows two sample aerogels of different structure with scattering size distributions and scanning electron microscopy images for comparison.

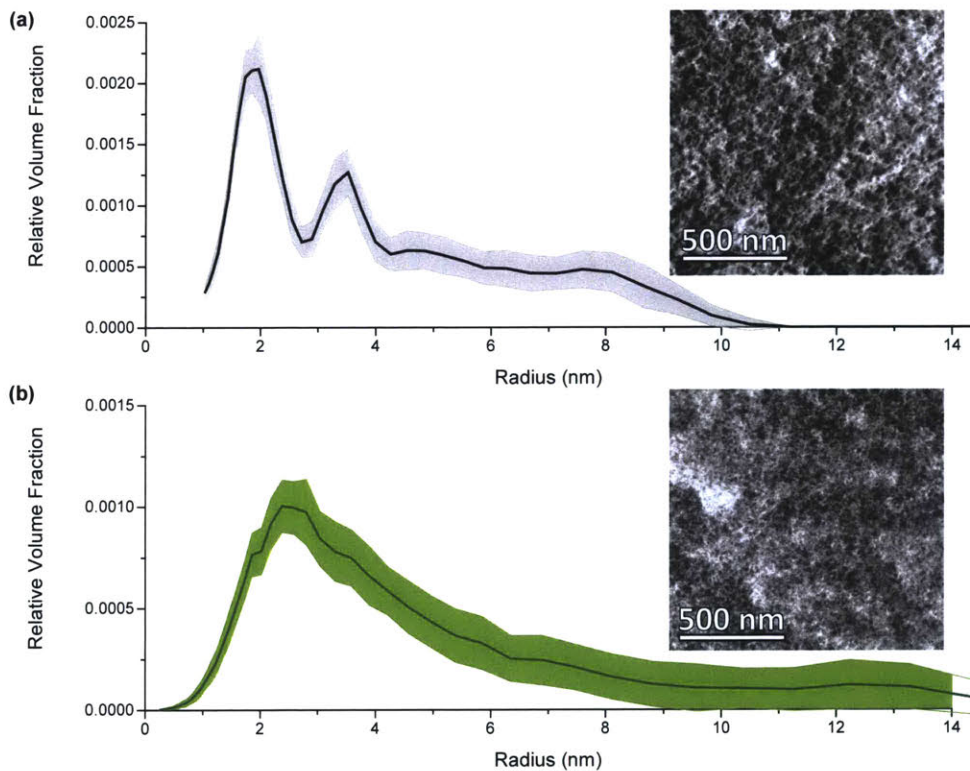


Figure 17: Effective scattering size (representing scattering from both pore and particles) and SEM images of silica aerogel. (a) Highly transparent (>96%) TMOS aerogel with a density of 220 kg/m³. (b) MS-51 aerogel with a density of 75 kg/m³.

3.2.2 Optical Performance Relation to Structural Features

The average scattering size can be used to relate the structural features within the aerogel to the optical performance, particularly the transmittance and haze. This provides a quantifiable way to measure and systematically increase the optical performance of the aerogel.

Optical properties in the visible spectrum were calculated from total hemispherical reflection and transmission data measured through the center of the samples. These measurements were performed on an Agilent Cary 5000 UV-Vis-NIR spectrophotometer on wavelengths from 250-2500 nm using a polytetrafluoroethylene coated integrating sphere (Internal DRA-2500, Agilent). After measurements, transmittance was averaged over the visible spectrum (380-780nm) and normalized by thickness (measured on a micrometer) using the method described in *Zhao et al*¹⁹. To calculate haze, we used the formal definition of haze as

$$Haze = \frac{T_{diffuse}}{T_{total}} \quad (5)$$

where T_{total} and $T_{diffuse}$ represent the total hemispherical transmittance and the diffuse component of the total hemispherical transmittance, respectively. By averaging haze over the visible spectrum, we can obtain a single representative haze value for the aerogel.

This average haze and average total transmittance can be predicted independently from the optical measurement by using the effective scattering size. If we assume that the scattering length within the aerogel is equivalent to a set of monodisperse spheres of the same diameter as the chord length, we can use the scattering size and density of the aerogels in the model presented in *Zhao et al*^{18,19} to predict the transmittance and haze. Figure 18 shows that the model agrees well with experimental results from the optical measurements. We see that while generally the model over-predicts optical performance (over predicting visible transmittance and under predicting haze) it does follow the general trends; haze increases more with increased scattering size, and generally increased transmittance also yields lower haze. This validates the use of SAXS and effective scattering size to predict the optical performance based on the nanostructure only. Additional factors such as surface defects, contaminants, or cracks will not be quantified by the effective scattering size, but those defects are also independent of the fundamental and repeatable steps within the synthesis process. Therefore, scattering size is a more repeatable and precise way to predict optical performance and guide optimization of the aerogel synthesis.

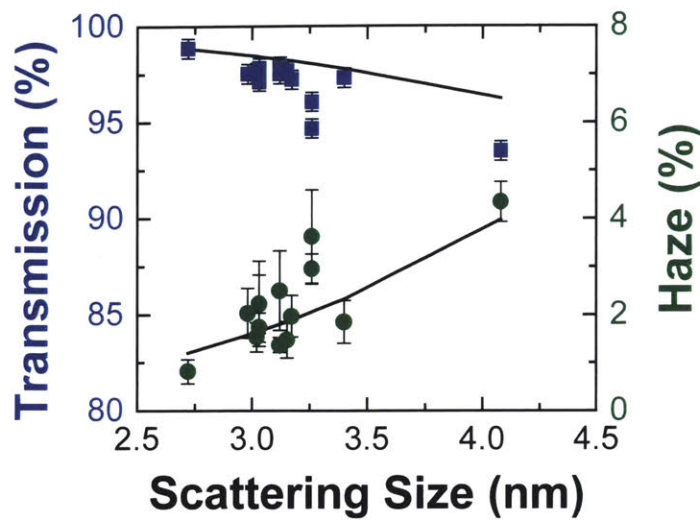


Figure 18. Visible transmittance and haze as a function of effective scattering size as characterized by Small Angle X-ray Scattering (SAXS). Scattering is the primary loss mechanism for visible transmittance and results in higher haze. The modeling lines shown are taken from the model described in Zhao *et al*^{18,19}.

3.3 STRUCTURAL DEPENDENCE ON AEROGEL SYNTHESIS

The established relationship between aerogel structure and optical clarity outlines a path to methodically optimizing the aerogel synthesis to achieve low-haze aerogels. The most important metric will be the haziness of the aerogel, used to quantify the optical clarity.

First, it is important to understand the influence of the chemical recipe on the clarity of the aerogel. For example, Figure 19 shows the visual results of varying the catalyst (ammonia hydroxide) within the base recipe. To methodically understand the effects of the recipe ratios, we performed 3 parametric sweeps of the chemical ratios, varying the ammonia (in the form of ammonia hydroxide), water, and methanol ratios normalized to the precursor amount (TMOS). Ratios were selected to span a range of haze values while still yielding “low-haze” aerogels (haze < 5% through 4 mm) based on prior works^{18,78,98}, while the base recipe selected was from the clearest aerogels fabricated to-date. These experiments were then repeated using the same recipe ratios with a different precursor (MS-51). The resultant aerogels were characterized structurally and optically to quantify scattering size and haze, respectively. Figure 20 shows the dependence of haze as each of the 3 chemical ratios is varied.



Figure 19. Images of samples of varied ammonia ratio made with TMOS precursor. Haziness can be seen by the blue color of diffusely scattered light of short wavelengths. From these images, it is clear to see the lowest haze sample is second from the right.

We see from Figure 20 that both precursors showed similar trends when ammonia hydroxide and water ratios were varied. Generally, higher ratios of the catalyst and reactant yielded lower haze, and TMOS reached lower haze than MS-51 for the same recipe. From our understanding of the solution-gelation process, higher catalyst and reactant ratios should result in a faster, more exothermic reaction. Fast nucleation of the silica nanoparticles in the solution generally creates smaller particles with greater number density. Small feature sizes will decrease scattering at a cubic rate, while the number density should increase scattering linearly. Therefore, within the low-haze regime, higher ratios of catalyst and reactant should decrease haziness. Also, since the MS-51 is a pre-polymerized structure, we expect it should form larger particle aggregates at the same chemical ratio, resulting in a hazier aerogel.

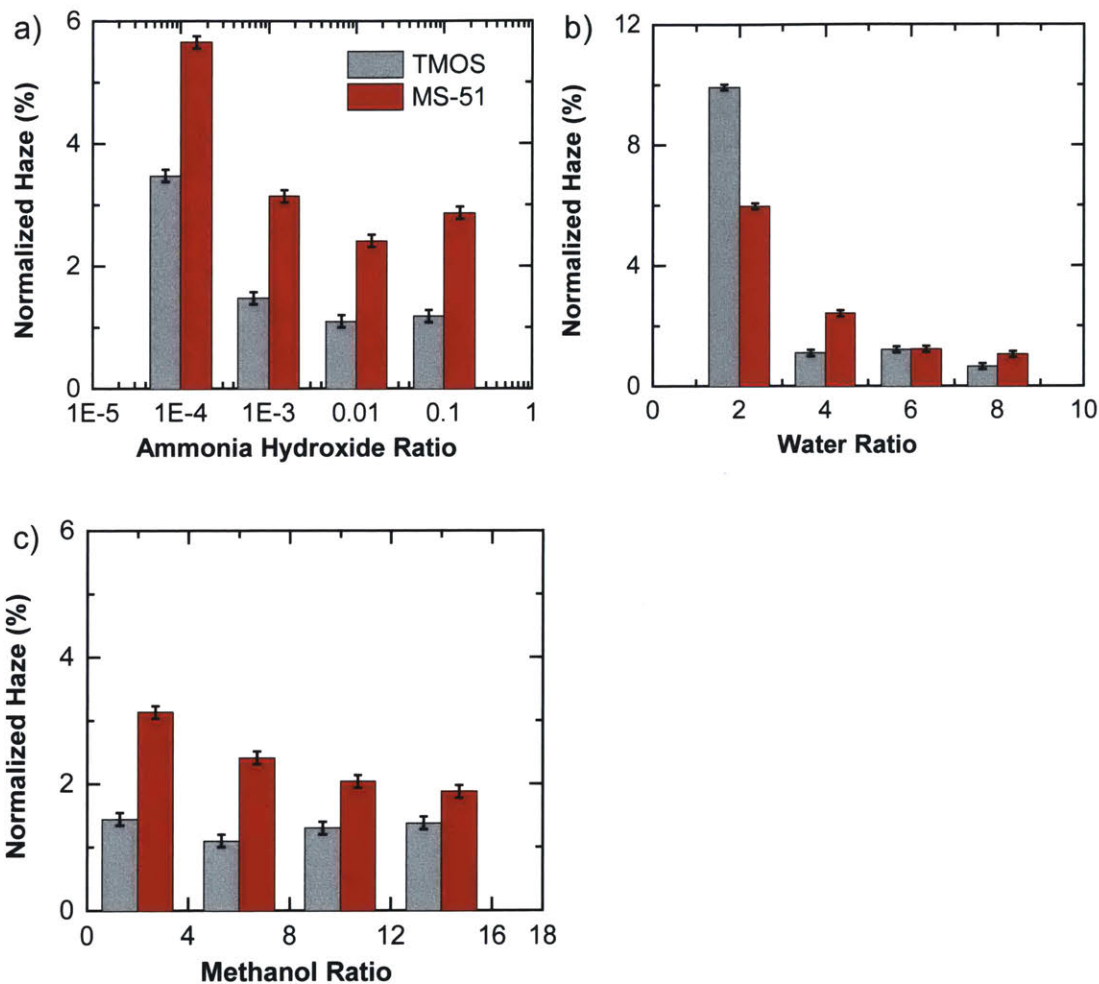


Figure 20. Influence of varying the chemical ratios normalized by precursor on the visible haze of silica aerogel. (a) Variation of ammonia hydroxide which functions as the catalyst. Both the TMOS and MS-51 precursors show an optimum ratio to minimize haze. (b) Variation of water, the reactant with TMOS and MS-51 respectively. Higher ratios show lowest haze. (c) Variation of methanol which serves to control concentration of reactants and catalyst, and also influences the density of the aerogels.

We see for Figure 20a that for both precursors there exists an optimum ratio. However, the trends in Figure 20b and c are less consistent, indicating a broader range is needed for full minimization of haze. Extending the ranges of reactants too broadly may cause additional factors to begin to influence the synthesis. For example, increasing the water ratio beyond 14 as seen in Figure 20c causes the gel to form so quickly it exceeds practical limitations for fabricating a sheet of aerogel. As a counter-example, reducing the catalyst ratio to below 10^{-5} can cause the recipe to gel very slowly, sometimes taking hours or days to fully form. This exposes the

solution to environmental conditions even longer than other recipes and causes challenges when trying to keep the other steps in the synthesis identical.

Despite the limited scope of optimization, this parametric sweep did demonstrate the ability to achieve low-haze aerogels across a variety of recipes. Of the 20 unique recipes, 17 achieved haze below 5%, which exceeds most prior works for silica aerogel. This implies that the optimum point for low-haze aerogels is broader than previously expected, allowing for small variations to the recipe to optimize other properties of interest.

Low-haze aerogels are also low-scattering aerogels, based on the modeling done in *Zhao et al*^{18,19}. This allows us to relate the structural properties to the optical properties, so that we can better optimize the aerogel recipe. Scattering is dependent on both density and effective scattering size, so we can approximate scattering intensity using the quantity ρd^3 . Using the dataset from Figure 20, we can then compare the independently measured structural properties (density and effective scattering diameter) to the measured optical haze, as shown in Figure 21.

Figure 21 shows good agreement between the modeled haze as predicted by *Zhao et al*¹⁸ and the measured haze. This validates the ability of the haze model presented in *Zhao et al*¹⁸ to predict the optical performance based on structural feature size, allowing us to optimize the chemical recipe with respect to scattering size.

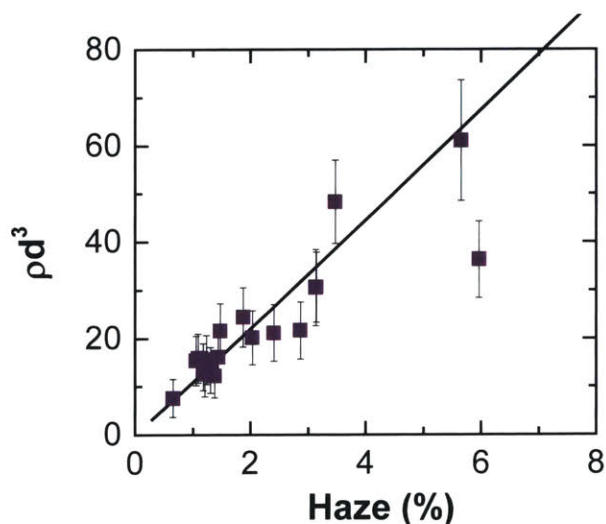


Figure 21. Relationship between the product of density and scattering diameter and visible haze. Density and scattering diameter influence the scattering coefficient and are therefore related to diffuse reflection and therefore haze. The modeling line was calculated using the model described in *Zhao et al*¹⁸.

After identifying the general trends that yield low-haze aerogels, 100 additional samples were fabricated and characterized using SAXS to determine effective scattering radius. **Figure 22** shows the results of the normalized recipes. In this ternary plot, each chemical ratio was normalized by maximum and minimum values. This was a ratio of 2-75 for methanol, 1-47 for water, and 0.002-0.30 for ammonia. We see that for the recipes shown, the lowest feature sizes are achieved at relatively high ammonia and water contents and lower methanol contents. However, it is important to remember that the chemical recipe is not the only influence on the aerogel nanostructure; drying of the aerogels can also have significant impact on the scattering size, and therefore the optical performance.

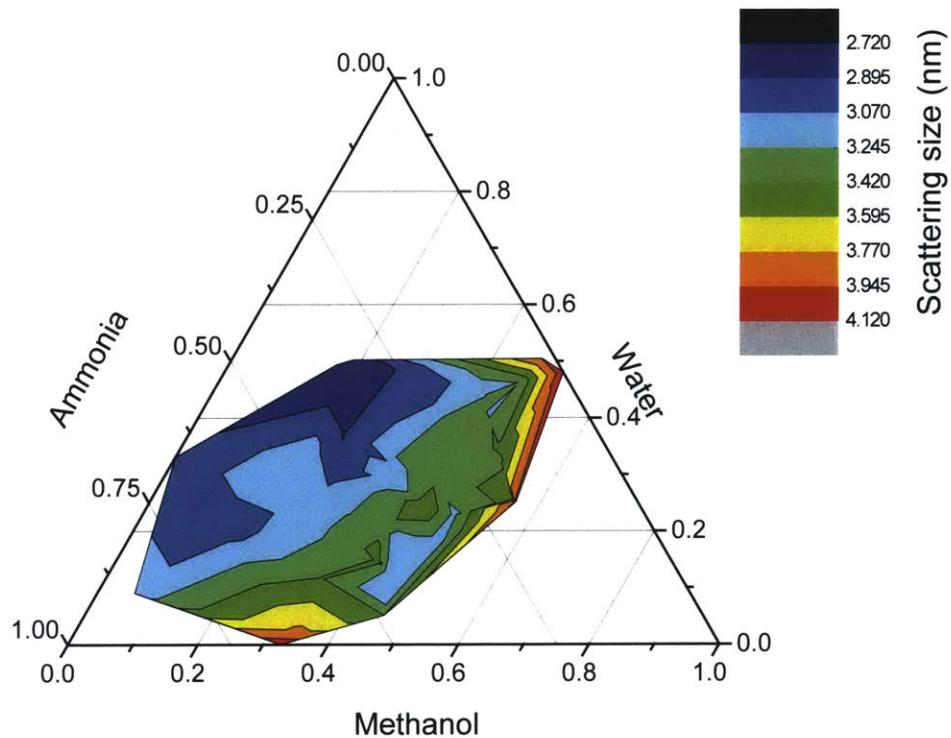


Figure 22. Effective scattering size achieved through various recipe ratios. Each axis is normalized by the minimum and maximum values selected for fabrication. This was a ratio of 2-75 for methanol, 1-47 for water, and 0.002-0.30 for ammonia. From the plot, we see that higher ammonia and water content results in consistently lower scattering size, and therefore higher clarity.

3.4 SUMMARY

High optical transmittance and low-haze are critical performance metrics for materials in traditional windows. Therefore, in this chapter we described the guiding principles necessary to achieving low-haze aerogels. First, we provide an overview of aerogel synthesis and structure,

highlighting the most important steps: gelation of a silane precursor and subsequent removal of liquid within the pore structure using critical point drying. Using small angle x-ray scattering (SAXS) and prior modeling works, it is possible to establish relationships between the fabricated structure and optical clarity, allowing us to tailor the nanostructure of traditional porous silica aerogel and create one of the lightest, most insulating solid materials with record-setting clarity (98% visible transmittance and haze less than 2%).

Next, we explore the relationship between the unique nanostructure and the optical properties, and use these relationships to optimize the aerogel chemical recipe to yield low-haze aerogels. We have fabricated and characterized over 50 samples using a variety of recipes and techniques to perform structural optimization for low-haze. This information enables the ability to achieve high clarity when recipe, batch size, and sample size is varied. This knowledge and control of fabrication provides us the necessary tools for scaling and optimizing the aerogel material for window applications.

4. Optimizing Transparent Aerogels for Windows

The characteristic sizes of pores and particles within the aerogel structure affects all relevant transport properties, such as light, heat, and sound transmission. With sufficiently small feature sizes (on the order of 10 nm or smaller), silica aerogel can achieve transparency higher than glass.¹⁸ However, for window applications the visual aesthetic, primarily clarity, is more important than total transmittance of the visible spectrum.⁹⁹ This is critical to the viability of the end result due to the extremely high expectations related to the use of aerogels in industry and the end application. Prior works have not addressed the intrinsic scattering of visible light as it travels through the aerogel structure. Here, we focus on developing a greater understanding of this visible haze in order to achieve an aerogel that is suitably clear for applications in traditional windows.

Figure 23 shows a plot of the high-clarity aerogel transmittance and haze compared to traditional float glass as measured using an UV-Vis-NIR spectrophotometer (Cary 5000, Agilent) on wavelengths from 250-2500 nm using a polytetrafluoroethylene coated integrating sphere and a Fourier transform infrared spectrometer (FTIR6700, Thermo Fisher) in the wavelength range of 1.5-18 μm . This shows the incredibly high transmittance (98% averaged over the visible spectrum), as well as the ultra-low haze (1.6% averaged over the visible spectrum) through a 4 mm sample. As described in the Section 3.3 and prior works such as *Zhao et al*^{18,19}, we find that this high clarity aerogel is not limited to a single unique recipe, but it is common among all aerogel samples with structural feature sizes and densities that are sufficiently small.

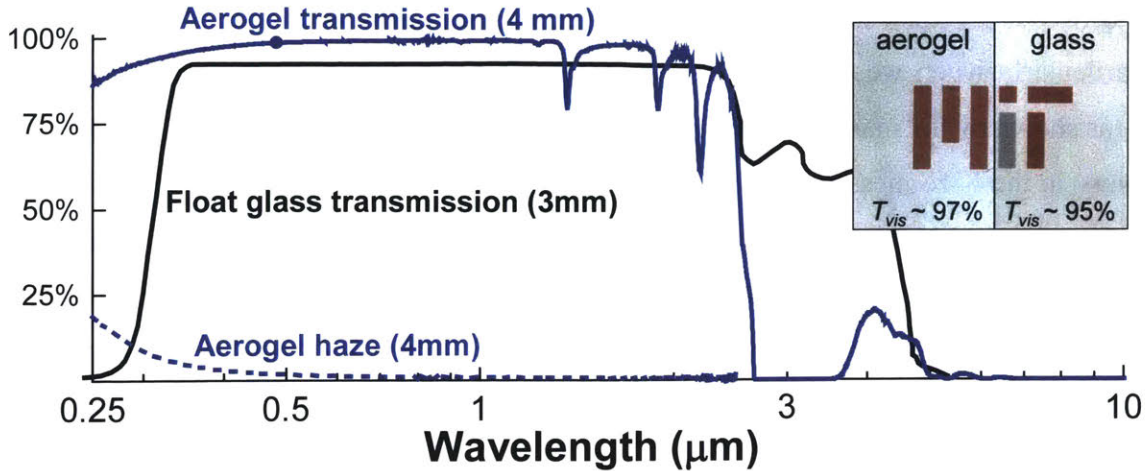


Figure 23. Transmission spectra of a 4 mm transparent aerogel compared to a 3 mm thick sample of traditional clear float glass. Haze spectra for the same aerogel is shown by the dashed line. Due to the low reflectance and high clarity of the transparent aerogel, total transmission in the visible spectrum (375-800nm) is higher than that of glass. However, glass haze is very consistent in the visible wavelengths (~0.5%, not shown) compared to the wavelength dependent behavior for the aerogel sample shown here (average haze 1.6% in visible wavelength range). Both transmission and haze of the aerogel are highly dependent on the nanofeature sizes, density, and thickness, providing an opportunity to tailor the material to achieve higher performance in application.

The primary transmission loss at low wavelengths (< 800 nm) is dominated by scattering losses. Therefore, an increase in scattering will decrease total transmittance and increase the haziness of a given sample. Figure 24a shows that as visible transmittance increases, the haze will decrease proportionately. As described in Zhao *et al*¹⁸, this should hold true when we consider the formal definition of haze as

$$Haze = \frac{T_{diffuse}}{T_{total}}$$

We see from this equation that for a material such as the silica aerogel where transmission losses are dominated by scattering, increased transmission directly correlates to a decrease in haze. These affects are largest at low wavelengths, often giving aerogels a characteristic blue hue.

Because the haze and transmission are directly related, it is generally assumed that the structural features that control visible transmittance similarly affect haze. Prior works have shown that transmittance is dependent on thickness, pore size, particle size, density, etc. In particular, Zhao *et al*¹⁸ has shown that scattering size (defined as a representative average radius of both pore and particle features) is the most influential material characteristic for achieving high transmittance and therefore low haze. Figure 24b shows the measured average visible haze as a function of independently measured scattering size (representative feature radius) by small angle x-ray

scattering (SAXS). We see that the various measured samples follow the model predicted behavior well, particularly when we consider the wide array of densities represented within the sample dataset (as shown by the margins on the model, representing densities from 89 to 249 kg/m³). The uncertainty in the haze measurement is relatively high in order to account for the small relative values of haze across the averaged spectrum (370 to 800 nm) as well as the thickness normalization to 4 mm (samples range from 2.5 to 4 mm in thickness). However, even considering this uncertainty and the varied fabrication of the samples within the dataset, the high clarity performance of the aerogel samples agrees well with the model prediction based on scattering size.

Density is the other most influential material property on the haze and visible transmittance. Figure 24c shows the effects of density variation on haze through the aerogel. Area and thickness were measured by image analysis against a known visual reference using ImageJ software¹⁰⁰. The mass of the aerogels was taken on an analytical balance (DV215, OHAUS Discovery DV215) in ambient conditions. Density was then calculated using area, thickness, and mass.

Here we see that the model-predicted trend is less representative of the measured data, but generally we anticipate that in this regime of nanofeature sizes that are significantly smaller than the visible wavelengths, lower density samples will scatter less due to fewer interfacial interactions of the light as it travels through the material. However, it has also been shown that density and scattering size are interdependent, which influences the ability to fabricate samples that represent bulk density changes for the same scattering size. This is illustrated by the large range of scattering sizes represented by the model uncertainty. Density measurements also contribute to the large uncertainty between the measured and predicted performance due to challenges in measuring thickness and mass. In particular, the fragile nature of samples and their water adsorption characteristics lead to large fluctuations within the material. While the attempt was made to limit effects of water adsorption and structural damage during density measurements (by controlling humidity conditions and limiting handling, respectively), it is realized that some influence of these affects were unavoidable as we performed multiple property and performance measurements on each sample over a range of months to compile these datasets.

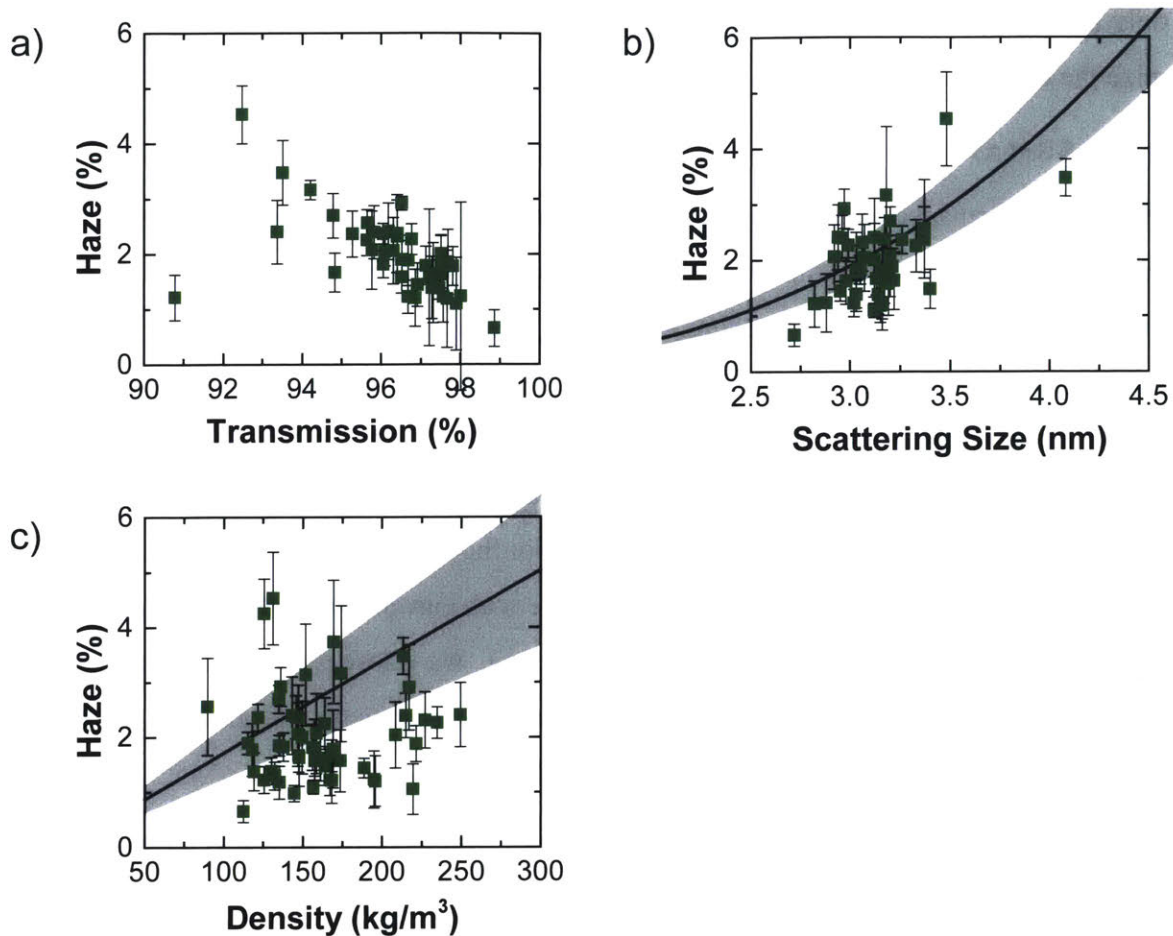


Figure 24. Transparent aerogel haze normalized to a 4 mm thickness (as described in *Zhao et al*¹⁹) as a function of a) average visible transmission, b) average scattering size, and c) bulk density. a) Haze and transmission are fundamentally related by the isotropic scattering that dominates optical loss in the visible and UV wavelengths as shown by the data trend.¹⁹ Since the threshold of desired haze is more limiting than visible transmission, by studying the property relationships of haze we can also meet acceptable visible transmission. b) Scattering size, as measured by SAXS, shows that haze is very sensitive to the average nanofeature size within the material. The modeled line shows good agreement with experimental results when banded by the range of densities within the experimental dataset (89 to 249 kg/m³). c) The relationship between density and haze is noisier experimentally than predicted by the model due to the high uncertainty when estimating density. The bands on the model capture the range of scattering sizes within the experimental dataset (2.72 to 4.08 nm).

Overall, the data from Figure 24 demonstrates our ability to fabricate silica aerogel samples with low haze, making them visually competitive with existing window solutions, such as electrochromic glazings.⁹⁹ These high quality samples are achieved across a variety of chemical recipes, aging and pinhole drying conditions, and post-processing treatments such as annealing primarily because of our ability to understand and control the pore and particle effective radii as represented by the scattering size. This versatility in performance across samples allows for us to

not only achieve one of the first truly clear aerogels, but also provides flexibility to control and optimize the thermal performance to have maximum impact in window applications.

4.1 THERMAL PERFORMANCE

Thermal performance of the aerogel in window applications is often quantified by the material thermal conductivity. Thermal transport is effected by many material properties, such as thickness, density, tortuosity, pore size and pressure, etc. When optimized for energy-efficient windows, the conductive, convective, and radiative modes of heat transfer through the aerogel material are often of similar magnitude. This allows us to describe the transport using an effective thermal conductivity, based on prior works by Hrubesh & Pekala¹⁰¹, that describes the thermal conductance for a prescribed thickness and boundary conditions. For the window application, we consider 2-10 mm to be of highest interest in order to be competitive with current products as well as achieve the high clarity needed for traditional windows. Therefore, we chose several samples across this thickness range to characterize via guarded hot-plate measurements (in ambient pressure and temperatures) as representative of both thickness and boundary conditions.

Figure 25 shows the measured effective thermal conductivity of 11 representative clear samples as a function of bulk density. The model shown is from Hrubesh & Pekala¹⁰¹, while the shaded areas represent the banded range of average pore sizes (as estimated by nitrogen sorption analysis ranging from 11-20 nm radius). We see that the characterized performance shows strong agreement with prior modeling work. We also see that for a fixed set of conditions (such as ambient temperatures and pressures) the model predicts an optimum density that minimizes heat transfer through the material.

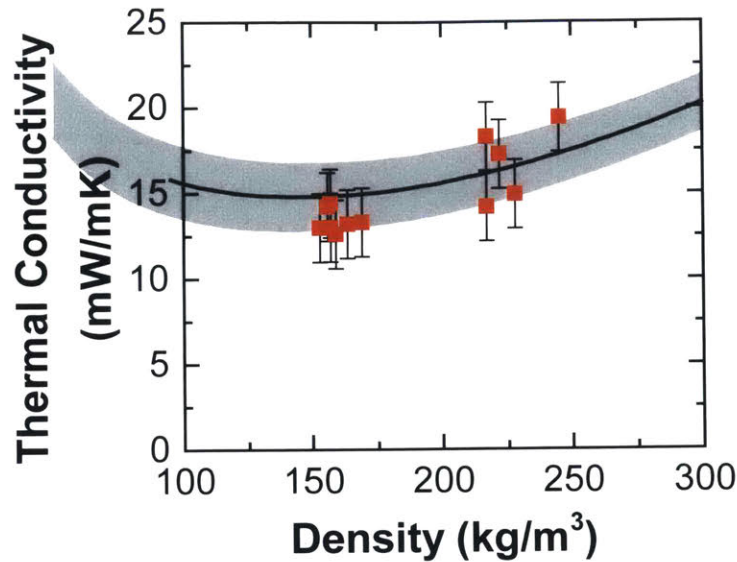


Figure 25. Effective thermal conductivity as a function of apparent density. Thermal conductivity was measured in a Netzsch 436 HFM on 12-15 cm diameter samples with thickness of 4 – 7 mm. The line represents predicted thermal conductivity at standard temperature and pressure from the relationships described in Hrubesh & Pekala¹⁰¹ with the bands representing the range of average pore diameter within the experimental dataset (11 – 20 nm), as measured by nitrogen sorption. Both the data and experimental characterization agree well and predict an optimum point at about 140 kg/m³.

As mentioned, there are many material properties that can be used to control the thermal conductivity. However, many of these properties also affect the visible transmittance, which is why we have identified the bulk density as the most influential and independent property to control thermal conductivity.

4.2 ACOUSTIC PERFORMANCE

Optimization of the visible transmittance and effective thermal conductivity is most critical for application, but there are many other properties of interest that provide additional value for windows. The sound transmission loss represents one of these potential value-added performance properties that we have investigated. Figure 26 shows a representative plot of the relative sound transmission loss of the aerogel compared to traditional float glass.

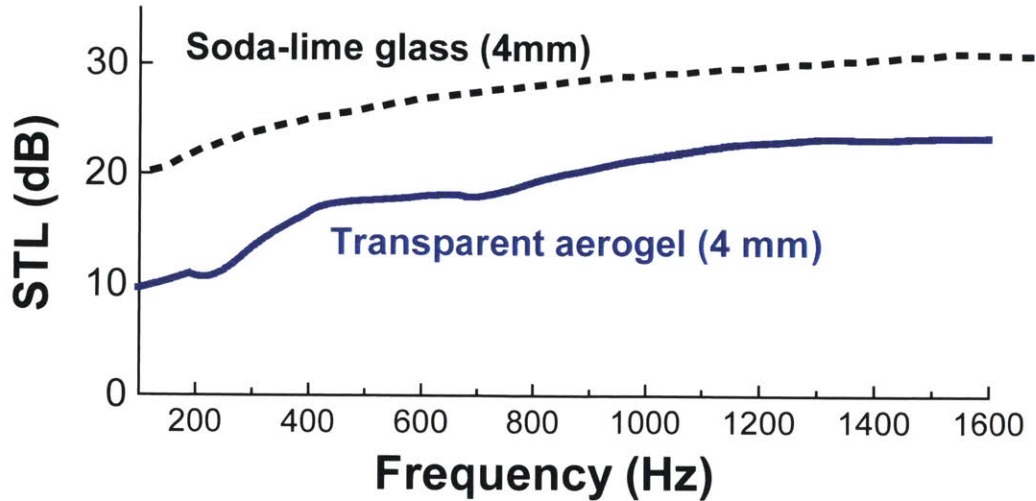


Figure 26. Sound transmission loss comparison of a 4 mm thick aerogel and a 4 mm glass sheet in ambient conditions as measured by an impedance tube. Reflection is the dominant sound transmission loss mode in both the aerogel and glass sheet, showing similar behavior.

The porous nature of aerogel combined with its solid backbone density allows it to intrinsically possess soundproofing properties that are highly favorable for window applications.¹⁰² Sound propagation through the aerogel is dependent on both the particle and pore structure, but is dominated by acoustic reflection caused by a rigid backbone and highly mesoporous network. By exploiting this understanding of acoustic loss through the material, we aim to increase the natural sound-proofing capabilities of the aerogel to increase its value as a high-efficiency window material.

Similar to bulk glass, the aerogel sound transmission loss is dominated by reflection and not absorption (representing a key difference in behavior between granular and monolithic aerogels).¹⁰³ While the sound transmission loss of the transparent aerogel is lower than traditional glass, it does have the potential to noticeably decrease sound transmission.¹⁰⁴ In a reflection-dominated porous material (see Figure 27) sound transmission loss is increased by changing transmission through the material backbone and/or through the pores. By increasing the overall mass or decreasing rigidity of the material, sound has a greater likelihood of being reflected due to its inability to propagate through the solid network. By decreasing the speed of sound through the porous structure (by controlling the gas or pressure within the pores) we can also increase porous sound reflection to reduce transmission. Because the thermal performance is critical for window application, it is most advantageous to optimize overall density for thermal properties and use the porous structure to optimize for acoustic properties. By decreasing the pressure within the

pores, we can limit the sound propagation speed and increase sound transmission loss. This results in coordinated strategies to improve both thermal and acoustic performance.

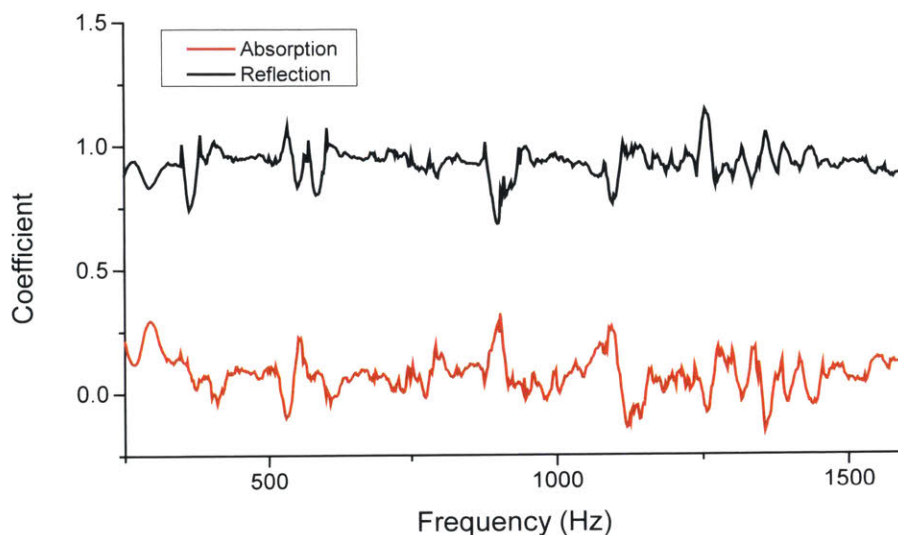


Figure 27: Absorption and reflection coefficients for a 3 mm thick TMOS aerogel. The reflection coefficient is measured by the ratio of the reflected amplitude relative to the incident amplitude and is the dominant sound transmission loss mode, indicating that increasing sound reflection in the pore and particle structure will increase overall sound loss.

We further investigated the dependence of sound transmission loss through the aerogel to determine the opportunity for improving acoustic performance (without detracting from optical and thermal performance). Within the range of our sample dataset, we found that thickness was the most influential property that changed sound transmission loss. This is related to the ability of the material to reflect additional sound as the overall mass per unit area of the aerogel increases. Figure 28 shows the average sound transmission loss in the 80-1600 Hz frequency range as a function of sample thickness. By comparing this to a model presented in Equation 2 in Tadeau & Mateus¹⁰⁵ describing sound transmission loss through single-pane glass, we find that our data agrees well with predicted performance. This indicates that by increasing the thickness of the aerogel we can directly increase the sound-proofing performance of the material, with particularly large improvements for samples at ~ 4 mm of thickness. Uncertainty in the measurement is largely influenced by the fragility of the aerogel and the challenge it represents in traditional acoustic characterization, which often requires a well-sealed edge and crack-free sample. Measurements were repeated three times for each sample and average values were used to represent performance.

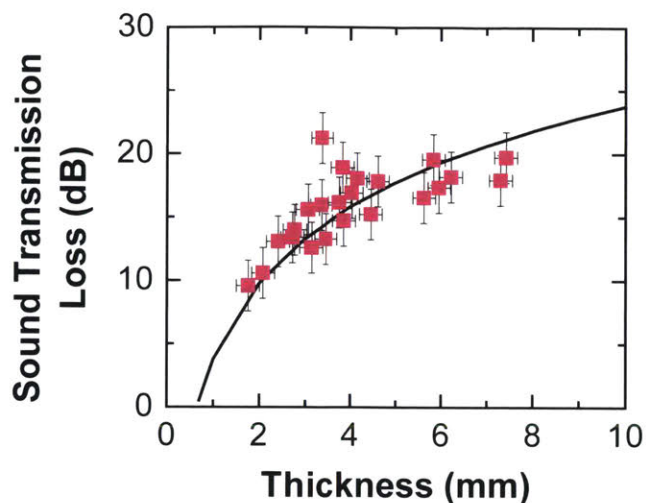


Figure 28. Sound transmission loss of the aerogel material averaged from 80-1600 Hz as a function of aerogel thickness. Each measurement was repeated at least 3 times and averaged to obtain each data point. The dependence of sound transmission loss on thickness indicates that sound is most impeded by an increase in overall aerogel mass, as predicted by prior works on glass panes.¹⁰⁵

Conversely, we saw no strong trends correlating sound transmission loss to variations in either density or pore and particle sizes. Some prior works have indicated that in the density range of our samples (89 to 249 kg/m³) the porosity should not strongly contribute to increasing sound reflection (the dominant sound loss mode for the clear, monolithic aerogels).¹⁰⁶ However, further characterization is planned to better understand the influence of other factors, such as water adsorption, pressure dependence, and pore and particle tortuosity. These additional properties, combined with our understanding of the thermal and mechanical properties of the material, will allow us to better understand and increase sound transmission loss of the material.

4.3 MECHANICAL PERFORMANCE

Sound transmission loss, thermal transport, and mechanical strength are highly interdependent properties of the material. While silica aerogel has intrinsic properties that make it a strong candidate for window applications, its primary limitation is its mechanical stability. This is problematic when considering the need for large, monolithic pieces that can survive 10-20 years in application. Additionally, the window application must meet rigorous mechanical standards due to daily consumer interaction with the product, wind and pressure loading, humidity considerations, etc. Therefore, it is crucial to characterize aerogel's mechanical properties to ensure they meet minimum load requirements, and improve strength and toughness as much as possible.⁶⁸

While aerogel is strong relative to its density, especially in compression, it is prone to breaking at relatively low bending stresses. Preliminary compression testing has been done on higher density TMOS aerogel in comparison to a lower density MS-51. Figure 29 shows that both of these synthesized aerogels are 2-3 times stronger than aerogels previously reported in literature, likely due to the small pore and particle sizes developed for high transparency. This data indicates that while compressive strength is a function of density¹⁰⁷, the MS-51 samples are already very strong at low densities compared to the much more dense TMOS. With further structural optimization, it may be possible to increase strength even further. However, further study into the limiting bending strength is needed before it is clear what strategies should be used to increase overall mechanical stability.

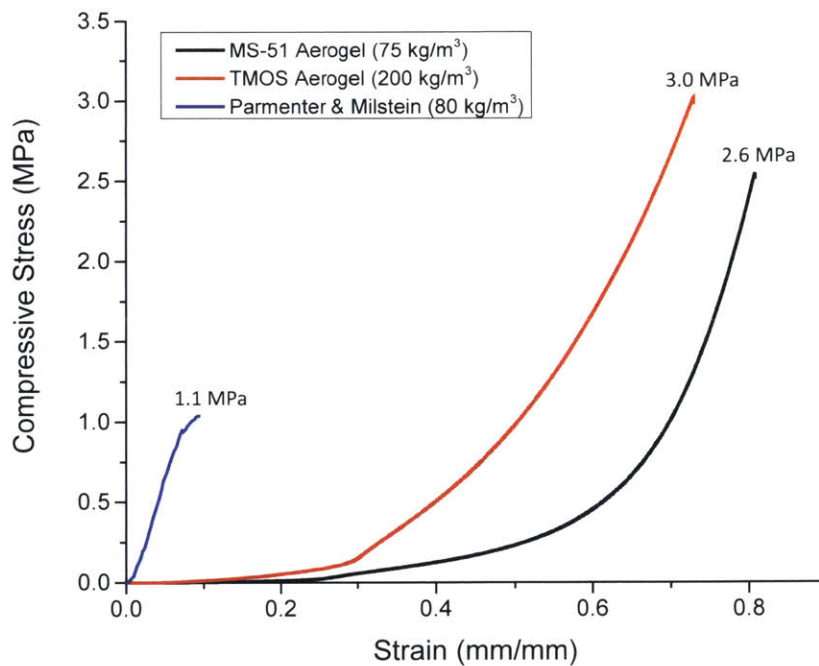


Figure 29: Compressive strength of TMOS and MS-51 aerogels fabricated in the Device Research Laboratory compared to typical literature values¹⁰⁸. While it is generally true that a denser aerogel has a higher compressive stress⁷⁷ we see that the less dense MS-51 aerogel still has a very high compressive strength, indicating it is a good candidate recipe for strong, lower density aerogels as needed in window applications.

For a better understanding of our clear aerogel structure, we also characterized the mechanical strength of all samples in the data set using indentation measurements. Figure 30 shows the Young's Modulus as calculated using the Hertz model¹⁰⁹ compared to the densities of the samples. Despite the wide variety of structures, fabrications methods, and thicknesses, we find that the

experimental data fits very well to the predicted empirical model described in Chapter 22 of the Aerogels Handbook.⁷⁷

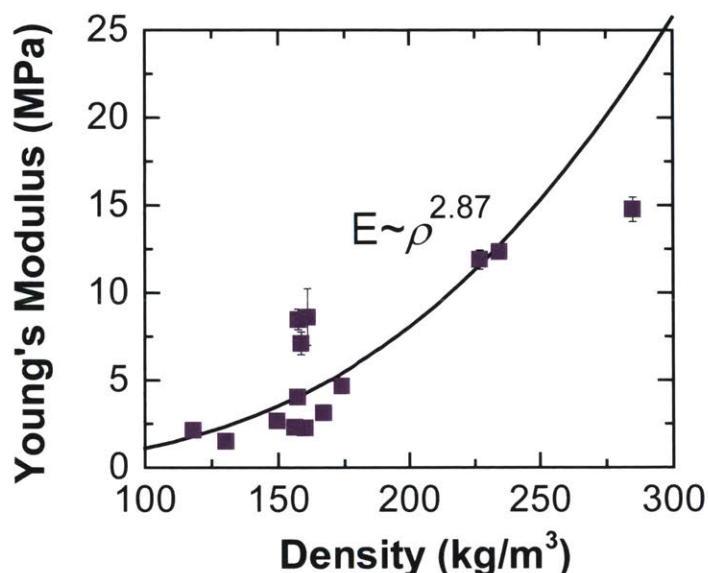


Figure 30. Young's Modulus as a function of apparent aerogel density. The values of E were determined by a slope fit of experimental data from a standard indentation test using the Hertz indentation theory. Previous literature indicates the exponential term of a power fit should fall in the range of 2.59 to 3.53. The data collected has a power fit of 2.87, agreeing well with prior works. This relationships also shows that while the strength can be improved by optimizing the material density, the aerogel still has a Young's Modulus that is 3 orders of magnitude lower than traditional float glass.

While samples vary in strength by almost an order in magnitude, the aerogels are still three orders of magnitude less than traditional glass used in window applications. Characterization of the mechanical properties show that optimization of the silica structure is unable to achieve a considerable improvement in strength when compared to the typical loading requirements of windows (transportation, installation, wind forces, cleaning, etc.). We consider the mechanical properties beneficial to understanding and predicting performance of the thermal and acoustic properties, but overall a relatively low priority in relation to optimizing the material for application. However, it is important to note that Young's Modulus describes mechanical strength in only one mode; in particular the bending strength of the material is the primary mode of failure for these monolithic silica aerogels. It has proven very challenging to make consistent samples for mechanical bending tests, such as a simple 3-point bending setup. For this reason we chose to first assess strength using indentation testing, but we have planned future works to measure the bending strength of the material to quantify improvements that can be made by controlling the material structure.

4.4 COMBINED PROPERTY OPTIMIZATION FOR APPLICATION

Successful application of the aerogel material requires full understanding and optimization of all relevant properties – optical, thermal, acoustic, and mechanical. However, it is the optical and thermal performance that has limited silica aerogel applications in the past (particularly when comparing the estimated costs to existing window products). Limitations in visual clarity have resulted in prior works being unable to truly optimize thermal performance for traditional transparent window applications. The achievement of our low haze silica aerogel combined with rigorous characterization and recipe agnostic performance has allowed us to quantify the relationship between transparent aerogel structure and thermal performance.

To fully understand the effects of aerogel thickness and density on window performance we must first translate effective thermal conductivity to U-factor, the measure of heat flow per area across a temperature difference (see Section 2.1.1). For the prescribed standard conditions (21 °C interior, -18 °C exterior), we can approximate the U-factor performance by creating a simple thermal flow diagram shown in Figure 31. By estimating R_{window} (the thermal resistance of the “window”) from the thermal conductivity aerogel, we can then use an iterative method to solve for the total heat transfer across the fixed conditions. This total heat flow across the “window” is normalized by the temperature difference to predict the U-factor. This method works especially well for the aerogel material as we measure effective thermal conductivity, and don’t have coatings or wavelength-dependent radiative transfer that needs to be accounted for in the heat flow.

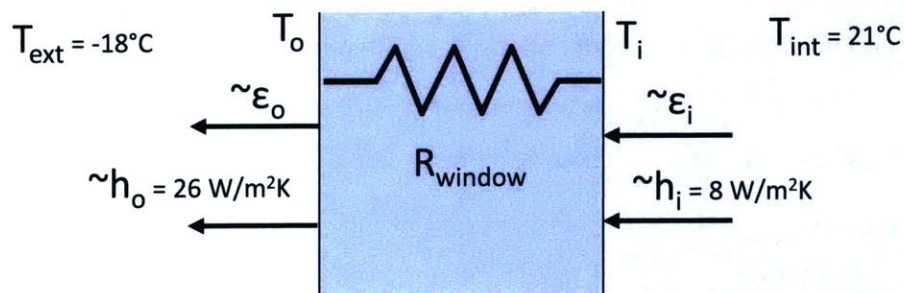


Figure 31. Diagram illustrating the simplified flow of heat from an interior chamber to an exterior chamber. Temperatures and convective coefficients are prescribed by the U-factor standards. Here, R_{window} can be calculated from modeled or experimentally measured effective thermal conductivity from the aerogel. As a note, the addition of glass to this model has no appreciable effect on U-factor due to the highly insulating nature of the aerogel (R_{window}) that is much large than any thermal resistance from the glass panes.

Figure 32 shows the performance of haze and U-factor as a function of material density and thickness. In both Figure 32a and Figure 32b, we see that these optical and thermal properties compete with each other for maximum performance, but that understanding the relationships allows us to reach the highest possible performance. In Figure 32a, we see that the flatness of the thermal performance with respect to density allows us to operate on the low-density side of the optimum to decrease haze without appreciably increasing thermal transport. Figure 32b shows that thickness dependence is particularly influential on thermal performance, allowing us to drastically increase performance with added thickness. However, it is noted that thickness is also highly tied to cost and manufacturability, which should be considered when targeting successful application.

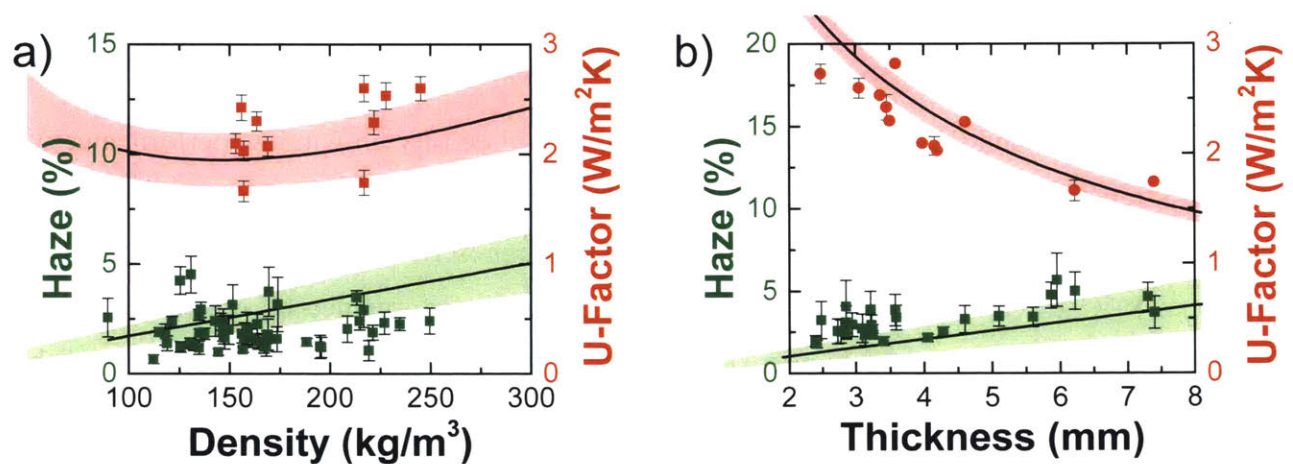


Figure 32. a) Haze and U-factor as a function of apparent density for the aerogel normalized to 4 mm thickness. Model bands encompass the average scattering size (2.72 – 4.08 nm) for haze and average pore diameter (11 – 20 nm) for U-factor that are represented by the included datasets. b) Haze and U-factor as a function of aerogel thickness. Model bands encompass the densities (112 – 249 kg/m³) for both haze and U-factor that are represented by the included datasets.

Another important factor to note is that the scattering size control of the material allows us to operate in a regime in which the haze dependence on both density and thickness is greatly reduced. As described in *Zhao et al*¹⁸, at low scattering sizes, density and thickness increases have less influence on increasing haze than at higher scattering sizes.

4.5 SUMMARY

The diverse needs of our buildings require consideration for the optical, thermal, acoustic, and mechanical properties of materials used in window designs. In this chapter, we provide a structurally-guided framework for optimization of high-clarity aerogels for windows. In prior works, the high-haze structure of aerogels has prevented a full consideration for how low-haze

feature sizes can limit thermal, acoustic, and mechanical performance. Here, we present the study and optimization of a high-clarity aerogel with a uniquely small nanostructure for windows.

Over 300 samples were made and characterized, enabling us to target and demonstrate nanostructures that achieve $< 3\%$ haze through a 4 mm sample across 20 unique recipes. Using experiments, validated with models, we demonstrate monolithic silica aerogel samples with thermal conductivity < 13 mW/mK, sound transmission comparable to a thin pane of glass, and mechanical strength comparable to other silica aerogels of similar density. These relationships were then used to guide optimization of clarity and thermal insulation in window applications. By removing the barrier to clarity, these low-haze aerogels represent the ability to achieve U-factors competitive with existing double-pane windows at relatively small insulating thicknesses.

5. Transparent & Stable Aerogels for Windows

Application of aerogels to the broader window market requires a high-quality visual experience. Even small defects or changes to the nanostructure can result in an “unacceptable” visual experience, such as visual aberrations, haziness, or coloration. Achieving high-clarity aerogels over a variety of recipes and synthesis (see Figure 33) is therefore limited unless defect-free monoliths can be fabricated. It is necessary to explore ways to increase the size and quality of defect-free aerogel samples to validate the performance of the material.

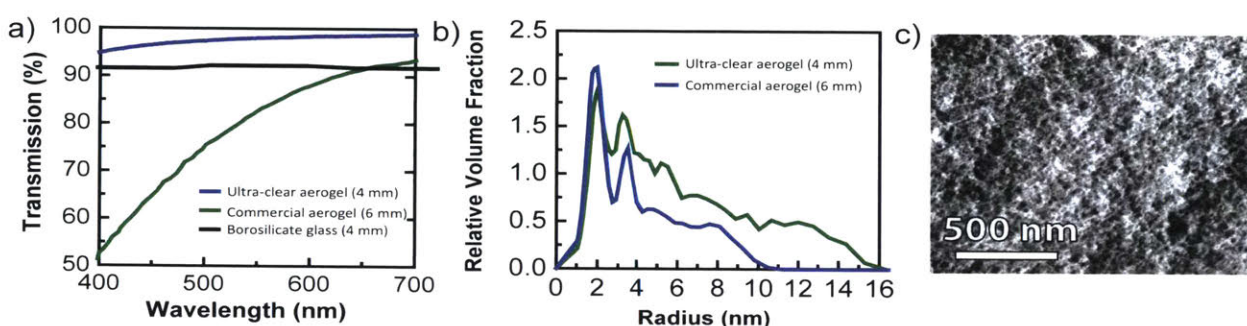


Figure 33: (a) Visible transmittance of the ultra-clear silica aerogel (blue) compared to borosilicate glass and commercial silica aerogel (from Aerogel Technologies). The ultra-clear aerogel is more transparent than bulk glass due to the reduction in reflectance from the highly porous aerogel. (b) Scattering size distribution (characterized by small angle x-ray scattering) comparing feature sizes of commercial aerogel to the ultra-clear structure. Scattering size quantifies both pore and particle features. (c) Scanning electron microscope image of the ultra-clear aerogel nanoporous structure, showing the complex particle and pore nanofeatures.

As discussed in Section 3.1.2 and 3.3, there are many steps within the aerogel fabrication process that influence the final aerogel properties. In the previous section, we extensively explored the optimization of the chemical recipe with respect to the relevant material properties (visible transmittance and haze, thermal conductivity, sound transmission loss, Young’s Modulus). However, each of the steps in the synthesis process can lead to changes in the structure ranging from the nanoscale to the macroscale. Therefore, it is important to control all steps of the fabrication to ensure large, defect-free sheets of aerogel are created. First, we consider the defects formed during solution-gelation.

5.1 GRADIENT-INDUCED STRESSES

Experimental observation of the aerogel synthesis for the samples from Section 3.3 indicate that the mixing of chemicals and the exothermic solution-gelation reaction cause gradients that drive convection that cause defects and non-uniformities. In particular, gradients in surface tension and density caused by the energy released during gelation create a characteristic surface pattern and create stresses that induce warping and cracking as shown in Figure 34a and Figure 34b . Similar effects have also recently been observed in adjacent fields, such as drying of colloidal films (Figure 34c).^{110,111}

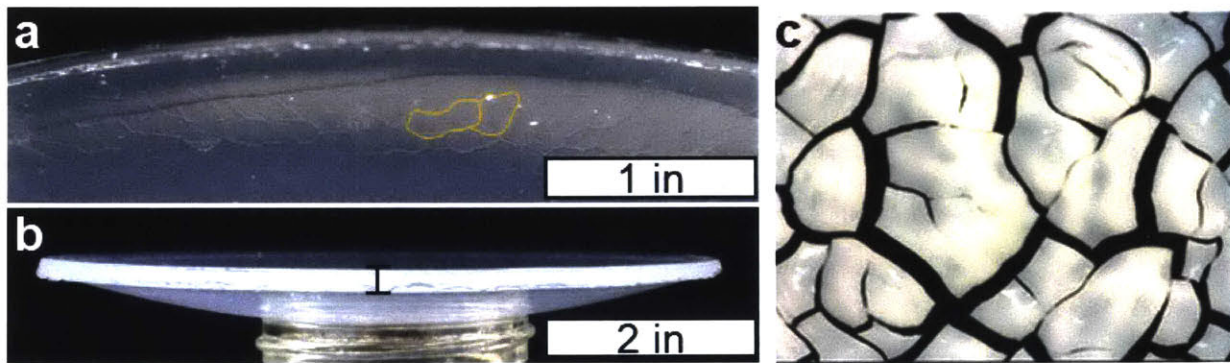


Figure 34: a) Surface defects on a monolithic aerogel sheet. Special lighting was used to accentuate the defects, which form cells with a characteristic period of ~ 0.2 in, consistent with typical Benard-Marangoni convection cell sizes observed in literature.¹¹² To aid the eye two cells have been traced in yellow. b) Side view of a monolithic aerogel sheet sitting on top of a beaker after supercritical drying. Non-uniform stresses in the sheet cause warping, preventing the formation of a flat sheet. The thickness of the sheet is marked in black. c) dried colloidal suspension with cracking and stresses due to Benard-Marangoni convection.¹¹⁰

The gelation process is exothermic, causing the solution to heat volumetrically while heat losses to the mold (container) and evaporation at the surface cool the liquid and lead to temperature gradients that drive convection (see Figure 35). Density driven convection is characterized by the Rayleigh number

$$Ra = \frac{\rho_0 g \beta \Delta T L^3}{\alpha \mu} \quad (1)$$

and surface tension driven convection is characterized by the Marangoni number

$$M = \frac{\rho_0 \gamma \Delta T L}{\alpha \mu} \quad (2)$$

where ρ_0 is the density of liquid at room temperature, g is gravitational acceleration, β is the coefficient of thermal expansion, ΔT is the temperature difference across the gelling sheet, L is the thickness of the sheet ($L \sim 3$ mm), α is the thermal diffusivity, μ is the viscosity, and γ is the temperature derivative of surface tension. Both quantities are affected by the temperature difference within a species, primarily experienced during the primary gelation (during which time the majority of the chemicals are reacting and a significant amount of evaporation can occur from the free surface).

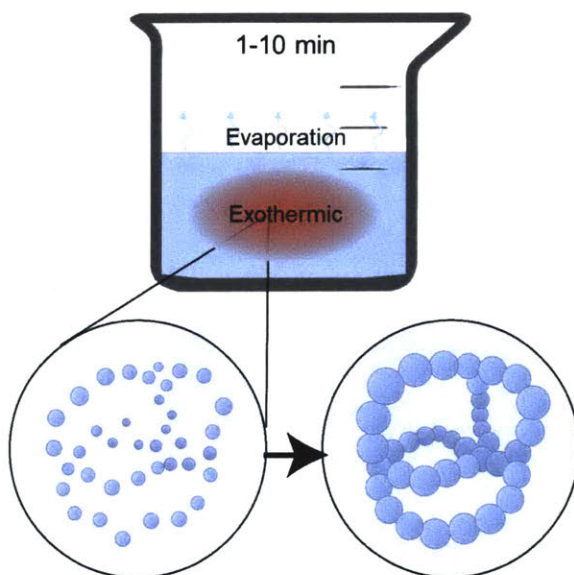


Figure 35. The exothermic reaction during gelation, evaporation at surfaces, and heat transfer through the mold (container), lead to temperature gradients within the mixture. These temperature gradients can drive both Marangoni convection and Rayleigh convection.

By fabricating samples over a range of reactant and catalysts ratios, it was observed that the exothermic heat generation during solution-gelation was dependent on both the speed of the reaction and the total volume of reactants used. Gels that formed more slowly and with less peak temperature rise showed less signs of surface patterning. Additionally, when the free surface was left uncovered during gelation, the surface defects also appeared with greater visibility. This evidence suggests that a slower, contained reaction results in less defects from gradient-driven sources. However, if the reaction rate must be fast (on the order of minutes) to achieve small nanostructure sizes (resulting in a lower haze aerogel), active temperature control of the solution during gelation could be used to reduce surface defects. Additional experiments that use a more

carefully controlled ambient environment during gelation also may eliminate enhancement of surface defects by surface evaporation.

5.2 NON-UNIFORMITY IN CRITICAL POINT DRYING

Drying of wet gels poses many challenges, and is often the step in which defects or cracks are created and/or revealed. Any non-uniformities in the wet gels can lead to stresses during drying that can cause warping or cracking, like that in Figure 34b. However, because the aerogels are so clear it can be difficult to find the causes of such defects with visual inspection. This creates challenges for identifying the source and severity of defects in dried aerogels. Birefringence of aerogels can be used to observe changes in stress gradients, providing a way to compare the severity of non-uniform stress.

Birefringence is an optical property when anisotropic propagation of light, commonly polarized light, is caused by differences in the refractive index of a material.¹¹³ In dried aerogels, the changes in refractive index can be used to quantify differences in density, species, etc.¹¹⁴ Stress patterns were observed in transparent dried aerogels by using two orthogonal polarized lenses with a white backlight. Since pure aerogels were used, we can assume the variation in birefringence indicates differences in density and/or stress, providing a picture of the non-uniformity and defects in the material.

For example, Figure 36a shows an aerogel that experienced an insufficient pressure during the drying step that resulted in the formation of a liquid-gas interface that damaged the sample. The liquid CO₂ never reached a stable critical point, and the internal surface tension gradients within the material caused cracks to form at the edge and propagate along existing lines of stress. These cracks along the high stress lines can be clearly seen in the image. For comparison, Figure 36b shows an almost stress-free aerogel that was produced from a similar recipe but with a well-controlled drying process.

Figure 36c represents a sample that shrank by more than 20% linearly while drying, but remained crack free. Looking closely at the photo, radial stress lines can be seen that are not present in Figure 36b. This circular monolith experienced significant shrinkage, but the radial gradients show that the sample was able to accommodate the shrinkage by densifying uniformly in the radial direction.

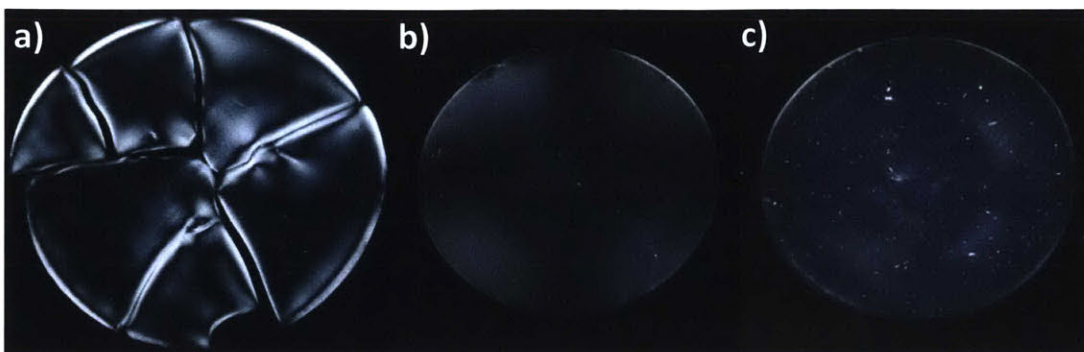



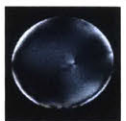
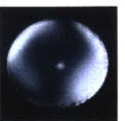

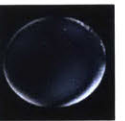
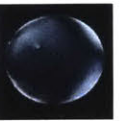
Figure 36: Birefringence variations within dried aerogel samples of 5 in nominal diameter showing relative changes to stress within the sample. (a) Sample that cracked during an error critical point drying. Stress build-up around the edges of the cracks show where non-uniform shrinkage lead to complete separation of the different sections within the sample. (b) Sample that was made with a similar process to (a) but was dried using a well-controlled process. While we still see some stress variations within the sample, overall the birefringence is much more uniform. (c) Sample that had significant shrinkage during critical point drying but was able to remain crack-free. Careful study of the photo shows stress lines that extend radially outward, but the changes in stress across these lines show less contrast than (a), The symmetry of stresses created and their low relative difference between the bulk sample resulted in this sample shrinking without cracking or warping.

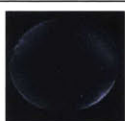




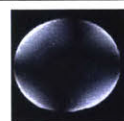
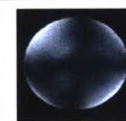
These selected samples show identical recipes dried under different conditions. However, when both the drying and the recipe are varied, it can become difficult to identify the true source of non-uniformities. It is important to make recipes consistently and repeat drying in several batches to truly validate trends shown in dry gels.

5.3 INTERDEPENDENT DEFECTS

The complexity of the aerogel synthesis makes it challenging to de-couple the solution-gelation step from drying. However, the birefringence property does provide a way to quantify defects in samples for a full process, enabling us to compare full processes including the chemical recipe, drying, and the resultant aerogel. Synthesis of these gels can be repeated and compared between batches to ensure repeatability. Table 3 shows a select sample from each of a range of recipes that were fabricated, dried, and imaged compared to the uniformity of gels based on chemical recipe ratios.

Table 3. Birefringence stress pattern of various aerogels made across a range of chemical recipes. All samples in this table were made using the same precursor (TMOS) and dried with similar process settings. The highest stress concentrations are seen in recipe ratios that have the highest and lowest catalyst (ammonia) and reactant (water) concentrations. Ammonia, water, and methanol ratios shown have all been normalized by precursor amount.

						
Sample	A	B	C	D	E	F
Ammonia	0.05	0.067	0.09	0.09	0.095	0.125
Water	0.5	0.5	0.47	0.47	0.47	0.75
Methanol	1.58	2.11	1.26	2.47	2	3

<i>(con't)</i>							
Sample	G	H	I	J	K	L	M
Ammonia	0.143	0.15	0.16	0.16	0.2	0.25	0.267
Water	0.49	1	0.6	0.8	0.75	1.5	1.33
Methanol	3.43	4	3	3.2	3.75	4	5.33

We see that at high at both high and low relative ammonia ratios, the non-uniformities induced in the aerogels increase. This agrees with the observations noted during synthesis of different recipes. In high-catalyst aerogels (samples K-M), the wet-gels are often very rigid and brittle. They are challenging to remove from molds but stand up to handling very well. At very low-catalyst ratios (samples A-D), the gels are very flexible, but also very weak. They tend to deform before moving and will flow off a substrate, making them very easy to damage during transfer or handling. It can be challenging to move these aerogels between synthesis steps, and it is less likely they will survive the drying step.

Another trend to note is the more un-symmetric nature of the birefringence pattern at low ammonia ratios (samples A-D). Generally, these gels form slower and have more time for mixing before gelation is complete, which may lead to more temperature-driven gradients within the gel (see Section 5.1 for details). At higher ratios we begin to see a transition to radially symmetric patterns, starting with sample G. However, more samples and repeated imaging of aerogels made with identical processes in different batches are needed to validate these observations.

5.4 POST-SYNTHESIS ANNEALING

The process for achieving the structure needed for high clarity aerogels often yields a material with high surface area (800-1000 m²/g) and residual stresses (see Section 5.3). This is caused by the nature of gelation – when the silica backbone forms the nanoparticles are small, disperse, and lightly interconnected. Small fluctuations in the interconnectivity of the particles within a sample and between different samples can change the surface energy and have significant effects on material properties such as water adsorption (particularly uptake of water into the internal surface in ambient conditions) and mechanical strength. One easy and scalable method of controlling the aerogel structure post-fabrication and reducing non-uniformities is through high temperature annealing.¹¹⁵

During annealing, the supporting network experiences structural relaxation and thermally-driven condensation. High temperature exposure decreases the viscosity of the silica particles and allows for the material to contract and rearrange itself into a less energetic state.¹¹⁵ By optimizing annealing temperature and time, it is possible to control the amount of structural contraction and modify the structure to the desired resultant aerogel. Prior works have shown that annealing can be used to modify effective pore and/or particle sizes, as well as density, providing an avenue for further optimization.^{78,98}

Annealing for high clarity silica aerogels also has the beneficial effect of reducing residual stress and burning off any potential contaminant species. Stresses and contaminants may affect haziness and/or the mechanical stability of aerogels in an application that requires long, stable lifetimes. Figure 37 shows an example of a transparent aerogel before and after annealing at 400 °C for two weeks, clearly showing the increase in transparency of an otherwise hazy recipe. Additionally, this sample became more mechanically stable after annealing, making it easier to handle for subsequent characterization. Each aerogel recipe has an optimum annealing time and temperature that is dependent on the initial structure as well as the desired properties, but several general trends have been found to provide favorable and consistent improvements to low-haze aerogels.



Figure 37: Transparent silica aerogel before and after annealing at 400 °C for 2 weeks. Transmittance is 97.6% in the annealed sample compared to 94.8% before annealing. However the sample also densified 4.5%, increasing effective thermal conductivity and indicating a need for optimization.

As discussed in Section 3.2.1, SAXS can be used to quantify the precise change to particle size, pore size, effective scattering size, and interconnectivity of the backbone. This provides an excellent quantification of the modification of the structure using non-destructive characterization to allow for optimization of annealing time and conditions. Past works have shown that at temperatures as low as 200 °C, the viscosity of the aggregated nanoparticles is decreased enough to allow for them to move relative to each other to achieve structural relaxation of the features.^{115,116} This results in a general shrinkage of the individual pore size and overall volume. However, as temperature increases further the viscosity of the particles becomes low enough that particle aggregation and densification dominate, which can result in detrimental effects to material transparency and thermal conductivity. At very high temperature, at or above the glass transition temperature of the aerogel of ~700-800 °C,⁸³ extreme densification and particle aggregation drastically change the nanostructure within hours (see Figure 38).

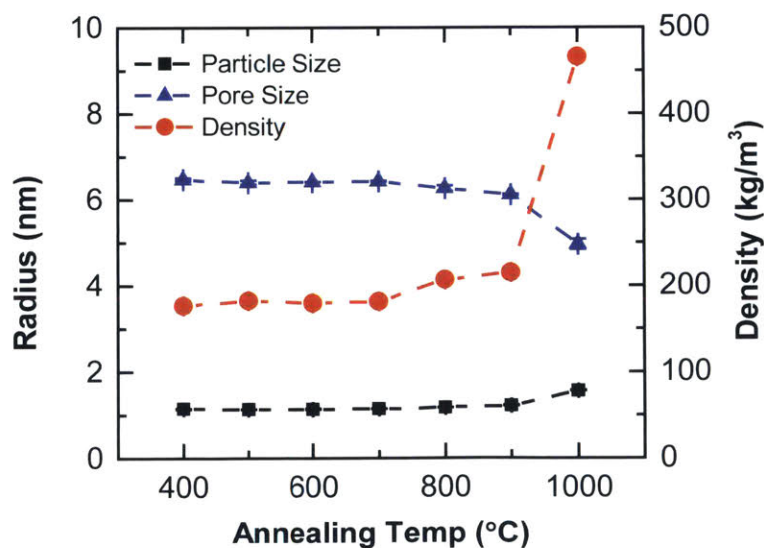


Figure 38: Structural change as measured by SAXS of a transparent silica aerogel annealed for 1 hour at progressively increasing temperatures. Average pore size, particle size, and overall density show appreciable change at higher temperatures, even with short exposure.

Longer exposure at a given temperature also increases the amount of structural change. Figure 39 shows the change in aerogel structure as a function of annealing time for a sample exposed to 400 °C for up to 336 hours. Structural data, characterized using SAXS, shows that initially the change to the structure is small for all relevant features. However, increased exposure results in more contraction of the pore sizes and reduction in the effective or mean scattering size. This decrease in effective scattering size results in a transmittance increase of more than 3%.

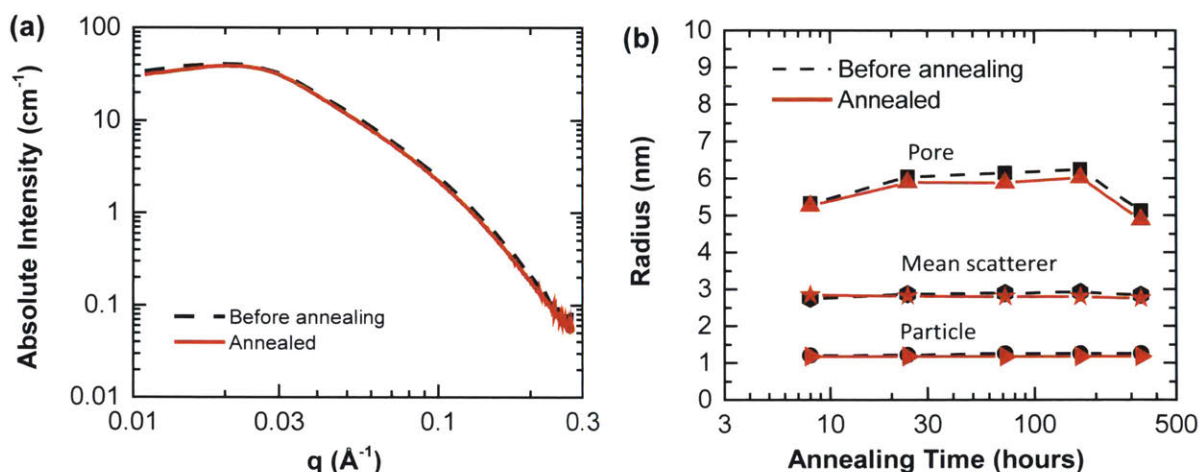


Figure 39. Small angle x-ray scattering (SAXS) data for TMOS samples annealed at 400 °C showing the structural characterization of the particle and pore network. (a) Scattering data of a sample before and after annealing for 336 h. Assuming that structural features are spherical, the particle ($q \sim 0.03$), pore ($q \sim 0.1$), and mean scattering size (full data range) can be found from the data¹². Because the data is spread over a large range of sizes, a subtle change to the raw scattering curve resulted in an appreciable change in size. (c) The structural feature changes of a TMOS sample annealed up to 336 h at 400 °C are shown. The data points for each annealing time represent the scattering radius before the indicated annealing time (Before annealing), and immediately after annealing (Annealed). Particle size was not affected significantly by annealing, but the pore size decreased more with annealing time, causing the mean scattering value to decrease with additional annealing.

Annealing offers another process for controlling and optimizing the structure of the aerogel. Generally, annealing at temperatures at or below 600 °C yields appreciable increase in transmittance, due to the structural decrease of effective scattering size. However, this change in structure also increases thermal conductivity due primarily to densification. It is important to consider annealing as another step in the process to achieve the optimal structure for a given set of application conditions.

5.5 SUMMARY

Fully optimized aerogels for windows must not only demonstrate high transmittance and clarity, but must also be free of optical defects for the lifetime of a window (>20 years). In this

chapter, we explore the various sources of defects unique to the high-clarity aerogel samples and how these defects can be minimized. Many of these defects are formed during solution-gelation and can be influenced by both the chemical recipe and the ambient conditions. However, these defects can be hard to quantify due to the high transparency of the material. Birefringence can be used post-drying to visually quantify defects and non-uniformities caused by structural changes in index of refraction. This same technique can be used to identify sources of damage during critical point drying. Additionally, in this chapter we discuss the benefits of using post-drying annealing to optimize the aerogel structure and density as well as reduce residual stress and remove contaminants. This knowledge used in combination with recipe optimization of the structure can yield high clarity, stable aerogels that are well-suited for a variety of window applications.

Chapter 6

6. Integrating Transparent Aerogels into Windows

Now that we have achieved high-clarity aerogels that can be optimized over a variety of recipes and synthesis methods, we can use validated models to consider the full performance of the aerogel in application. By placing the aerogel material between two panes of glass to create an aerogel double-pane (Figure 40), we can increase insulating performance of traditional windows while protecting the fragile aerogel for the anticipated 10+ year lifetime of window products. However, there are many additional considerations for integrating the aerogel into a full window product, including full window performance of optical, thermal, and acoustic transport.

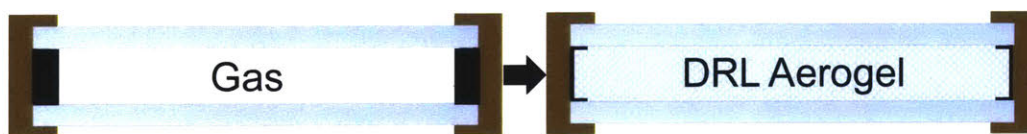


Figure 40. Proposed double-pane window design using DRL aerogel. The aerogel will replace the gas-filled gap and the edge-spacers of a typical double-pane (left) to achieve superior performance (right).

6.1 INITIAL AEROGEL DOUBLE-PANE PROTOTYPES

As discussed in Section 4.3, a major hurdle for aerogel windows has been their low mechanical strength. However, several prior works have proposed replacing some or all of the traditional gas-fill with aerogel as a means to improve thermal performance while protecting the material.^{68,69,72} This integration approach allows the aerogel to increase the thermal insulation of the window, as the aerogel has a thermal conductivity 30% lower than even argon gas. The development of highly transparent aerogels in this work (see Figure 41a) allows aerogel windows to overcome optical limitations that have prevented adoption of any window using monolithic aerogel for traditional applications. This allows for the fabrication, characterization, and optimization of transparent aerogel double-pane prototypes.

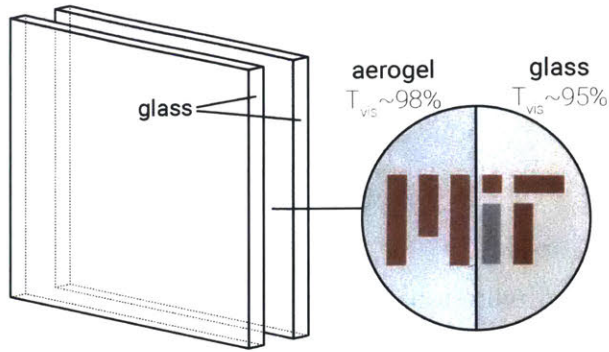


Figure 41. a) Ultra-clear aerogel sheet (6" diameter) with a porosity of 94%. Average pore and particle feature sizes are <10 nm diameter, allowing transmittance >98%, haze <2.0%, and thermal conductivity <13 mW/mK through 3 mm thickness. b) Proposed aerogel double-pane window with inset showing the ultra-clear aerogel compared to float glass. The aerogel replaces the air gap in a double-pane window.

6.1.1 Prototype Optical Performance

The first aerogel prototypes were designed to validate the optical properties of the high-clarity aerogel when combined into various stack configurations. These prototypes were made by sealing circular aerogel monoliths between two panes of glass using polyisobutylene, a sealant commonly used in the insulated glass industry. The aerogel sheets were made and/or cut to sizes that fit within the glass shape and size required for testing (typically ~5 in diameter circles) and sealed within the gap between two panes of glass as shown in Figure 42. Various spacer sizes were used to accommodate different aerogels and stack configurations in order to validate optical performance.

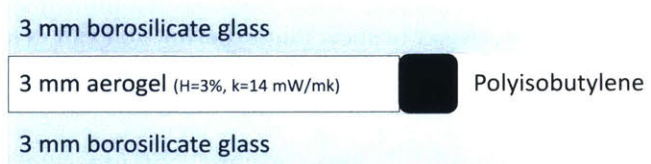


Figure 42. Double-pane window prototype using DRL aerogel. The aerogel will replace the gap traditionally filled with gas and the edge-spacers support the double-pane structure.

High-clarity aerogels primarily transmit incident light; it is expected that including aerogels will have very little effect on total transmittance. However, glass also has a small amount of haze (~0.5%) and some optical aberrations (such as waviness) that could exemplify optical imperfections when combined with the aerogel. We therefore fabricated several aerogels of 5 different high-clarity recipes to first test independently, and then each one combined in a double-pane stack configuration. We measured both visible transmittance and haze using a spectrophotometer and the same process described in Section 3.2.2 and compared the predicted stack performance (based on a model combining the optical properties of the glass and aerogels) to the full stack characterization. Results are shown in Figure 43 with a 1:1 line drawn to illustrate the deviation from prediction.

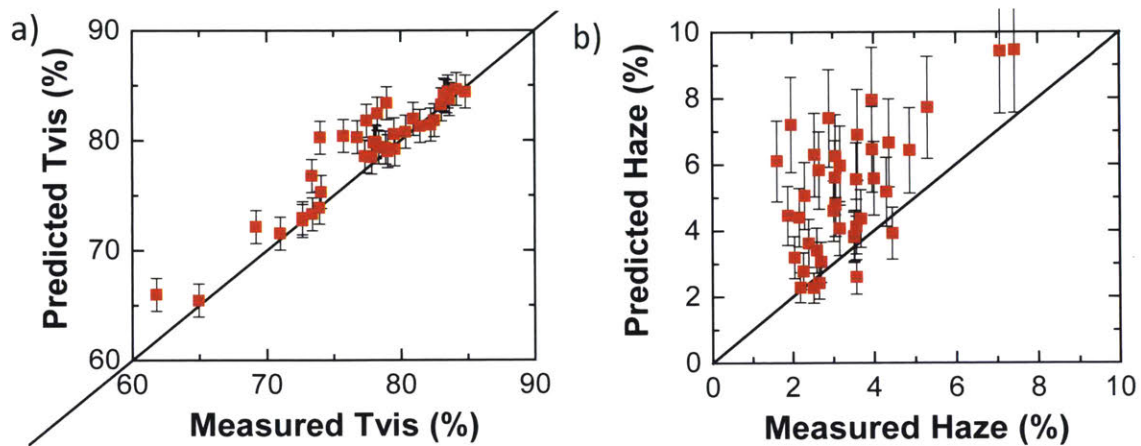


Figure 43. (a) Experimental visible transmission plotted against predicted visible transmission. A line of $y=x$ was added to the graph to show that experimental values align very well with predicted values. (b) Experimental haze plotted against predicted haze. A line of $y=x$ was added to the graph, which shows that experimental haze values differ more as the predicted haze value increases.

We see that visible transmittance of the stacks agrees well with predictions based on the individual stack components. The total hemispherical transmittance is not affected by placing the glass and aerogel into a stack configuration. However, the visible haze does measure as significantly higher than predicted at high absolute haze. During aerogel-only measurements, we have observed that any distance between the sample and the opening of the detector aperture increases the amount of scattered light that is measured by the detector. In the definition of haze, we see that increased diffuse transmittance results in a higher haze. When the aerogel is placed in a stack, the distance between the scattering-dominated aerogel and the aperture opening is increased. Therefore, by nature of the measurement the amount of scattered light when combined with a glass

stack will be higher than predicted. As the aerogels become hazier and/or thicker, this mechanism of scattering increases and results in more error at higher hazes.

As discussed in Section 2.2, window designs are customized for climate, occupancy, building type, etc. Aerogel windows must also be able to meet the diverse needs of buildings, which extends beyond the optical clarity to also include control of the solar heat gain. High-clarity aerogel also has a high solar transmittance, often transmitting >90% of the solar spectrum. For applications where this solar energy is not desired, such as in cooling dominated locations, aerogel windows can utilize the same low-cost solar filtration coatings to reduce heat gain.

Since the aerogel is volumetrically dominated by air and has an effective index of refraction of 1.02 (close to air) we expect that for wavelengths < 3 μm the optical properties of the aerogel prototype will behave similarly to that of an air-filled prototype. Figure 44 shows that when adding aerogel in combination with a solar-control coating, the results are almost identical to a prototype filled with air. This demonstrates that the aerogel does not limit the performance of traditional solar and optical tints/coatings, giving it a broader range of applications within the window market.

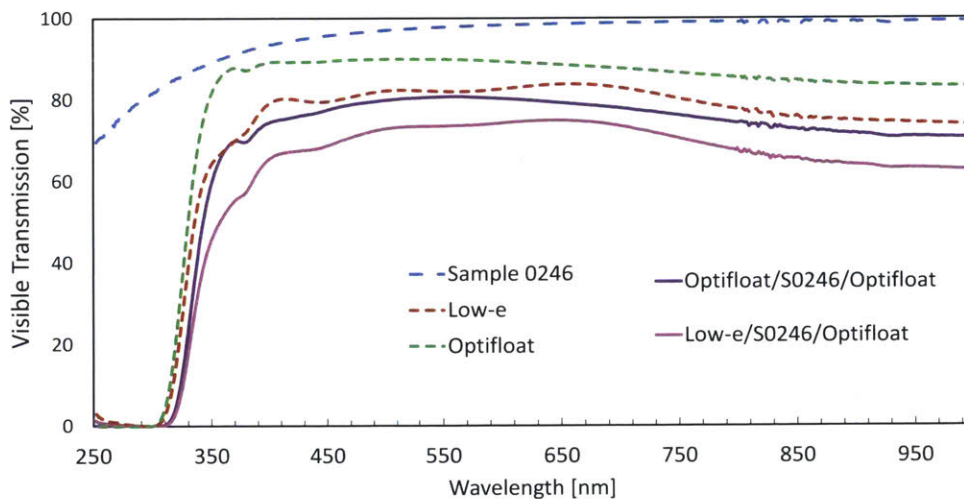


Figure 44. Visible light transmission of aerogel Sample0246 compared to Pilkington’s Energy Advantage low-e coating and Optifloat glass, as well as transmission of insulated glass unit stacks that include Sample0246 with the glass. Due to the aerogel’s high transparency, it does not significantly affect other strategies to control SHGC.

The aerogel material is highly solar transparent, while being very opaque to long-wave radiation. Experiments have shown that the aerogel has a SHGC > 0.90, but that it can be controlled using traditional coatings to be customized for each window application. Figure 23 from Section 4 shows the transmission of float glass compared to the transmission and haze of a

4 mm thick sheet of aerogel. Due to the high transparency, the aerogel can be used with other strategies to control SHGC, UV, IR, etc., without adversely affecting their performance in visible wavelengths. Further testing is required to determine the effect on IR wavelengths and low-e coatings, however, insulated glass unit stack configurations (discussed in Section 6.2) that use a high-clarity aerogel with a gas gap would not adversely affect the low-e coating performance.

6.1.2 Prototype Acoustic Performance

As discussed in Section 4.2, sound transmission is a value-added property of the aerogel that can improve occupant comfort. The porous nature of aerogel combined with its solid backbone density allows it to intrinsically have soundproofing properties. However, the sound-proofing fundamental behavior is similar to glass, meaning that the aerogel has limitations to the incremental sound-proofing capabilities. The aerogel still provides a benefit (~4-8 db reduction, see Figure 45) over a gas-filled window, but the benefit is less than other strategies in use today, such as laminated glass.

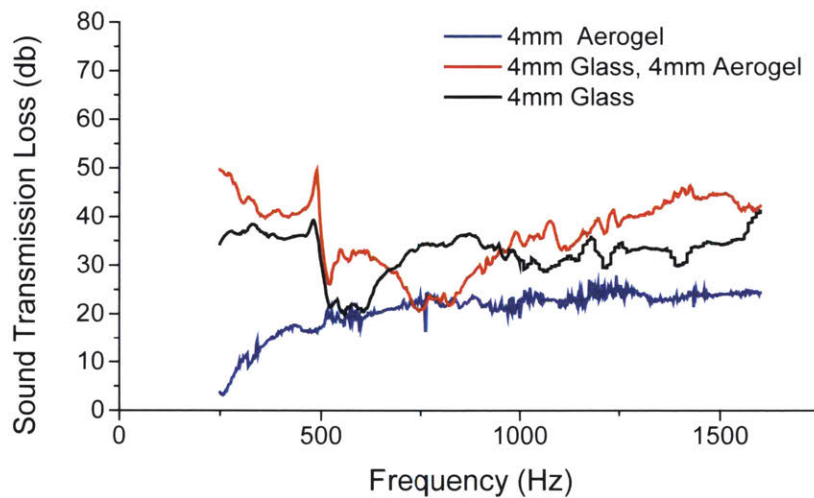


Figure 45: Sound transmission loss comparison of a 4 mm thick aerogel and a 4 mm glass sheet in ambient. Reflection is the dominant sound transmission loss mode in both the aerogel and glass sheet. The data shows that sound transmission can be increased by adding the aerogel layer to the glass layer, with large enhancement expected when the aerogel pore pressure is decreased.

However, if an aerogel window is also evacuated, the sound reduction can be increased. To investigate the sound-proofing potential further, we sealed several samples of aerogel between glass at a pressure of ~ 1 kPa. These samples were then tested in an impedance tube using the same procedure as described in Section 4.2. Results are shown in Figure 46.

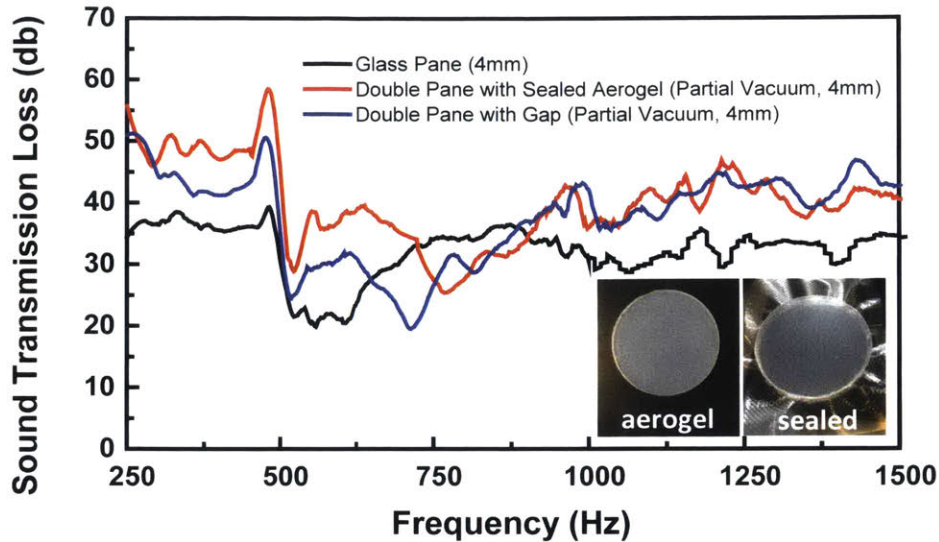


Figure 46: Sound transmission loss comparison of a 4 mm thick aerogel sealed in a double-pane, a 4 mm air gap at ~ 1 kPa, and a 4 mm glass sheet in ambient. Reflection is the dominant sound transmission loss mode in both the aerogel and glass sheet. The data shows that sound transmission can be increased by adding the partially evacuated aerogel layer to the glass stack.

Figure 46 shows that evacuated aerogel reduces sound transmission by 10-15 dB across the majority of the frequencies shown compared to glass. In particular, the low frequency regime is better insulated than compared to a double-pane gap at the same partial pressure (~ 1 kPa). Comparing to a traditional double-pane window at full pressure, this provides a promising improvement in sound performance that is worth investigating further.

6.1.3 Prototype Thermal Performance

The U-Factor is a standard measure of the total window heat transfer coefficient as described in Section 2.1.1. Primarily, this is used as a measure of “how well a product can keep heat from escaping from the inside of a room”.¹¹⁷ While the U-Factor of the aerogel may be very low as a standalone material (see Figure 47) due to the low thermal conductivity, when the aerogel is packaged into a window, sealed at some pressure, and installed with a frame, the total window U-Factor may be much higher than anticipated due to the necessary additional components. It becomes important to understand the effects of the aerogel and window design on the final U-Factor with respect to other properties, given that the full design optimum might not be the same as for the aerogel on its own.

Using the aerogel thermal properties that have been validated at room temperature and pressure by measurements, we can approximate performance as a function of insulating gap thickness.

Figure 47 shows the modeled performance of various window configurations, including an aerogel in ambient conditions and sealed at a reduced pressure. Compared to air, aerogel can achieve the same U-values at significantly reduced thickness, with modeling indicating that aerogel can be competitive at as little as 2 mm of thickness.

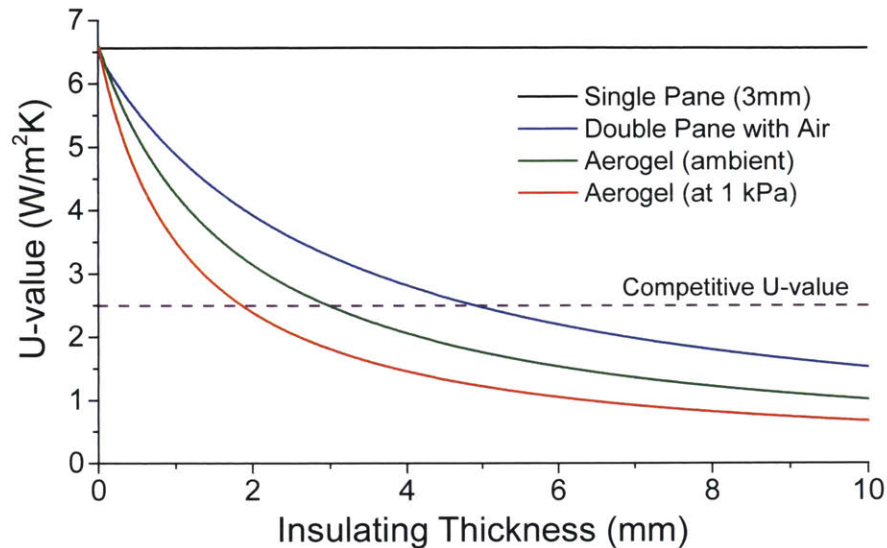


Figure 47: U-values at center-of-pane for different window designs as modeled from thermal conductivity (no consideration for convection) per the NFRC standard conditions. To be competitive in the window market, it is necessary to be at or below 2.5 W/m²K. Aerogel at both ambient and modestly reduced pressure show significantly better performance at reasonable thicknesses.

However, these U-factor values represent the material properties, and not the full unit assembly. In order to fully quantify the optical and energy performance, it is necessary to test the window unit as a whole. This can be done by testing the insulated glass unit, which for our design includes the aerogel sealed between two panes of glass using a desiccant spacer and a silicone seal at the edge, similar to the small prototypes shown in Figure 42.

6.2 FULL-SCALE AEROGEL PROTOTYPE

Fabrication of pristine aerogel samples were initially limited in number and size, making the small prototypes best suited for optical and acoustic characterization. However, full window unit thermal testing requires a large area to accurately estimate heat loss during standardized conditions (as described in Section 2.1.1). Thermal measurements must be done on prototypes of sufficiently large area so that edge effects and local property fluctuations (such as cracks) don't create a dominant thermal pathway that adds error and uncertainty to the measurement. To achieve this, we fabricated a full window prototype of size 1 x 1 sqft featuring the same sealing strategy used

in small prototypes. However, because the aerogels cannot be fabricated in sizes larger than 8” diameter with the lab scale equipment, several batches of samples were fabricated using the same recipe and cut to a standard size. Hexagons were chosen as the shape used because of their tight close packing and their ability to maximize the usable material from the standardized circular molds used to form the raw aerogel material. The aerogel samples were made using identical processes and handling to the greatest degree possible. Also, as samples were cut and assembled, the excess material was saved for characterization to quantify uniformity within the prototype. Figure 48 shows an image of this prototype.

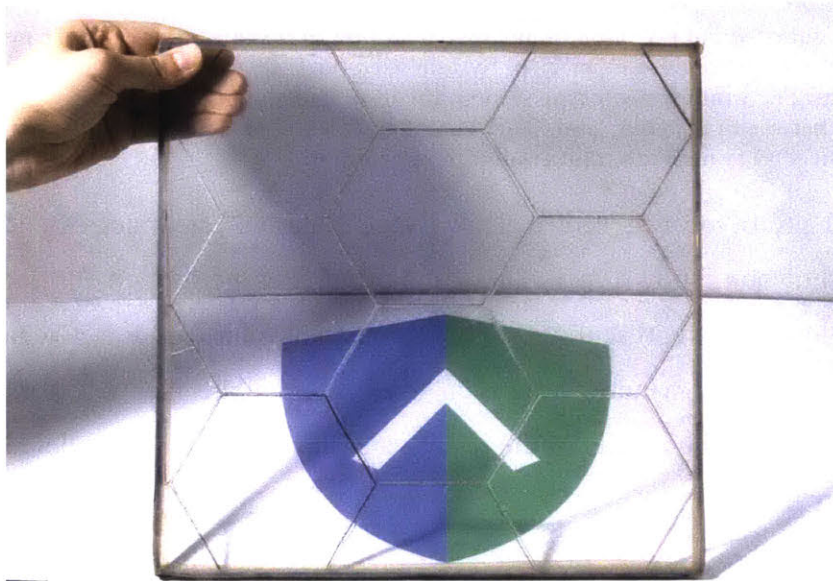


Figure 48. Aerogel double-pane prototype made of ~ 4 inch tiled hexagons. The full prototype is 12” x 12” featuring a 2 mm thick layer of nominally identical aerogels.

The U-factor is tested using the prescribed conditions in Section 2.1.1, but it is not trivial to simulate these conditions with accuracy at a relevant scale. One common approach is to use a rotatable guarded hot box (see ASTM standard C1363²⁶) that uses chambers separated by an insulating material to simulate the heat flow into or out of a building. The chambers are set at fixed temperatures and the meter chamber is used to quantify the energy needed to maintain the temperature difference (very similar to the guarded hot-plate method described in Section 4.1). The energy needed to maintain the “hot” metering is used to calculate the effective thermal transfer through the area of the prototype, representing the U-factor.

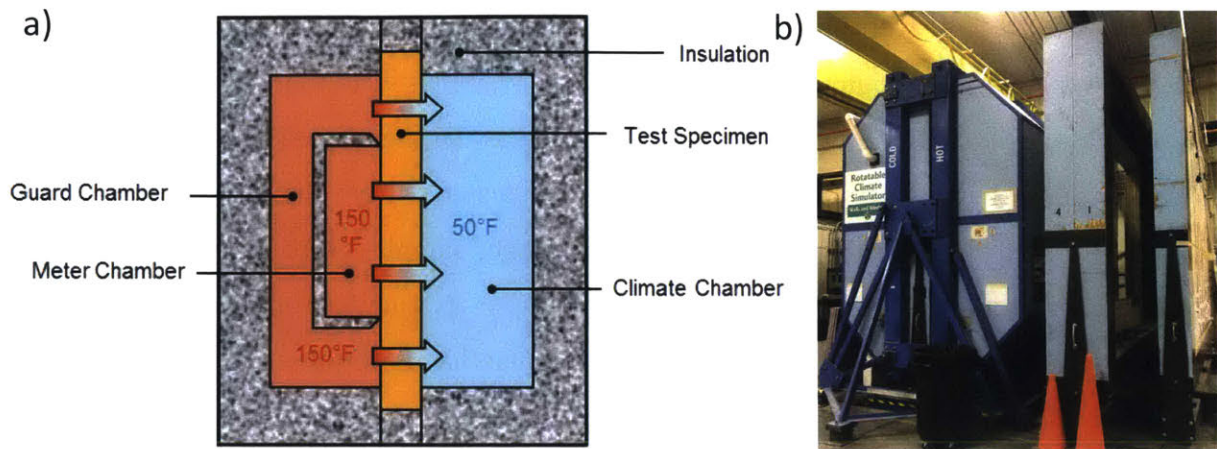


Figure 49. Rotatable guarded hot box used to measure heat flow across a wall area. (a) Diagram showing general design of metered chamber system.¹¹⁸ (b) System used for U-factor characterization at Oak Ridge National Laboratories. For window prototype testing, the insulated glass unit is mounted into the center wall section and sealed in between the “cold” and “hot” chambers. Heat flow across the prototype is measured by monitoring the heat needed to maintain the setpoint temperatures.

Our 1 x 1 sqft prototype was sent to Oak Ridge National Laboratories and tested in their rotatable guarded hot box, shown in Figure 49. Testing was performed for 3 different sets of temperature set points, each representing ~ 22 °C temperature difference between chambers. The flow of energy through the window was then used to calculate the U-factor for each set of conditions. Table 4 shows the results of the testing and the performance modeled using the same approach is Section 4.4.

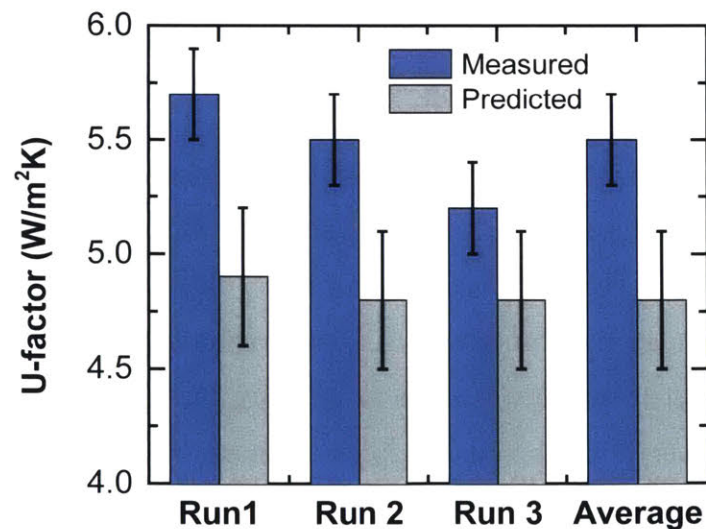


Figure 50. Experimental and modeled U-factor of 1 x 1 sqft aerogel double-pane prototype. Experimental measurements were performed in a rotatable guarded hotbox at conditions described in Table 4. The prototype window was made using tiled 2 mm aerogel samples.

Table 4. Experimental results from rotatable guarded hotbox thermal measurement. Temperature difference across the chambers was held at 22.2 °C for all runs.

	Hot Chamber Temperature	Cold Chamber Temperature
Run 1	35.0 °C	12.8 °C
Run 2	1.7 °C	23.9 °C
Run 3	-17.8 °C	4.4 °C

We find that the model over-predicts insulating performance (under-predicting U-factor) across all runs. We also notice that the measurement is more influenced by absolute chamber temperature than predicted by the model. Both of these trends may be attributed to inconsistencies across the various samples used, and the relatively small area of the prototype. At small thicknesses, the U-factor of the aerogel can vary by up to 30% per millimeter of material. The highest percent difference between the model and experiment is 15% (during Run 1 conditions), corresponding to a 0.5 mm error in thickness. The samples used in the prototype were measured in only 2 locations on the edge of the sample in order to avoid damaging the fragile material. It is likely that samples have deviation from the 2 mm target thickness, and that they also may not be of uniform thickness. Unlike the select samples taken for thermal characterization using the guarded hot-plate (see Section 4.1), the large number of samples used in this prototype limited precision, and may have resulted in the differences seen between the model and measured performance. Additionally, it is very uncommon for industry to test insulated glass units smaller than 5 sqft, which also results in the measurements of this prototype having more error than a standard test. Considering these factors, the results do indicate superior performance to air, and are a step toward validating full window performance with an aerogel.

The goal of measuring the U-factor of this initial prototype was primarily to validate the modeled performance and demonstrate viability of creating aerogel insulated glass stacks at window-relevant sizes. We can now take the measured performance and use our model to investigate pathways to increasing performance beyond this demonstration. Figure 51 shows the modeled improvement in performance for the measured and predicted prototype performance that can be achieved using model-guided optimization per the improvements described in Table 5. We see that the final performance for the measured performance of the prototype is 1.5 W/m²K.

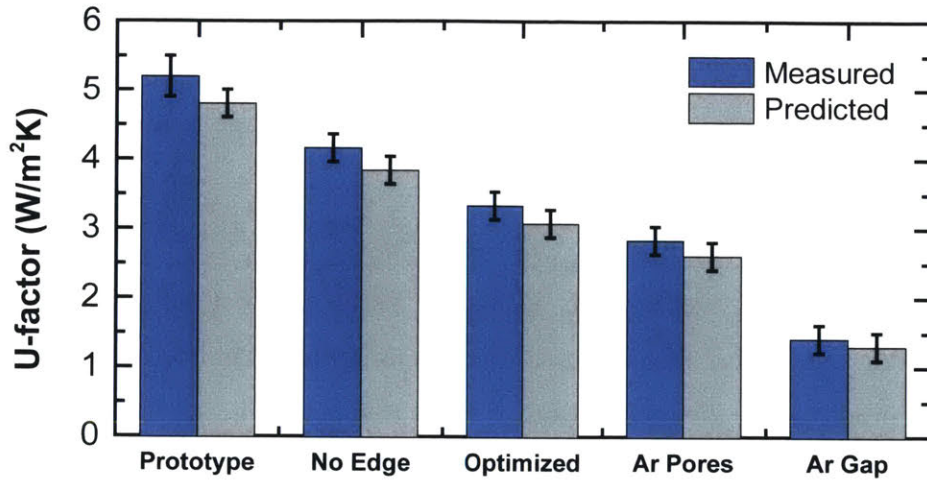


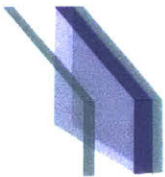
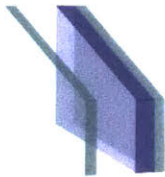

Figure 51. Experimental and modeled U-factor of 1 x 1 sqft aerogel double-pane prototype utilizing various additional design strategies to improve insulating performance. Description of model-suggested design improvements are shown in Table 5. Both the experimental and model predictions of the prototype can be improved significantly by utilizing optimized aerogels in combination with argon gas-fills.

Table 5. Experimental results from rotatable guarded hotbox thermal measurement. Temperature difference across the chambers was held at 22.2 °C for all runs.

Legend	Improvement	Description
Prototype	-	Measured and predicted performance of prototype as fabricated
No Edge	20%	Eliminating edge effects (achieved by fabricating a sufficiently large prototype)
Optimized	20%	Using a continuous optimized aerogel recipe of uniform 3 mm thickness
Ar Pores	15%	Replacing air in aerogel pores with >90% argon gas
Ar Gap	50%	Using 3 mm aerogel and 9 mm argon gap with low-e coating

Using this same approach, we can also explore many other integration strategies that may provide more improvement of thermal performance for the same technical and material costs. The material itself is >95% void, making it too weak to take the structural purpose of a pane of glass. However, the aerogel material does add more structural integrity than a traditional gas-fill, creating opportunity to redesign windows to use less bulk glass and framing elements. Table 6 explores several integration strategies that have promising advantages for U-factor performance while still fitting within the traditional double-pane footprint and weight requirements.

Table 6. Potential insulated glass unit stack configurations with predicted performance. Images show proposed stack designs where the aerogel (darker blue sheet) replaces some or all of the traditional gas-fill in a double-pane configuration. The aerogel material is bonded to and supported by at least one pane of glass.

			
Stack Configuration	<ul style="list-style-type: none"> • 3 mm glass • low-e coating • 9 mm Ar • 3 mm aerogel • 3 mm glass 	<ul style="list-style-type: none"> • 3 mm glass • low-e coating • 9 mm Kr • 3 mm aerogel • 3 mm glass 	<ul style="list-style-type: none"> • 3 mm glass • 9 mm aerogel in Ar • 3 mm glass
U-factor (BTU/ft²·hr·F)	0.195	0.137	0.171
Visible Transmittance	0.76	0.76	0.70

6.3 DOUBLE-PANE DURABILITY

Another important aspect of full window performance is the durability. Homeowners spend 10 years on average in their homes, so consumers are unlikely to invest in any product or replacements with lifetimes shorter than that threshold. Additionally, the embodied energy and cost of installation for replacing windows far outweighs the benefits unless the current products have significant issues, such as leaks, fogging, condensation, breakage, etc. These failure mechanisms are caused by a variety of environmental sources that compound over decades in the building envelope. Thermal cycling, UV-degradation, freezing, humidity, etc. can all cause the materials and interfaces to break down with time. Therefore, durability and compatibility of the aerogel with the other materials in windows is very important to application.

Silica aerogel is made using a process that results in a pure glass material and do not contain any coatings, polymers, or fine structures that degrade with time. We have performed rigorous study of thermal exposure up to 600 °C (with some cycling) as well as early exposure testing using accelerated UV and condensation testing. These results show promising resistance to degradation; however, we plan to quantify this exposure more explicitly in future works as we create prototypes large enough to undergo industry testing.

6.3.1 Extreme Environmental Exposure

Thermal cycling was explored in the presence of a high-humidity environment. The test setup was designed to expose the aerogel to extreme conditions: 400°C with ~1 atm air with >80% humidity for 8 to 24 hour increments. After exposure the aerogel was measured and subsequently re-exposed to the same conditions until total exposure time exceeded 100 hours. The primary properties of interest were the total visible transmittance, measured by spectrophotometer, and the effective thermal conductivity.

The durability test was conducted in an environment at ~1 atm with >80% humidity, while the aerogel sample was held at a temperature of ~400 °C. Figure 52 shows a photograph of the setup which consists of a commercially available ultrasonic humidifier connected to a stainless steel chamber. The aerogel samples (>8 mm thick) were kept in a ceramic dish on the hotplate which was maintained at 450 °C to ensure a sample temperature of >400 °C. Steam from the humidifier was continuously introduced into the sample chamber to ensure humidity >80%.

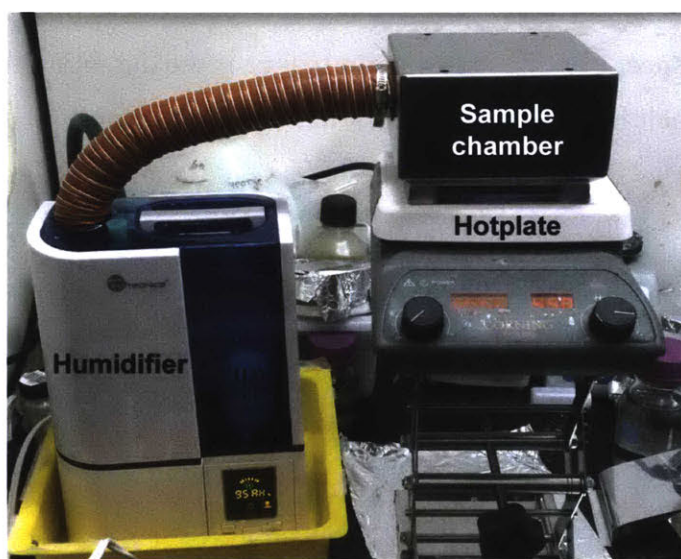


Figure 52. Experimental setup for extreme environmental testing. The hot plate exposes the aerogel to >400 °C on the bottom surface while the humidifier continues to bring in room temperature air at >80% humidity. The sample is exposed to these conditions for 8 to 24 hour increments and then characterized for optical performance.

We measured the transmittance of the aerogel samples before, during and after durability testing. The results show an increase in the total transmittance due to an annealing effect that leads to structural relaxation and a decrease in average scattering size observed at temperatures >300 °C.⁷⁸ Figure 53 compares the transmittance of the aerogel sample fabricated using the TMOS

precursor before, during and after durability testing in high humidity conditions. It is important to note that this annealing effect was mostly due to the high temperature. However, high humidity may have caused the small fluctuations in transmittance over time. Overall, the transmittance increased from 92.6% before the testing to about 95% after the completion of testing. Fluctuations in transmittance over the course of testing can be attributed to the high humidity as mentioned previously, as well as increased defects in the sample due to repeated handling.

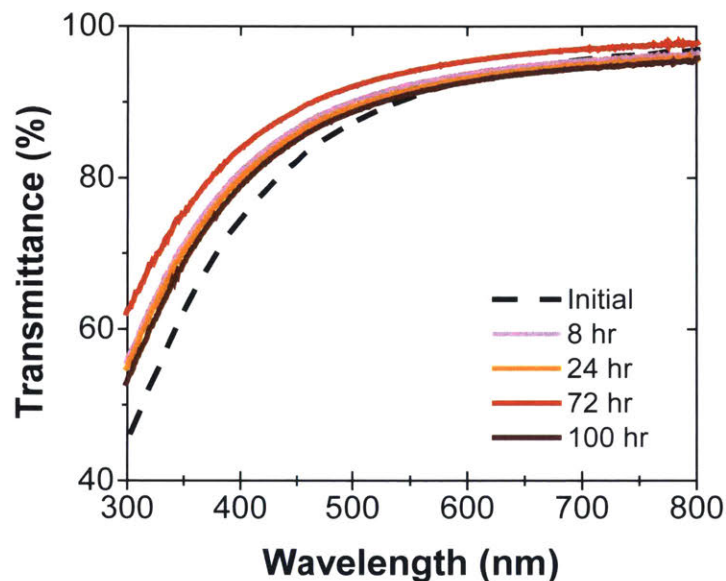


Figure 53. Total transmittance comparison of TMOS sample before, after 8, 16, 32 and 100 hours of annealing at 400°C in 80% humidity. Transmittance is shown to increase with exposure to high-temperature annealing, with no adverse effects caused by the exposure to the high humidity environment.

In addition to the optical properties, the heat transfer coefficient of the aerogel sample was measured before and after exposure for 100 hours. Table 7 summarizes the thermal measurement results of the durability testing of aerogel samples fabricated using both TMOS and MS-51 precursors. The heat transfer coefficient was measured between a hot junction temperature of 400 °C and cold junction temperature of ~250 °C. ($T_H = 400$ °C, $T_C = 150$ °C for MS-51 post-cycling test; result shown in Table 7 scaled to $T_H = 400$ °C, $T_C = 250$ °C).

While the measured heat transfer coefficient decreased for the TMOS sample after durability testing, it increased for the MS-51 sample. The reason for the change in heat transfer coefficient is not entirely clear at this point. The change in IR absorption is possibly due to physical/chemical modification of the aerogel, degradation of samples due to handling, or a combination of both. Overall, accounting for the decrease in heat transfer coefficient when the cold junction temperature

is maintained at 50 °C (as opposed to 250 °C for the results shown), the pre- and post-cycling heat transfer coefficients are expected to be <10 W/m²K for both TMOS and MS-51 aerogel samples.

Table 7. Result summary of thermal durability testing shows measured heat transfer coefficients (between $T_H = 400$ °C and $T_C = \sim 250$ °C).



Sample	Thickness (mm)	Heat transfer coefficient (W/m ² K)	
		Pre-cycling	Post-cycling
TMOS	8.76	6.44 ± 0.3	5.32 ± 0.4
MS-51	8	9.60 ± 0.5	10.6 ± 0.7

6.3.2 Hydrophobicity & Condensation

A major potential failure mode for aerogel is exposure to liquids or humidity. Silica aerogel is naturally hydrophilic, but the small, distributed pores within the surface cannot sustain the induced capillary pressure mismatch when a water-vapor interface is introduced. Any liquid interface is capable of destroying the nano-features. One commonly proposed solution is to chemically make the surface conformally hydrophobic by treatment during the wet-gel stage as proposed by Günay *et al.*¹¹⁹ However, generally aerogels made hydrophobic by chemical treatment tend to have higher IR transmission and are less effective at suppressing heat losses at high temperatures.¹²⁰

To validate these assumptions, several samples were made chemically hydrophobic using hexamethyldisilazane and the process described in Tabata *et al.*⁹⁰ Table 8 shows the comparison of hydrophobic properties to its non-hydrophobic sibling. Here we see that a hydrophobic coating on the low-haze aerogel does not improve the relevant optical and thermal properties.

Table 8. Comparison of naturally hydrophilic silica aerogel compared to a hydrophobic aerogel. The hydrophobic coating has almost no effect on the visible transmittance, but increases the average scattering radius and decreases density.

	Hydrophilic	Hydrophobic
		
Visible Transmittance	96.0%	95.8%
Scattering Radius (nm)	3.12	3.37
Density (kg/m³)	165	147

Next, we wanted to explore the failure mechanism for extreme condensation conditions for the hydrophilic and hydrophobic samples. To approximate conditions for application, a solid copper surface was mounted to a cooling loop and set to $-8\text{ }^{\circ}\text{C}$. This block was then placed inside of a transparent box with a programmable humidifier and temperature and humidity sensors set to test the ambient conditions. Two samples of aerogel, a hydrophilic and hydrophobic sample made from the same recipe, were attached to the copper block using thermal paste. Figure 54 shows the mounted aerogels and the copper plate hooked up to a cooling loop. The aerogels were then exposed to increasingly higher relative humidity until failure.

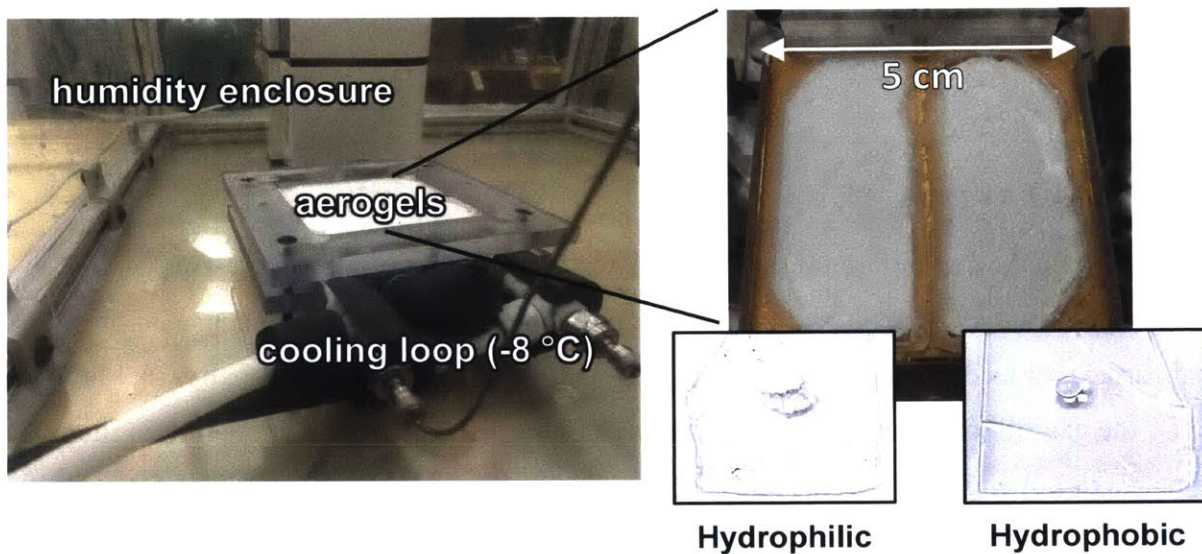


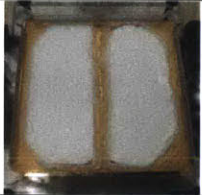


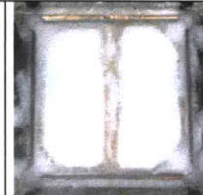
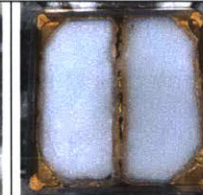
Figure 54. Hydrophilic (left) and hydrophobic (right) aerogel samples mounted on a copper block. The copper block is cooled via a cooling loop to $-8\text{ }^{\circ}\text{C}$ and then placed into a humidity chamber.

Table 9 shows the progression of both aerogels from initial exposure to failure. At relative humidity $< 70\%$, both aerogels remain undamaged macroscopically. However, above 70% ice begins to form all around the copper block. At this point, vapor began to condense not only around the aerogel, but at the bottom surface of the aerogel. Initially, this started only on the hydrophilic aerogel, but after several hours of exposure the hydrophobic aerogel experienced the same mode of failure.

From the setup, it is unclear if the same mechanism of failure would occur if the interface of the aerogel and the copper block were more perfectly mated, however it is apparent that if there is an opportunity for the aerogel to condense at the bottom surface of the aerogel, that is where failure will start. Once failure began at the bottom surface, this nucleation site grew very quickly and damage for both aerogels occurred within an hour of continual exposure. After the aerogels were

destroyed, the humidity conditions were removed gradually and the aerogel was allowed to dry. The result was a densified and cracked aerogel, with both the hydrophobic and hydrophilic samples completely damaged.

Table 9. Hydrophilic (left) and hydrophobic (right) aerogel samples exposed to increasing relative humidities. The aerogel is attached to a cooled copper block to which the aerogel is attached with thermal paste.

					
Base Temperature	-8.0 °C	-7.7 °C	-7.6 °C	-7.2 °C	25 °C
Relative Humidity	35.8 %	55.0 %	68.8 %	89.4 %	34.6 %

6.3.3 Seal Failure

A common method of failure for double-pane windows is failure of the seal. This can allow moisture to permeate into the interior surface which can degrade coatings, condense on the internal surface, or lead to outgassing and fogging within the window. Additionally, seal failure can cause the gas-fill, often argon, to lose pressure or leak that can cause degradation in thermal performance or bowing of the sealed unit.

The aerogel reduces the performance degradation of a window during seal failure. In the event of seal failure, the difference in aerogel performance in air (~13 mW/mK) compared to performance in argon (~10mW/mK) is small compared to the difference between air and argon (26 mW/mk compared to 17 mW/mK, respectively). Figure 55 shows a comparison of two insulated glass units (no coatings) as argon is replaced by dry air over the lifetime of the window. As described in ASTM E 2188, when the window is below 50% argon fill the window has effectively failed. We see that the aerogel window requires an extra 25% decrease in argon content before reaching the same U-factor as the standard double-pane.

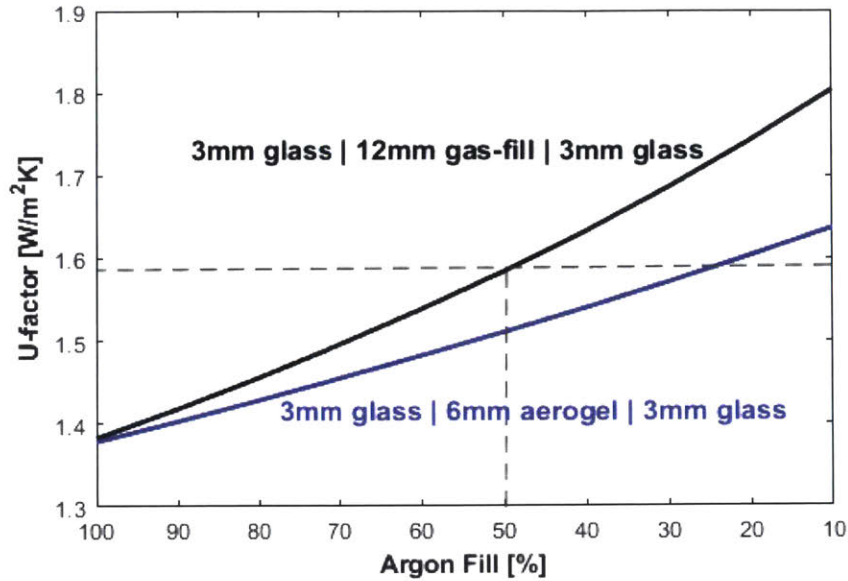


Figure 55. Comparable insulated glass units illustrating the degradation of performance as the argon fill is replaced by air. The aerogel insulated glass unit can undergo an additional 25% fill loss before reaching the same U-factor at failure as the gas-filled window.

6.3.4 Accelerated Ultraviolet Exposure

We also investigated accelerated UV exposure to ensure there were no adverse effects to the aerogel for extended sunlight exposure. To do this, we placed an aerogel sample under a UV source with a long-wave output peaking at 365 nm at a power of 100 W for a 0.01 m² spot size (equivalent to ~250 suns of UV exposure). After running the lamp for 20 hours, we removed the sample and characterized the properties (density, scattering size, visible transmission, thermal transmission). Results show that there was no appreciable change or degradation of any properties for an as-made aerogel (see Table 10). This is expected as the base material of our aerogel is silica, which is known to have high UV stability. However, if additional modifications, coatings, or layers (such as the hydrophobic coatings discussed above) are to be used in the design of the receiver, it is important to consider the effects of UV stability.

Table 10. Comparison of aerogel before and after accelerated UV exposure (~250 sun equivalent for 20 hrs). Solar UV exposure was simulated with a lamp with peak output of 365 nm at 100 W. A sample from each of the two fabricated sample batches (discussed in the main paper) was selected to investigate the changes to structure and performance. None of the relevant properties showed any significant change.

Sample	Scattering Radius (nm)		Visible Transmittance (%)		Density (kg/m ³)	
	Before exposure	After exposure	Before exposure	After exposure	Before exposure	After exposure
Batch 1	3.17	3.20	96.4	96.1	176	174
Batch 2	3.22	3.22	95.5	95.2	182	204

6.4 SUMMARY

In this chapter, we present the development and testing of optimized aerogels into double-pane insulated glass unit prototypes. This integration strategy was based on the limitations of the aerogel mechanical properties, as well as consideration for the existing building requirements. These prototypes were used to characterize optical and acoustic performance of full insulated glass units and full U-factor performance of a 1 x 1 sqft prototype window. Experimental measurements provide sufficient concept validation to allow exploration of different integration strategies for different potential window products.

Durability and potential lifetime are also important considerations for aerogel insulated glass units. Therefore, we also explore possible failure modes of application conditions including extreme thermal exposure, high humidity and condensation, seal failure, and accelerated UV exposure. The results of these early experiments are very promising, indicating that aerogel is able to withstand temperature > 200 °C, relative humidity > 60%, and ultraviolet exposure for more than 6 months without degradation of the nanostructure or optical quality.

Chapter 7

7. Techno-economic Viability of Aerogel Windows

While optical clarity and thermal performance are important to the function of a window, it is the cost-benefit of building fenestration that dictates the effectiveness. For example, installing a triple-pane window in a home in a cold climate such as Duluth, Minnesota will yield energy savings of about ~14%.¹²¹ However, these energy savings will require more than 30 years to recover the upfront cost of the window, making it a poor choice for the average homeowner who lives an average of 10 years in their home. Now consider a home in New York that has the original single pane windows and frames installed 60 years ago. Winter drafts and cold, radiative glass make indoor comfort a nightmare. In this home, the building owner may value his or her thermal comfort more highly than the potential energy savings and the payback period may be given little consideration. It becomes very important to understand the practical considerations for purchasing window products in order to better develop innovative solutions for consumers.

In particular, most of state-of-the-art strategies in development today do not lead to reasonable payback periods at the current stage. However, there are still applications for more efficient, sustainable windows. One of the biggest drivers for energy efficient window development is the end user's desire to reduce energy consumption and carbon emissions. Increases in the number of passive homes and energy certified buildings has shown that building owners and occupants care about the environmental impact of inefficient buildings. These markets drive thermal innovations within the fenestration field, but that also means that solutions must be sustainably sourced. If products rely on a high upfront energy cost or exotic materials, their overall impact will be greatly reduced. It is important to keep the full window lifecycle in mind when designing new products.

Another important practical consideration for windows is the tradeoff between their benefits in regard to lighting and aesthetics compared to their high thermal losses. In fact, codes have been established in many cities that limit the total percentage of windows installed in a building's envelope.¹²² However, these codes can be circumvented if the building can demonstrate its total energy consumption is less than an equivalent amount. One strategy to overcome this prescribed limitation is to select windows that are nearly as insulating as traditional walls. In this case, the

application of high-performance windows is highly valuable, but only if total cost and weight of the full window assembly is not prohibitive.

7.1 AEROGEL COST

The complex manufacturing chain that is typical for window products (often including 4+ stakeholders) leads to a lack of motivation and/or influence by any single entity to dramatically innovate or change the status quo. We have spoken to over 200 stakeholders within the window value chain to understand the value we can provide to customers. In the United States market, “Industry is now facing a revolution. It’s getting harder to get better” per Barry Corden of Guardian Glass Industries. The current insulating strategies (air gaps, coated glass, etc.) are reaching the limitations of cost-effective improvement, leaving manufacturers without a clear path to enhance performance to satisfy building code. A solution like high-clarity aerogel prevents conduction, convection, and radiation heat losses in one technology, providing significant improvement. However, a technology must also show a clear path for low-cost manufacturing in order to be widely adopted. With a price to consumers of less than \$3-4 /sqft, transparent aerogel has the same potential as low-e coatings, which are found on virtually all new windows. This is a significant consideration if the time and energy expended in research is to be successful in making the transition to market and obtainable for the benefit of everyman.

7.1.1 Integration into Existing Manufacturing

The most cost-effective commercialization plan for transparent aerogel is to supply the material directly to insulated glass unit (IGU) manufacturers (see Figure 56). An entity can produce and sell aerogel to these manufacturers, who assemble and seal it into the IGU for residential houses and commercial buildings. This is the most technically feasible approach to incorporate into existing products, as it allows us to take advantage of existing manufacturing equipment and established sales channels. The custom nature of window manufacturing makes third-party suppliers a highly advantageous business model – this strategy is already being used for window coatings. Furthermore, using existing manufacturing channels allows us to serve a diverse market comprising windows with different styles, sizes, and designs without additional equipment or costs.

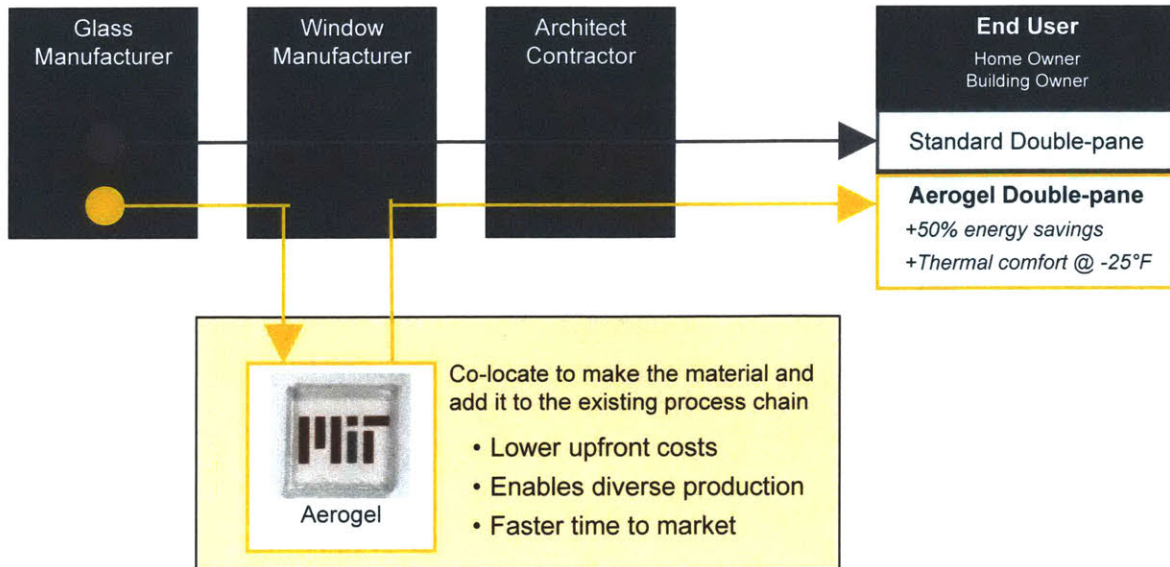


Figure 56. Typical manufacturing process for windows including the aerogel material. Insulated Glass Unit (IGU) manufacturers simply buy and seal the aerogel into a glazing unit, replacing gas fills in the current process. For production launch, aerogel manufacturing will be co-located and include pilots targeted to reduce any impact the aerogel material has on traditional manufacturing. Selling directly to IGU manufacturers allows us to take advantage of the existing equipment and distribution channels.

7.1.2 Aerogel Production Costs

The window industry as a whole is characterized by its cost-competitive nature. Therefore, adoption of aerogel in windows is driven by its amazing performance at relatively low cost. However, currently the ultra-clear aerogel technology exists only in lab-scale sizes (6 inch diameter samples). We have demonstrated the ability to achieve clarity competitive with glass and thermal properties competitive with exotic gases, but with lab-scale sizes and unit economics. To estimate the cost and price of the aerogel at scale, we must account for materials, processing, and labor needed in a commercial process.

The major costs from this process come from capital expenditure and cost of goods sold, with long term costs driven by chemicals (39%) and the amortization of capital equipment (18%). The capital expenditure is dominated by large drying equipment (\$2 million per 340,000 sqft of annual material capacity) needed for production. However, by taking advantage of long equipment lifetime (20+ years demonstrated in industry) and key partnerships with existing glass manufacturers who are also familiar with capital intensive manufacturing, scale-up can be cost competitive. At established production levels, amortization of each dryer normalized per sqft of aerogel produced will be 0.32 \$/sqft.

Costs of goods per unit produced (per square foot of material at a 3 mm thickness) is driven by a variety of sources. The production process requires well-established chemicals. In addition to water, ammonia, pure alcohol, and carbon dioxide, the primary chemical is tetramethyloxysilane, a ubiquitous and relatively low-cost silicate precursor. Other unit costs include:

- Labor for production (1 worker can operate 3 dryers for 3 shifts per day)
- Royalties (to license various patents)
- Non-operating capital and facilities
- Maintenance
- Utilities

These factors drive the unit cost to be \$1.52 /sqft by the time production reaches 4.5 million sqft of annual production. While initial costs are expected to be higher (~\$3.5 /sqft at a 0.3 million sqft production volume), costs can be reduced through material optimization, development of better production processes, and increasing production to favorable economies of scale.



Figure 57. Unit cost of aerogel production driven by chemicals needed for production. This cost can be reached at a 4.5 million sqft production volume.

Additionally, these financial projections also represent a conservative estimate for market adoption and government incentives. The following are all possibilities that accelerate market penetration and/or increase internal rate of return:

- Government incentives, rebates, and subsidies
- Increased demand due to dynamic weather trends and events
- Additional cost savings by optimizing full window design for use with aerogel
- Long-term contract sales to normalize production to demand
- Secondary markets for “unfit” produced material to recover costs

7.1.3 Sensitivity and Risk Analysis

In addition to base cost estimate, there are four key assumptions that have the largest impact on pricing and adoption of the material. These assumptions have a key role in the successful scaling of the aerogel as a product sold to the existing value chain.

Product demand

Key assumptions: We assume that strategic establishment and growth in the market will allow sales to reach 4.5 million sqft production within 5 years of full launch. The driving assumption behind this expansion rate initially conservative to allow distribution channels to accommodate a new technology throughout the downstream value chain. We assume a 6 month lead time between purchasing additional production capacity and implementing the production.

Sensitivity: If adoption is significantly less than predicted, the expansion plan can be reduced to match. For example, decreasing the projected production plan by 33% only adds 20 months (1.75 years) to anticipated payback time for equipment.

Price per sqft

Key assumptions: We assume that for entry into the initial market, customers (insulated glass manufacturers) will pay \$6/sqft. As production expands, costs can be incrementally driven down to \$5/sqft through improvements in yield, fill factor for production equipment, and continued material development. In the following years, reduction in cost continues within the commercial sector until price reaches \$3/sqft.

Sensitivity: If product does not sell at \$6/sqft in our initial market, production is still feasible but internal payback is increased. For example, reducing initial price from \$6/sqft to \$5/sqft increases payback time by 16 months (1.25 years).

Material yield

Key assumptions: We assume that after 2 years of pilot production (no revenue), yield of drying equipment can reach 95% yield at production launch. This yield then reaches ~100% by the time the aerogel reaches 4.5 million sqft of annual production.

Sensitivity: If yield issues cannot be solved during pilot production (caused by batch mixing variations, damage during transportation between manufacturing processes, or drying events), it will affect internal rate of return. For example, if production launch yield is decreased from 100% to 90% internal rate of return drops by nearly 1.5%. However, it is very likely production can achieve >85% yield based on similar synthesis techniques currently used in industry.

Dryer utilization

Key assumptions: We assume that at the outset of production, dryers can be utilized at 85% capacity. This is made possible by the extensive piloting to develop precise production schedules and maintenance routines that complement the manufacturing process. By the time production reaches significant market share (~1 million sqft), it is assumed dryer utilization reaches 95%, facilitated by the addition of additional dryer capacity and the establishment of optimal labor training.

Sensitivity: If utilization of the dryers is limited, it poses a large risk to our success. In particular, reduction in long term utilization from 95% to 85% reduces internal rate of return by around 7%. To mitigate this risk, pilot production should be used to develop procedures that maximize dryer output. Additionally, production can be scaled back to increase dryer capacity until optimum utilization can be achieved, mitigating the effects on internal return rate.

Key risks to projected growth are shown in Figure 58, where key risks revolve around manufacturing challenges and adoption of aerogel. To mitigate these risks our projections assume conservative growth within markets with high willingness to pay. Furthermore, even if sales growth is slower than projected, the breakeven point for capital equipment is unchanged as long as output per facility meets expectations. Therefore, by choosing our revenue model and growth strategically, we can significantly reduce risk and reach a breakeven point at a sales volume far below our projections. Similarly, increased sales growth would allow production to be increased more quickly while remaining cost competitive.

	Risk	Mitigation Strategy
1	Low willingness to pay	Limit early production to demanding clients (extreme climates, passive homes, etc.)
2	Early manufacturing challenges	Strong partnership with launch customer willing to undergo extensive testing
3	Building energy regulations or incentives relax	AeroShield is cost competitive with existing solutions without incentives/regulations
4	Fragility of AeroShield panes limits handling	Co-locate with launch customers to directly integrate AeroShield
5	Complex training and manufacturing process	Prioritize knowledge sharing & create specialized training procedures

Potential Impact	High		1	
	Medium			2
	Low	5,3		
		Unlikely	Likely	Probable
		Probability		

Figure 58. Key risks, probability of occurrence, potential impact, and mitigation strategies for commercial production and integration of the aerogel into the existing manufacturing chain.

7.2 COST-EFFECTIVENESS OF AEROGEL WINDOWS

Currently, there are no window products that can match the performance and price of the aerogel material. Existing products rely on 3 primary strategies to improve performance: 1) add more layers of glass, 2) fill the space between the glass layers with insulating gases, 3) add solar and thermal coatings to one or more of the glass panes. By adding more layers and insulating gases, thermal performance can be significantly increased, but it also raises the cost of the product significantly – sometimes quadrupling the cost. While adding solar and thermal coatings to glass panes is a cheap, effective solution to reduce radiative losses, it can't prevent convection or conduction through the window and has, therefore, reached its limit for effectiveness. These strategies can be used in combination to meet the diverse needs of buildings, but results in a large variance in price. Double-pane windows cost anywhere from \$25 to \$70 per sqft, while high-performance triple-panes can cost as much as \$90 per sqft. Figure 59 compares nominal values of these technologies to the modeled aerogel double-pane.

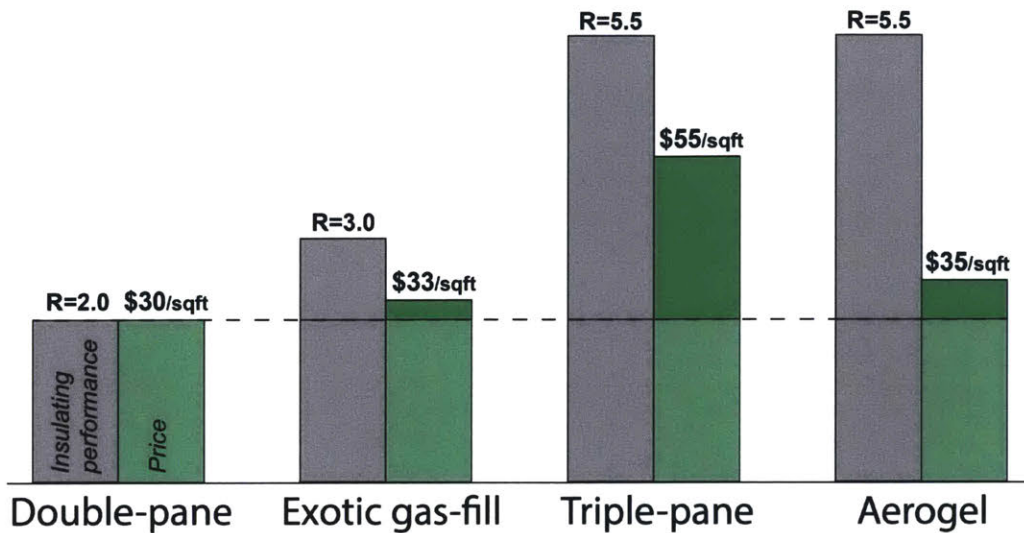


Figure 59. Comparison of cost added to a simple double-pane window for various solutions to increase thermal performance. The aerogel material can be added to a double-pane window at a price point significantly lower than triple-pane, with up to 50% better performance than exotic gases.

Other emerging products, such as vacuum-insulated glazing, face technical challenges that affect lifetime or costs, making them orders of magnitude (10x) more expensive than existing solutions. Porous materials that can compete with the thermal performance of aerogel face clarity and stability challenges that preclude them from entering the traditional window market at this stage in their development. Some have demonstrated favorable properties such as flexibility, but without the clarity that is fundamentally linked to their larger nanofeatures, these materials will not be adopted for traditional windows (as validated by our primary customer research). Additionally, these materials have yet to prove cost-competitiveness with our offering. Compared to these solutions, high-clarity aerogel has the potential to dramatically increase the insulating performance of windows and glazing without adding substantial cost.

7.2.1 Performance Modeling

Aerogel windows have the potential to provide significant energy savings. The Building Technologies Office Baseline Energy Calculator web tool estimates the residential homes lose over 2 quads of primary energy each year through heating and cooling losses due to low performance insulation in windows. A simple case study in Duluth, Minnesota shows that we can save 30-50% of these losses at a simple payback period <5 years. Indirect cost savings such as window lifetime, reduction in upfront construction costs, and reduced heating and cooling equipment make the aerogel window solution even more attractive. However, considering energy

savings alone, cold climate residences could save 2.6 GWh of energy each year simply by adding aerogel material into new construction windows.

Table 11. Comparison of energy performance for proposed aerogel double-pane compared to traditional window options. The case study considered a typical new construction single family home located in Duluth, Minnesota modeled in LBNL’s RESFEN energy package. Payback was calculated as the number of full year energy savings to cover the initial cost difference for the more insulating products compared to the standard double-pane needed to meet building code for an average home (2,000 square feet, 20 windows). Lifetime savings is the value of energy saved after payback compared to double-pane, assuming a 30 year window lifetime.

	Double-pane U=0.34 BTU/h/ft ² /F	Triple-pane U=0.18 BTU/h/ft ² /F	Aerogel double-pane U=0.20 BTU/h/ft ² /F
Window Cost	\$30/sqft	\$50/sqft	\$35/sqft
Energy Savings	—	14 MBTU	13 MBTU
Payback Period	—	25 years	7 years
Lifetime Savings	—	\$650	\$2750

7.3 SUSTAINABILITY & IMPACT OF AEROGEL WINDOWS

Sustainable window products face a unique set of challenges – in an industry where the dominant material has an embodied energy of 10 MJ/kg¹²³, adding materials to insulate quickly becomes cost and/or performance limited. However, there is still opportunity for more efficient, sustainable windows. Increases in the number of passive homes and energy certified buildings has shown that building owners and occupants care about the environmental impact of inefficient buildings. This means that the future of sustainable windows is not gated by low cost in market entry, but simply that there must be a path to balance cost, lifecycle, and installed performance.

We see the underserved intersection of the affordable and efficient markets as an opportunity to leverage our innovative material into the existing manufacturing chain to achieve both high performance and affordability. By placing high-clarity aerogel between two panes of glass to create a double-pane window, we can achieve performance competitive with triple-pane windows while having the cost and installation ease of a double-pane. This results in a product that can be up to 50% more energy efficient than 80% of windows installed in today’s homes, but with a payback period that is 3-5 times faster than triple-pane windows. In fact, If current single and double-pane windows were replaced with aerogel windows across the United States, buildings would be lighter, more comfortable, and more efficient – saving over 100 million tons of CO₂ and \$10 billion in reduced heating, cooling, and building construction costs.

Additionally, the aerogel is a platform solution for windows, and can provide an increased window lifetime and reduction in total materials needed, leading to a more sustainable product line. Typical double-pane windows can have lifetimes as short as 10 years due to failure of the seal inside the windows and degradation of coatings. As discussed in section 6.3.3 the aerogel can prevent and mitigate the effects of these failures, increasing lifetime for windows.

The sustainability of the production process of aerogels proves a challenge. The highest clarity aerogels are made of silica, but to reach peak performance they require high energy intensity and expensive capital equipment that does not have advantageous economies of scale. The embodied energy of aerogel is on the order of 50 MJ/kg, making it 5-10 times more energy intensive than glass.¹²⁴ However, significantly less material is needed to provide the same insulation (15-20 times less material per window), resulting in a 2-4x reduction in embodied energy and GHG of an additional air gap and pane. If aerogel performance can be pushed to extremes, it is possible that aerogel-filled windows could outperform triple-panes in cost-effectiveness and reduction in GHG.

7.4 SUMMARY

Successful application of silica aerogels in windows requires consideration for the cost-effectiveness of their insulating performance. To assess this, it is necessary to consider both the cost and price of the aerogel compared to traditional solutions. In this chapter, we propose a commercialization strategy in which the aerogel material is manufactured and supplied into the existing window manufacturing chain. Therefore, the cost premium for aerogel double-pane windows is driven by manufacturing equipment and cost of goods needed to manufacture the material.

Simplified building models were used to compare the potential homeowner energy and cost savings to the cost premium of other available products. In both cost-effectiveness (primarily quantified by simple payback) and energy savings, the proposed aerogel double-pane outperforms triple-pane windows. These results show promising potential for aerogel windows to enable windows that can save billions of dollars in energy for new buildings each year.

Chapter 8

8. Summary, Perspective, and Future Work

As the world's population grows, more buildings are needed to create work and home environments. This means there is an ever-growing need to provide bigger, better, more affordable buildings that optimize energy. For daylighting, this means finding the best way to use every photon to its highest potential, and the achievement of transparent aerogel provides a promising path for windows. In this work, we have achieved unprecedented visible transmittance of >98%, visible haze <2.0%, and thermal conductivity of <13 mW/mK through a 3 mm monolithic slab in ambient conditions, enabling window designs that can achieve a center-of-glass U-factor of 0.20 BTU/h/ft²/F without adverse effects on visual clarity. This results in a product that can be 50% more insulating than double-pane windows, and achieve performance comparable to triple-panes.

First, it is important to understand the current insulating window designs. In Chapter 2, we introduced the industry standard figures of merit and the fundamental principles of heat transfer and how they influence window designs. We also examined state-of-the-art technologies to understand the opportunity that still remains for cost-effective, high performance solutions.

In Chapters 3-5, we discussed the important considerations for optimized high-clarity aerogel for windows. This requires an understanding of the interdependent relationship between fabrication, the resultant nanostructure, and the relevant performance properties. These chapters present a framework for fabricating optimized aerogels that can be used to tailor performance properties relevant to a particular window application.

In Chapters 6-7, we discuss practical aspects of aerogel windows, including proof-of-concept performance at the prototype scale and considerations for full building performance. These practical considerations for commercialization and performance at full-window scale are critical to achieving cost-effective aerogel windows, particularly in an industry where durability and price are top considerations for end-users.

8.1 FUTURE WORK

The work presented here is a strong foundation for the consideration of aerogel windows. However, there are many areas of development that can increase the commercialization of these materials.

8.1.1 Sound Reduction

Value-added properties such as sound reduction offer an interesting opportunity for further development. In urban and metropolitan areas, sound pollution is a growing problem with very few products offering cost-effective results. In areas like New York City, noise pollution has led to a 50-100% increase in noise complaints.¹²⁵ Noise can also have an impact on a residents' health and is responsible for loss of 1.0-1.6 million "disability adjusted life-years".¹²⁶ An insulating solution like transparent aerogel that can address the acoustic needs of urban environments with low-frequency noise reduction could lead to higher adoption rate of energy-efficient windows. However, more development of the aerogel's acoustic properties is needed before this impact could be achieved.

In particular, early results of the sound transport through the aerogel indicates that in ambient conditions, sound reduction is only slightly better than a sealed gas gap. The transparent aerogel structure has been optimized for optical and thermal, but additional study of the nanofeatures and surface chemistry could yield improvements on the sound proofing potential of the material without adversely affecting the other properties. It is expected that pore pressure, porosity, tortuosity, and water uptake due to adsorption all influence acoustic transport. Developing a more rigorous understanding through the use of modeling and carefully designed characterization is needed to fully quantify the potential for aerogel sound-proof windows. More development of the understanding could uncover strategies to improve the material and/or window designs.

8.1.2 Increasing Sizes

Currently, the high clarity aerogel is fabricated at lab-scale sizes (6 inch diameter samples). This has demonstrated the ability to achieve clarity competitive with glass and thermal properties competitive with exotic gases, but at limited scale. The next step towards a realized product is to demonstrate the viability of a full aerogel window. This requires resources to fabricate larger aerogel samples and assembly into a full window prototype.

Scaling of the material to demonstrate manufacturability requires each needs to be translated from lab-scale into pilot scale. Considerations for how to cost-effectively achieve monoliths greater than 4 sqft include developing ways to cleanly mix and cast gels, method and equipment for drying, as well as repeatable handling for integration into double-pane units. Future works that can increase the success of such a pilot process includes adjusting chemical ratios and conditions

for increased solution-gelation, developing molding and transport techniques to prevent damage and defects, and achieving high-yield in critical point drying.

8.1.3 Prototype Development

In Chapter 6, we presented characterization of a 1 x 1 ft prototype to validate model predictions. However, we need to validate this performance with industry standardized testing of continuous aerogels of larger area to fully validate aerogel performance. This includes testing for both the center-of-glass and full window performance with framing elements. If larger sizes can be demonstrated, these prototypes would be significantly easier to assemble and test.

Additionally, considerations for varied stack configurations should be validated with prototypes as well. In Chapter 6, we propose designs such as argon fills and air gaps that can significantly increase performance, but these predictions have not been validated experimentally. Prior works have also explored the use of vacuum evacuation of aerogel pores, which may be another path to higher thermal efficiency. Successful commercialization of these designs requires rigorous proof of the aerogel's ability to integrate and perform. Extensive exploration and development is needed with regards to design and manufacturing of aerogel into double-pane units.

Large prototypes also enable investigation of the mechanical stability of the material during the lifetime of operation. Residential customers have high expectations for the structural stability of their windows; wind loading, cleaning, and weather events need to be designed and tested for. As the material technology is developed for optical, thermal, and mechanical properties, we also need to demonstrate the feasibility and performance of the material for end-users.

8.1.4 Full Building Model

Another important aspect of aerogel windows is their full impact on building comfort. In Chapter 7 we presented a simple building energy analysis based on predicted window performance. However, there are many considerations for different building types, climates, configurations, window types, etc. that influence the full performance of a window in a building. Select case studies for applications where aerogel windows can provide additional benefits may be highly advantageous in increasing commercialization potential.

For example, in extremely cold climates the benefits of high-performing windows reach beyond energy savings. Homes in locations like Manitoba and Saskatchewan, Canada have a huge need for high thermal performance, but have also demonstrated a high willingness to pay for

thermal comfort and window lifetime. Of the 10,000 new homes built each year in these provinces, customers are 8 times more likely to choose triple-panes than the national average despite the higher cost and payback period.⁷ This is a market that needs high performance just to maintain acceptable thermal comfort.

8.2 PERSPECTIVE ON THE FUTURE OF DAYLIGHTING

The next generation of daylighting systems will rely on material innovations and advancements. The most universal truth for buildings is that no two are exactly the same, and this means the needs of our buildings vary. Architects and engineers demand a diverse set of affordable materials to achieve optimum solutions, especially as our needs change and grow with time. Current advances include transparent insulating materials (TIMs), such as porous films or the transparent aerogels presented in this work, that overcome the thermal limitations that cause large windows to be impractical in many climates. Other material development is being used to create transparent/translucent photovoltaic cells that can harvest unused solar energy outside the visible spectrum. Additionally, many of the materials and elements currently being used in daylighting (such as reflectors, prisms, collectors) are constantly being improved to increase performance through careful study and optimization of structures and material properties.

The future of daylighting will also rely on advances in automation and control.¹²⁷ Automated control that can reduce energy needs has the potential to save considerable amounts for owners and tenants. Adaptive controls have the ability to reduce or eliminate varying non-idealities that can cause issues for occupants or processes. Instantaneous control allows for people and spaces to create the best environment for their productivity and comfort. Systems that use one or more of these approaches are becoming more and more prevalent, and will soon be an essential part of daylighting in new constructions.

Many daylighting elements already serve multiple purposes, such as thermal management or aesthetic elements, but future systems will include even more multi-functionality. As we push the limits of versatility and design, the same elements that provide natural light can also address other issues, such as energy collection and acoustic control. By combining advancements in materials, controls, and overall design, the future of daylighting, and aerogel's place in that endeavor, is indeed bright.

Bibliography

1. Office of Energy Efficiency & Renewable Energy. *Buildings Energy Data Book*. Department of Energy; 2011.
2. Department of Energy, Building Technologies Office. *Windows and Building Envelope Research and Development: Roadmap for Emerging Technologies*. 2014.
3. Chao J. Super Window Could Save Billions. News Release. <https://windows.lbl.gov/news/article/super-window-could-save-billions>. Published 2018. Accessed March 20, 2019.
4. Phillips D, Gardner C. *Daylighting: Natural Light in Architecture*; 2012. doi:10.4324/9780080477053
5. Carmody J, Haglund K. Measure Guideline : Energy-Efficient Window Performance and Selection. *Build Technol Progr*. 2012;(November).
6. Residential Energy Consumption Survey (RECS). 2015.
7. Centre CBEE-UD and A. A Comparison of Energy-Related Characteristics of Residential Dwellings and Technologies across Canada and the US. <https://sites.ualberta.ca/~deyoung/myweb/Comparison.pdf>.
8. Chao J. 'Super Window' Could Save \$10 Billion Annually in Energy Costs. News Release. <https://newscenter.lbl.gov/2018/06/06/super-window-could-save-billions-in-energy-costs/>. Published 2018. Accessed March 20, 2019.
9. Haranath D, Pajonk GM, Wagh PB, Rao AV. Effect of sol-gel processing parameters on thermal properties of silica aerogels. *Mater Chem Phys*. 1997;49(2):129-134. doi:10.1016/S0254-0584(96)01924-4
10. Svendsen S. Solar collector with monolithic silica aerogel. *J Non Cryst Solids*. 1992;145(C):240-243. doi:10.1016/S0022-3093(05)80464-8
11. McEnaney K, Weinstein L, Kraemer D, Ghasemi H, Chen G. Aerogel-based solar thermal receivers. *Nano Energy*. 2017;40(May):180-186. doi:10.1016/j.nanoen.2017.08.006
12. Reichenauer G. *Aerogels Handbook*. Springer US; 2011. doi:10.1007/978-1-4419-7589-8
13. Zhao J-J, Duan Y-Y, Wang X-D, Wang B-X. Experimental and analytical analyses of the thermal conductivities and high-temperature characteristics of silica aerogels based on microstructures. *J Phys D Appl Phys*. 2013;46(1):015304. doi:10.1088/0022-3727/46/1/015304
14. Soleimani Dorcheh A, Abbasi MH. Silica aerogel; synthesis, properties and characterization. *J Mater Process Technol*. 2008;199(1):10-26. doi:10.1016/j.jmatprotec.2007.10.060
15. Caps R, Fricke J, Germany W. Infrared Radiative Heat Transfer in Highly Transparent Silica Aerogel. *Sol Energy*. 1986;36(4):361-364.
16. Emmerling A, Petricevic R, Beck A, Wang P, Scheller H, Fricke J. Relationship between optical transparency and nanostructural features of silica aerogels. *J Non Cryst Solids*. 1995;185(3):240-248. doi:10.1016/0022-3093(95)00021-6
17. Tabata M, Adachi I, Ishii Y, Kawai H, Sumiyoshi T, Yokogawa H. Development of transparent silica aerogel over a wide range of densities. *Nucl Instruments Methods Phys Res Sect A Accel Spectrometers, Detect Assoc Equip*. 2010;623(1):339-341. doi:10.1016/j.nima.2010.02.241
18. Zhao L, Strobach E, Bhatia B, et al. Theoretical and experimental investigation of haze in transparent aerogels. *Opt Express*. 2019;27(4):A39. doi:10.1364/oe.27.000a39
19. Zhao L, Yang S, Bhatia B, Strobach E, Wang EN. Modeling silica aerogel optical performance by determining its radiative properties. *AIP Adv*. 2016;6(2). doi:10.1063/1.4943215
20. National Fenestration Rating Council. Procedure for Determining Fenestration Product U-factors. *NFRC 100*. 2014;(301).
21. National Fenestration Rating Council. Procedure for Determining Fenestration Product Condensation Resistance Values. *NFRC 500*. 2017;(301).

22. Rogers TG. Considerations for the condensation resistance of fenestration assemblies. *Proc BEST2 Conf.*:1-22.
23. National Fenestration Rating Council. Procedure for Determining Fenestration Product Solar Heat Gain Coefficient and Visible Transmittance at Normal Incidence. *NFRC 200*. 2014;(301).
24. National Fenestration Rating Council. Procedure for Determining Translucent Fenestration Product Visible Transmittance at Normal Incidence. *NFRC 202*. 2017;(301).
25. ASTM International. Standard Test Method for Haze and Luminous Transmittance of Transparent Plastics. *ASTM D1003*. 2000;06:1-6. doi:10.1520/D1003-07E01.2
26. ASTM International. Standard Test Method for Thermal Performance of Building Materials and Envelope Assemblies by Means of a Hot Box Apparatus 1. *ASTM C1363 – 11*. 2014;90:1-44. doi:10.1520/C1363-11.2
27. ASTM International. Standard Test Method for Steady-State Heat Flux Measurements and Thermal Transmission Properties by Means of the Guarded-Hot-Plate. *ASTM C177*. 2013:1-23. doi:10.1520/C0177-13.2
28. Energy Star. ENERGY STAR: The Simple Choice for Energy Efficiency. <https://www.energystar.gov/>. Published 2019. Accessed March 20, 2019.
29. National Fenestration Rating Council. NFRC Certified Products Directory. <http://essearch.nfrc.org/>. Published 2019. Accessed March 20, 2019.
30. Muneer T, Abodahab N, Gilchrist A. Combined conduction, convection, and radiation heat transfer model for double-glazed windows. *Build Serv Eng Res Technol*. 1997;18(4):183-191. doi:10.1177/014362449701800401
31. Sharpe LT, Stockman A, Jagla W, Jägle H. A luminous efficiency function, $V^*(\lambda)$, for daylight adaptation. *J Vis*. 2006;5(11):3. doi:10.1167/5.11.3
32. International Organization for Standardization. Determination of light transmittance, solar direct transmittance, total solar energy transmittance, ultraviolet transmittance and related glazing factors. *ISO 9050*. 2003;9050.
33. Ariosto T, Memari AM. Evaluation of Residential Window Retrofit Solutions for Energy Efficiency. *Pennsylvania Hous Res Cent*. 2013;(111).
34. McCluney WR. Sensitivity of fenestration solar gain to source spectrum and angle of incidence. *ASHRAE Trans*. 1996;102(2):112-122.
35. Carmody J, Selkowitz SE, Lee ES, Arasteh DK. *Window Systems for High-Performance Buildings*. New York, NY: W. W. Norton & Company, Inc.; 2004.
36. Lawrence Berkeley National Lab. WINDOW: Windows and Daylighting. <https://windows.lbl.gov/software/window>. Published 2019. Accessed February 15, 2019.
37. Korpela SA, Lee Y, Drummond JE. Heat Transfer Through a Double Pane Window. *J Heat Transfer*. 1982;(August 1982):539-544.
38. ElSherbiny SM, Raithby GD, Hollands KGT. Heat Transfer by Natural Convection Across Vertical and Inclined Air Layers. *J Heat Transfer*. 1982;104(1):96-102.
39. Bakonyi D. The thermal modeling of traditional double-skin box type windows. *PhD Thesis, Budapesti Univ Technol Econ*. 2016:132.
40. Arici M, Karabay H, Kan M. Flow and heat transfer in double, triple and quadruple pane windows. *Energy Build*. 2015;86:394-402. doi:10.1016/j.enbuild.2014.10.043
41. Salazar J, Sowlati T. Life cycle assessment of windows for the North American residential market: Case study. *Scand J For Res*. 2008;23(2):121-132. doi:10.1080/02827580801906981
42. Cabeza LF, Rincón L, Vilariño V, Pérez G, Castell A. Life cycle assessment (LCA) and life cycle energy analysis (LCEA) of buildings and the building sector: A review. *Renew Sustain Energy Rev*. 2014;29:394-416. doi:10.1016/j.rser.2013.08.037
43. Jelle BP, Hynd A, Gustavsen A, Arasteh D, Goudey H, Hart R. Fenestration of today and tomorrow: A state-of-the-art review and future research opportunities. *Sol Energy Mater Sol Cells*. 2012;96(1):1-28. doi:10.1016/j.solmat.2011.08.010
44. Weir G, Muneer T. Energy and environmental impact analysis of double-glazed windows. *Energy*

Convers Manag. 2002;39(3-4):243-256. doi:10.1016/s0196-8904(96)00191-4

45. Gläser HJ. History of the development and industrial production of low thermal emissivity coatings for high heat insulating glass units. *Appl Opt.* 2008;47(13):C193. doi:10.1364/ao.47.00c193
46. Sharma M, Chua ST, Wong TI, et al. Color tunable low cost transparent heat reflector using copper and titanium oxide for energy saving application. *Sci Rep.* 2016;6(1):1-14. doi:10.1038/srep20182
47. Dalapati GK, Kushwaha AK, Sharma M, et al. Transparent heat regulating (THR) materials and coatings for energy saving window applications: Impact of materials design, micro-structural, and interface quality on the THR performance. *Prog Mater Sci.* 2018;95:42-131. doi:10.1016/j.pmatsci.2018.02.007
48. Ferrara M, Castaldo A, Esposito S, D'Angelo A, Guglielmo A, Antonaia A. AlN–Ag based low-emission sputtered coatings for high visible transmittance window. *Surf Coatings Technol.* 2015;295:2-7. doi:10.1016/j.surfcoat.2015.12.015
49. Pilkington. Pyrolytic Advantage. <https://www.pilkington.com/en/us/architects-page/pilkington-pyrolytic-advantage>.
50. Babaizadeh H, Hassan M. Life cycle assessment of nano-sized titanium dioxide coating on residential windows. *Constr Build Mater.* 2013;40:314-321. doi:10.1016/j.conbuildmat.2012.09.083
51. Eames PC. Vacuum glazing: Current performance and future prospects. *Vacuum.* 2008;82(7):717-722. doi:10.1016/j.vacuum.2007.10.017
52. Kalnæs SE, Jelle BP. Vacuum insulation panel products: A state-of-the-art review and future research pathways. *Appl Energy.* 2014;116(7465):355-375. doi:10.1016/j.apenergy.2013.11.032
53. Zhao J, Luo S, Zhang X, Xu W. Preparation of a transparent supporting spacer array for vacuum glazing. *Vacuum.* 2013;93:60-64. doi:10.1016/j.vacuum.2013.01.002
54. Cuce E, Riffat SB. Vacuum tube window technology for highly insulating building fabric: An experimental and numerical investigation. *Vacuum.* 2015;111:83-91. doi:10.1016/j.vacuum.2014.10.002
55. Thapliyal PC, Singh K. Aerogels as Promising Thermal Insulating Materials: An Overview. *J Mater.* 2014;2014:10. doi:10.1155/2014/127049
56. Rubin M, Lampert CM. Transparent silica aerogels for window insulation. *Sol Energy Mater.* 1983;7(4):393-400. doi:10.1016/0165-1633(83)90012-6
57. Gao T, Jelle BP, Gustavsen A. Building Integration of Aerogel Glazings. *Procedia Eng.* 2016;145(1877):723-728. doi:10.1016/j.proeng.2016.04.090
58. Lolli N, Andresen I. Aerogel vs. argon insulation in windows: A greenhouse gas emissions analysis. *Build Environ.* 2016;101:64-76. doi:10.1016/j.buildenv.2016.03.001
59. Schultz JM, Jensen KI. Evacuated aerogel glazings. *Vacuum.* 2008;82(7):723-729. doi:10.1016/j.vacuum.2007.10.019
60. Zinzi M, Rossi G, Anderson AM, Carroll MK, Moretti E, Buratti C. Optical and visual experimental characterization of a glazing system with monolithic silica aerogel. *Sol Energy.* 2019;183(August 2018):30-39. doi:10.1016/j.solener.2019.03.013
61. Buratti C, Moretti E. Glazing systems with silica aerogel for energy savings in buildings. *Appl Energy.* 2012;98:396-403. doi:10.1016/j.apenergy.2012.03.062
62. Garnier C, Muneer T, McCauley L. Super insulated aerogel windows: Impact on daylighting and thermal performance. *Build Environ.* 2015;94(P1):231-238. doi:10.1016/j.buildenv.2015.08.009
63. Gao T, Jelle BP, Ihara T, Gustavsen A. Insulating glazing units with silica aerogel granules: The impact of particle size. *Appl Energy.* 2014;128:27-34. doi:10.1016/j.apenergy.2014.04.037
64. Gross J, Fricke J, Hrubesh L. Sound propagation in SiO₂ aerogels. *Acoust Soc Am.* 1992;91(4):2004-2006. doi:10.1121/1.403684
65. Gronauer M, Fricke J. Acoustic Properties of Microporous SiO₂- Aerogel. *Acustica.* 1986;59:177.
66. Gibiat V, Lefeuvre O, Woignier T, Pelous J, Phalippou J. Acoustic properties and potential applications of silica aerogels. *J Non Cryst Solids.* 1995;186:244-255. doi:10.1016/0022-3093(95)00049-6
67. Pajonk GM, Elaloui E, Chevalier B, Begag R. Optical transmission properties of silica aerogels

- prepared from polyethoxidisiloxanes. *J Non Cryst Solids*. 1997;210(2-3):224-231. doi:10.1016/S0022-3093(96)00600-X
68. Duer K, Svendsen S. Monolithic silica aerogel in superinsulating glazings. *Sol Energy*. 1998;63(4):259-267. doi:10.1016/S0038-092X(98)00063-2
 69. Wittwer V. Development of aerogel windows. *J Non Cryst Solids*. 1992;145(C):233-236. doi:10.1016/S0022-3093(05)80462-4
 70. Buratti C, Moretti E. Experimental performance evaluation of aerogel glazing systems. *Appl Energy*. 2012;97(July 2016):430-437. doi:10.1016/j.apenergy.2011.12.055
 71. Venkateswara Rao A. Synthesis of hydrophobic aerogels for transparent window insulation applications. *Mater Sci Technol*. 2001;17(3):6. doi:http://dx.doi.org/10.1179/026708301773002572
 72. Venkateswara Rao A. Synthesis of hydrophobic aerogels for transparent window insulation applications. *Mater Sci Technol*. 2001;17(3):6. doi:http://dx.doi.org/10.1179/026708301773002572
 73. Zhao L, Strobach E, Bhatia B, et al. Theoretical and experimental investigation of haze in transparent aerogels. *Opt Express*. 2019;27(4):A39-A50. doi:10.1364/OE.27.000A39
 74. Kim GS, Hyun SH. Synthesis of window glazing coated with silica aerogel films via ambient drying. *J Non Cryst Solids*. 2003;320(1-3):125-132. doi:10.1016/S0022-3093(03)00027-9
 75. Maleki H, Durães L, Portugal A. An overview on silica aerogels synthesis and different mechanical reinforcing strategies. *J Non Cryst Solids*. 2014;385:55-74. doi:10.1016/j.jnoncrysol.2013.10.017
 76. Fricke J, Emmerling a, Hubland A. Aerogels — Recent Progress in Production Techniques and Novel Applications. *J Sol-Gel Sci Technol*. 1998;13:299-303. doi:10.1023/A:1008663908431
 77. Aegerter M, Leventis N, Koebel M. *Aerogels Handbook (Advances in Sol-Gel Derived Materials and Technologies)*.; 2011. doi:10.1007/978-1-4614-1957-0
 78. Strobach E, Bhatia B, Yang S, Zhao L, Wang EN. High temperature annealing for structural optimization of silica aerogels in solar thermal applications. *J Non Cryst Solids*. 2017;462:72-77. doi:10.1016/j.jnoncrysol.2017.02.009
 79. Reim M, Reichenauer G, Körner W, et al. Silica-aerogel granulate - Structural, optical and thermal properties. *J Non Cryst Solids*. 2004;350:358-363. doi:10.1016/j.jnoncrysol.2004.06.048
 80. Sutherland RL. *Handbook of Nonlinear Optics*. Vol 36.; 2003. doi:10.1117/1.601248
 81. Stover JC. *Optical Scattering: Measurements and Analysis, Third Edition (SPIE Press Monograph PM224)*.; 2012. doi:10.1117/3.975276
 82. Modest M. *Radiative Heat Transfer*. 3rd ed. Oxford: Academic; 2013. doi:10.1016/B978-0-12-386944-9.50021-2
 83. Scherer C. B and GW. *Sol-Gel Science: The Physics and Chemistry of Sol- Gel Processing*.; 1990.
 84. Pons A, Casas L, Estop E, Molins E, Harris KDM, Xu M. A new route to aerogels: Monolithic silica cryogels. *J Non Cryst Solids*. 2012;358(3):461-469. doi:10.1016/j.jnoncrysol.2011.10.031
 85. Venkateswara Rao A, Nilsen E, Einarsrud MA. Effect of precursors, methylation agents and solvents on the physicochemical properties of silica aerogels prepared by atmospheric pressure drying method. *J Non Cryst Solids*. 2001;296(3):165-171. doi:10.1016/S0022-3093(01)00907-3
 86. Pajonk GM. Transparent silica aerogels. *J Non Cryst Solids*. 1998;225:307-314. doi:10.1016/S0022-3093(98)00131-8
 87. Reichenauer G. Thermal aging of silica gels in water. *J Non Cryst Solids*. 2004;350:189-195. doi:10.1016/j.jnoncrysol.2004.07.073
 88. Yoda S, Ohshima S. Supercritical drying media modification for silica aerogel preparation. *J Non Cryst Solids*. 1999;248(2):224-234. doi:10.1016/S0022-3093(99)00250-1
 89. Adachi I, Tabata M, Kawai H, Sumiyoshi T. Study of transparent silica aerogel with high refractive index. *Nucl Instruments Methods Phys Res Sect A Accel Spectrometers, Detect Assoc Equip*. 2011;639(1):222-224. doi:10.1016/j.nima.2010.08.125

90. Tabata M, Adachi I, Kawai H, Sumiyoshi T, Yokogawa H. Hydrophobic silica aerogel production at KEK. *Nucl Instruments Methods Phys Res Sect A Accel Spectrometers, Detect Assoc Equip.* 2012;668:64-70. doi:10.1016/j.nima.2011.12.017
91. Tillotson TM, Hrubesh LW. Transparent ultralow-density silica aerogels prepared by a two-step sol-gel process. *J Non Cryst Solids.* 1992;145(C):44-50. doi:10.1016/S0022-3093(05)80427-2
92. www.aerogeltechnologies.com.
93. Emmerling A, Fricke J. Small angle scattering and the structure of aerogels. *J Non Cryst Solids.* 1992;145(C):113-120. doi:10.1016/S0022-3093(05)80439-9
94. Svergun DI, Feigin L a, Taylor GW. *Structure Analysis by Small-Angle X-Ray and Neutron Scattering.*; 1987. doi:10.1007/978-1-4757-6624-0
95. Pauw BR. Everything SAXS: small-angle scattering pattern collection and correction. *J Phys Condens Matter.* 2013;25(38):383201. doi:10.1088/0953-8984/25/38/383201
96. Butler P, Alina G, Hernandez RC, et al. SASView for Small Angle Scattering Analysis.
97. Pauw BR. McSAS: A package for extracting quantitative form-free distributions. *J Appl Crystallogr.* 2014:1-18.
98. Strobach E, Bhatia B, Yang S, Zhao L, Wang EN. High temperature stability of transparent silica aerogels for solar thermal applications. *APL Mater.* 2019;7(8). doi:10.1063/1.5109433
99. Strobach E, Bhatia B, Zhao L, Wang EN. Thermal Performance of High-Efficiency Window Technologies. *Annu Rev Heat Transf.* 2019:59-97. doi:10.1615/annualrevheattransfer.2019030886
100. Abràmoff MD, Magalhães PJ, Ram SJ. Image processing with imageJ. *Biophotonics Int.* 2004;11(7):36-41. doi:10.1117/1.3589100
101. Hrubesh LW, Pekala RW. Thermal properties of organic and inorganic aerogels. *J Mater Res.* 1993;9(3):731-738. doi:doi:10.1557/JMR.1994.0731
102. Gibiat V, Lefeuvre O, Woignier T, Pelous J, Phalippou J. Acoustic properties and potential applications of silica aerogels. *J Non Cryst Solids.* 1995;186:244-255. doi:10.1016/0022-3093(95)00049-6
103. Gross J, Fricke J, Hrubesh LW. Sound propagation in SiO₂ aerogels. *J Acoust Soc Am.* 2005;91(4):2004-2006. doi:10.1121/1.403684
104. Scientific C, Ryde N, Narang PP. A theoretical study of sound transmission through aerogel glazing systems. *Appl Acoust.* 1991;34(4):249-259. doi:10.1016/0003-682X(91)90008-3
105. Tadeu AJB, Mateus DMR. Sound transmission through single, double and triple glazing. Experimental evaluation. *Appl Acoust.* 2001;62(3):307-325. doi:10.1016/S0003-682X(00)00032-3
106. Gross J, Fricke J, Hrubesh LW. Sound-Propagation in SiO₂ Aerogels. *J Acoust Soc Am.* 1992;91(4):2004-2006. doi:Doi 10.1121/1.403684
107. Gross J, Reichenauer G, Fricke J. Mechanical properties of SiO₂ aerogels. *J Phys D Appl Phys.* 1988;21:1447-1451. doi:10.1088/0022-3727/21/9/020
108. Parmenter KE, Milstein F. Mechanical properties of silica aerogels. *J Non Cryst Solids.* 1998;223(3):179-189. doi:10.1016/S0022-3093(97)00430-4
109. Scherer GW. Bending of gel beams: Effect of deflection rate and Hertzian indentation. *J Non Cryst Solids.* 1996;201(1-2):1-25. doi:10.1016/0022-3093(95)00629-X
110. Sobac B, Colinet P, Pauchard L. Influence of Bénard-Marangoni instability on the morphology of drying colloidal films. *Soft Matter.* 2019. doi:10.1039/c8sm02494d
111. Bassou N, Rharbi Y. Role of Bénard-Marangoni instabilities during solvent evaporation in polymer surface corrugations. *Langmuir.* 2009. doi:10.1021/la802979a
112. Maroto JA, Pérez-Múuzuri V, Romero-Cano MS. Introductory analysis of Bénard-Marangoni convection. *Eur J Phys.* 2007. doi:10.1088/0143-0807/28/2/016
113. Pedrotti FL, Leno M. *Introduction to Optics.* Addison-Wesley; 2006.
114. Cui Y, Ke Y, Liu C, et al. Thermochromic VO₂ for Energy-Efficient Smart Windows. *Joule.* 2018;2(9):1707-1746. doi:10.1016/j.joule.2018.06.018
115. Brinker CJ, Scherer GW. Structural changes during heating: Amorphous systems. *Sol-Gel Sci Phys Chem Sol-Gel Process.* 1990;555.

116. Aravind PR, Mukundan P, Krishna Pillai P, Warriar KKG. Mesoporous silica-alumina aerogels with high thermal pore stability through hybrid sol-gel route followed by subcritical drying. *Microporous Mesoporous Mater.* 2006;96(1-3):14-20. doi:10.1016/j.micromeso.2006.06.014
117. No Title. <http://www.nfrc.org/>.
118. Holstein A, Bohnhoff D. The Design and Fabrication of a Rotatable Guarded Hot Box (RGHB) Capable of Static Pressure Application. In: Vol 1. ; 2013. doi:10.13031/aim.20131578832
119. Günay AA, Kim H, Nagarajan N, et al. Optically Transparent Thermally Insulating Silica Aerogels for Solar Thermal Insulation. *ACS Appl Mater Interfaces.* 2018;10(15):12603-12611. doi:10.1021/acsami.7b18856
120. Wagh PB, Ingale S V. Comparison of some physico-chemical properties of hydrophilic and hydrophobic silica aerogels. *Ceram Int.* 2002;28(1):43-50. doi:10.1016/S0272-8842(01)00056-6
121. Huang YJ, Mitchell RD, Arasteh D, Selkowitz SE. Residential fenestration performance analysis using RESFEN 3.1. *Therm Perform Exter Envel Build VII, Conf Proc.* 1998;(February):587-598.
122. Humphries C. Boston wants to fight climate change. *The Boston Globe.* <https://www.bostonglobe.com/ideas/2017/07/14/boston-wants-fight-climate-change-why-every-new-building-made-glass/bPHKGwPxuuwsxHHTdlwmNJ/story.html>. Published 2017. Accessed February 15, 2019.
123. Citherlet S, Di Guglielmo F, Gay JB. Window and advanced glazing systems life cycle assessment. *Energy Build.* 2000;32(3):225-234. doi:10.1016/S0378-7788(98)00073-5
124. Dowson M, Grogan M, Birks T, Harrison D, Craig S. Streamlined life cycle assessment of transparent silica aerogel made by supercritical drying. *Appl Energy.* 2012;97:396-404. doi:10.1016/j.apenergy.2011.11.047
125. No Title.
126. Fritschi L, Brown AL, Kim R, Schwela D, Kephelopoulos S. Burden of disease from environmental noise: Quantification of healthy life years lost in Europe. *World Heal Organ.* 2011:1-106. doi:10.1080/13504630.2011.629519
127. Konstantoglou M, Tsangrassoulis A. Dynamic operation of daylighting and shading systems: A literature review. *Renew Sustain Energy Rev.* 2016;60:268-283. doi:10.1016/j.rser.2015.12.246